Physics of Fluids

REVIEW ARTICLE | APRIL 16 2024

A review on flow instability in hydro-viscous drive

Jianzhong Cui (崔建中) ; Hui Tang (唐辉)

Physics of Fluids 36, 041301 (2024)
https://doi.org/10.1063/5.0203298

Physics of Fluids REVIEW pubs.aip.org/aip/pof

A review on flow instability in hydro-viscous drive

Cite as: Phys. Fluids **36**, 041301 (2024); doi: 10.1063/5.0203298
Submitted: 12 February 2024 · Accepted: 28 March 2024 ·
Published Online: 16 April 2024

Jianzhong Cui (崔建中)[1,2,a)] and Hui Tang (唐辉)[3,b)]

AFFILIATIONS

[1]Yancheng Institute of Technology, Yancheng 224051, People's Republic of China
[2]Southeast University, Nanjing 211189, People's Republic of China
[3]Department of Mechanical Engineering, The Hong Kong Polytechnic University, Kowloon, Hong Kong, People's Republic of China

[a)]**Author to whom correspondence should be addressed:** cuijianzhong21@163.com
[b)]**Electronic mail:** h.tang@polyu.edu.hk

ABSTRACT

Hydro-viscous drive (HVD) plays a significant role in smoothly transferring torque and flexibly regulating the velocity of the disks. By hydro-viscous drive, we mean that the viscous shear stress of the thin oil film between a multi-layer assembly of rotating parallel disks is generated to transmit torque and power. The laminar-to-turbulent transition is an extremely complicated issue due to the combined effects of squeeze and shear on the oil film within the microscale friction pair system. Hence, a comprehensive and thorough analysis of flow instability in fluid-thermal-solid interaction of tribodynamic behavior is highly desirable. Following a brief introduction of fundamentals of HVD, this paper provides an overall review on the instability mechanisms for three types of canonical flow dynamic models, i.e., plane squeeze flow, plane shear flow, and rotating-disk flow. The effects of various aspects of wall conditions and working media, such as surface microstructure, and temperature-dependent viscosity, on flow instability are then summarized, which can serve as a reference and guidance for optimizing the design of friction pair systems. Based on the review of the former progress, this paper not only explores the in-depth mechanisms regarding the laminar-to-turbulent transition in microchannel flow, but also provides the possibility of bridging the gap between flow instability and tribodynamic behavior.

I. INTRODUCTION

A. Background

Hydro-viscous drive (HVD) utilizes the viscous shear stress of the thin film between a multi-layer assembly of rotating parallel disks to transmit torque. As the lubricant oil serves as the working medium, it has been successfully used for speed regulation or soft-start of high-powered industrial equipment, such as tunnel boring machines (TBM), wind-driven generators, belt conveyors, controlled start transmission (CST) systems, etc.[1] Based on both the squeezing and shearing of the oil film, the torque transmission mechanism of HVD is similar to that of the wet clutch system, as shown in Fig. 1. During the process of torque transfer, the disks are immersed in a cooling lubricating fluid that flow through the working intake. Simultaneously, the oil flows through the control intake and then into the hydraulic actuator, which is used for regulating the film thickness between the disks. The HVD system transmits torque or rotation between shafts by engaging, while the input shaft is driven by the engine, and the output shaft is connected to the transmission or some other device. It links these two rotating shafts to be connected together and rotate at the same speed, or be separated and rotate at different speeds. In the hydrodynamic lubrication stage, as the clearance between the disks decreases, the hydrodynamic torque increases due to the squeeze action. After reaching its peak value, the torque starts to decrease until a constant level is established in the high-speed range. At this partial lubrication stage, the film thickness is reduced to an extent that surface asperities come in contact with each other. Then, the friction torque due to the contact pressure at the asperity level begins to develop, which significantly influences the tribodynamic behavior. For this typical friction pair system (consisting of two disks and the oil film), the lubrication regime undergoes a transition from hydrodynamic to mixed or boundary lubrication regime,[2,3] as shown in Fig. 2.

B. Flow configuration and flow instability

The transmission performance of the friction pair system in HVD largely depends on the dynamic characteristics of the oil film between the disks. Actually, in contrast to the breadth of the disks, there is a distinct smaller order of the film gap where the oil film is given by a combination of squeeze-film flow and rotating shear flow.[3] When the disks move normally to each other with a prescribed time-dependent speed, i.e., squeeze-film flow only, the velocity field

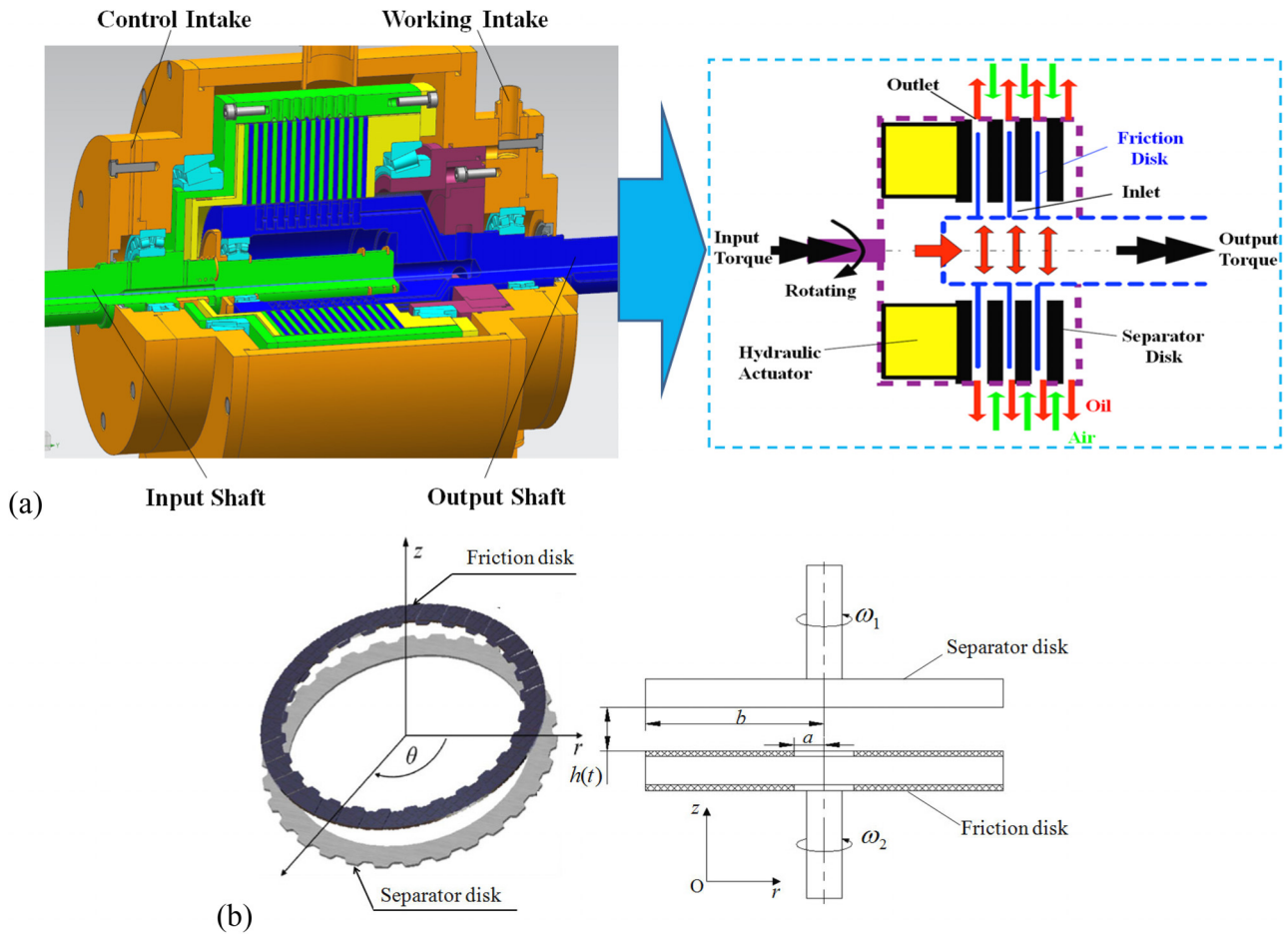

FIG. 1. Schematic of HVD: (a) Multi-layer model; (b) Single simplified friction pair system.

developed in the thin layer of fluid can be approximately identified as plane Poiseuille flow (PPF). Then the magnitude of the flow velocity is dependent on time and also on the coordinate parallel to the planes. It should be noted that PPF still exists under the assumption that there is no relative movement between the two disks. This is due to the fact that the oil film flows from the inner to the outer radius, effectively lubricating the space between the disks. On the other hand, viscous shear stress is generated when the driving and driven disks rotate at different speeds (in rpm) without axial motion, which can be classified as plane Couette flow (PCF). If the cooling effect of the oil flowing through the microchannel is also considered, it can be seen as the so-called plane Couette–Poiseuille flow (PCPF). PCF and PCPF are the most elementary types of laminar motion, and are widely investigated for hydrodynamic stability. Such kind of working conditions correspond to the *open mode* of HVD.[4] When HVD is open, the drag torque depends on the viscosity of the oil film and is also affected by the presence of air bubbles that may be trapped between the disks. However, there is a great discrepancy between PCF and viscous shear of HVD. As shown in Fig. 3, the rotating flow between parallel disks is located in a cylindrical polar coordinate system (r, θ, z) where the r-axis is on the driven disk surface. The fluid particle in the flow is assumed to rotate about z axis with relative angular velocity ω. Then the driving shear force is balanced by the Coriolis force component $2\rho\omega v_r \mathrm{d}V$ (ρ is the density, v_r is the radial velocity component and dV is the volume of fluid particle), while the centrifugal force $\rho r\omega^2 \mathrm{d}V$ and

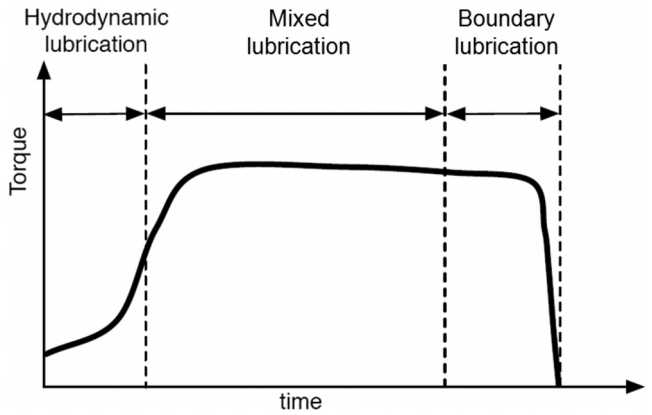

FIG. 2. Torque vs time: Typical soft-start process.

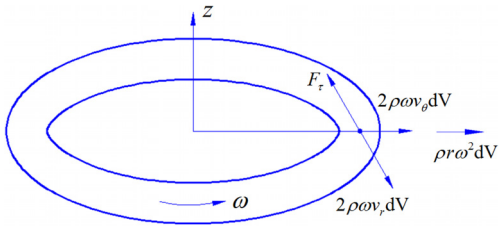

FIG. 3. Diagram of force balance on a fluid particle in the driven disk surface.

the Coriolis force component $2\rho\omega v_\theta dV$ (v_θ is the tangential velocity component) will accelerate the flow of the fluid particle in the radial direction.[5] Therefore, it can be seen that both the centrifugal force and the Coriolis force have a significant effect on the rotating flow.

To some extent, HVD may be approximated as rotating plane Couette flow (RPCF) or Taylor–Couette flow (TCF); however, almost all the RPCF flows consider channel flow driven by the in-plane motion of the parallel channel walls, subject to a system rotation about a spanwise axis instead of the wall-normal axis. In addition, TCF is the closed motion of fluid lying between concentric cylinders driven by the rotation of these cylinders about their shared axis, which is governed by the combined effects of rotation, shear, and curvature of the walls. Whether about the centrifugal force or the Coriolis force or the shear force, it is obvious that the viscous shear of HVD will have absolutely different effects on film dynamics as compared to RPCF and TCF.[6] Regarding the common mode of speed-regulating or soft-start, the flow configuration generated within the film can be taken as a combination of PPF and PCF in the coaxial rotating system. Due to viscous dissipation and also interaction of asperity contact, a large amount of frictional heat is generated, which greatly affects the hydrodynamic torque and the overall operational stability. Moreover, thermal stresses may be developed in the bounding surfaces when the temperature rise exceeds the cooling capacity of the oil film.[7]

Based on the viscous shear effects of the oil film, HVD can be used for transferring the torque from the engine or motor to the transmission output shaft, thereby affecting the overall driven-train efficiency. For speed-regulating or soft-start mode, in order to adequately realize the flexible transmission potential, i.e., hydro-viscous flexible drive, it is necessary to keep the friction pair system at either hydrodynamic or mixed lubrication regime.[7] Although the friction pair system appears simple, it is difficult to predict the highly nonlinear tribodynamic behavior, characterized by the complexity of physical mechanisms about microscale wall-bounded hydrodynamic lubrication and fluid–thermal–structure interaction. It is closely related to the response of a stable flow system to any amplitude of disturbance, i.e., flow instability. More specifically, flow conditions are always assumed to be laminar due to oil viscosity and gap dimensions in HVD. Wall effects may suppress turbulence in the oil film over the entire range of rotational speeds.[8] Nevertheless, according to Huang *et al.*,[6] flow behavior can be predicted by tangential Reynolds number Re_θ as follows:

$$Re_\theta = \frac{\omega r^2}{\upsilon}, \tag{1}$$

where υ is the kinematic viscosity of the oil film. The transition to turbulence can be observed as Re_θ exceeds a critical value (of the order 3×10^5). As a result, the laminar flow may evolve into a more complicated state when subjected to small disturbances. Inevitable irregular fluctuations of the multi-physical field within the thin oil film occur, which will have a dramatic effect on the original dynamic equilibrium of the squeeze and shear film process. Therefore, a good understanding of the flow stability of the microscale oil film between the sliding disks is necessary to accurately capture the tribodynamic torque characteristics.

Flow instability is undesirable because sustained flow oscillations may cause premature occurrence of critical heat flux as well as other undesirable secondary effects, such as torque oscillations. Additionally, flow instability can also disturb effective control of the film thickness and cause operational problems about HVD.[9,10] Over the years, several kinds of instabilities have been observed in microchannel flow system excited by different mechanisms. Because of the multi-physics aspects of the flexible drive process, the stability of fluid flows in HVD usually depends on various influencing factors. A bifurcation occurs provided that one of the parameters reaches the critical value. Then, the friction pair system starts evolving toward a new state, either steady or unsteady. As a typical fluid–thermal–solid interaction system, the main influencing factors are: wall boundary (surface microstructure, porous media of the friction material, and surface roughness) and working medium (temperature-dependent viscosity, non-Newtonian fluids and cavitation). A number of research works, in fact, have already been done to determine the effects of the above factors on flow instability in modern engineering and industrial applications, e.g., microelectromechanical systems, microchannel flow boiling, and microchannel heat sink. However, it can be observed that the friction pair system in HVD is required to transfer torque smoothly via the oil film when suffering from extremely demanding microscale conditions.[11] Whether the established model is accurate or not, it is very difficult to specify how the realistic transition-to-turbulent flow occurs in microchannels. In general, the true mechanisms of flow instability are either unknown or very poorly defined. In order to offer physical insights into complex flexible transmission behaviors, the influencing mechanisms of various factors on the stability of plane microchannel flow are examined.

C. Objectives of present work

It is worth emphasizing that, although consistent efforts have been made to identify the effects of various factors on the transmission performance of HVD, the underlying mechanisms regarding the tribodynamic behavior within the friction pair system are yet to be fully explored. For example, most of the existing studies reported the performance based on the assumption of laminar flow. Obviously, it does not correspond to the real situation and may not satisfy the design requirements, either. In fact, flow instability like velocity fluctuations, pressure drop oscillations, and flow maldistribution in the microchannel, can cause an irreversible failure of the system. Therefore, to bridge the gap, the objective of this work is to provide a comprehensive review of flow instability of oil film in HVD. It should be noted that the fluid in the microgap is in motion due to the relative rotation of the disks, which is similar to in other applications, such as hydrodynamic journal bearings, cylinder linear-piston ring systems in internal combustion engine, piston cylinder interface in axial piston pump, mechanical seals, and microelectromechanical systems (MEMS), etc. Therefore, even though this present work is focused on HVD, we believe that it

will also be of significant value for the above applications. More importantly, this work could highlight broad aspects of causes of complicated tribodynamic behavior that is caused by flow instabilities within microscale flow system.

The paper is divided as follows: Sec. II summarizes the flow instability characteristics of three basic flow models in HVD, namely plane squeeze flow, plane shear flow, and rotating-disk flow. Section III analyzes the effects of two main influencing factors from the fluid–solid interaction system, including the wall conditions and the working media, on the flow instability of the oil film. Finally, Sec. IV presents conclusions and proposes some perspectives.

II. INSTABILITY CHARACTERISTICS OF BASIC FLOW MODELS

A. Plane squeeze flow

HVD is featured by an incompressible viscous squeeze flow in a thin gap. For such a small aspect ratio of the gap separating the two parallel disks $G = h/r$ (h is the gap), flow stability may be neglected over a controllable timescale. However, it is clear that, whether soft-start or speed-regulating, squeeze film flow does not vary smoothly but fluctuates in a quite disordered manner.[12] Related studies can be traced back to the Reynolds lubrication theory, which is recognized as an important problem in fluid mechanics since it appears in many practical applications such as printing, human joints, injection molding, shock absorbers, and lubrication systems, etc.

The simplest means of investigating hydrodynamic stability is through approximation methods, such as the perturbation method. One of the earliest attempts to analyze the unsteady laminar flow of an incompressible fluid in a narrow gap between two parallel disks was made by Ishizawa,[13] in which a multifold power series solution was developed as the gap varies arbitrary with time. The analysis showed that the varying hydrodynamic force acting on the wall surface becomes distorted in the wave form. There is a coupling between a time-dependent inviscid core flow and the growth of an unsteady boundary layer.[14] According to the linearized solutions of the resulting nonlinear partial differential equations, thin layers of vorticity are initially concentrated at the surfaces due to the initial impulsive movement. The vorticity then diffuses out from the surfaces, and the radial velocity profiles tend to become parabolic.[15]

For the first time, Stuart *et al.*[16] established a two-dimensional viscous squeeze-flow model in which two parallel plates were moved normally to each other with a time-dependent speed. They systematically derived the Orr–Sommerfeld (O-S) equation governing the squeeze-flow stability at a Reynolds number *Re*. Then the relationship between time-dependence and flow instability was obtained through both linear and quadratic approximations. They found an asymptotic solution to the equations governing the growth of Tollmien–Schlichting (T-S) waves, which reflects PPF with amplitude varying slowly in time and space. Furthermore, Hall and Papageorgiou[17] investigated the instability of time-periodic oscillatory squeeze bearing flows subjected to wave or vortex disturbances. It was concluded that if the basic flow is disturbed slightly, the growth and decaying of the disturbance are closely related to linear stability. Whether the plates are squeezed together or pulled apart, both kinds of squeeze flows are characterized by the equivalent Reynolds number, which considers the disturbance wave at or near a particular station. With the increase in the equivalent Reynolds number, chaotic flow resulting from a quasi-periodic flow is closely associated with the amplitude of oscillation, especially in the presence of unsteady periodic flows. Obviously, these methods and their numerical applications fall under the linear theory of hydrodynamic stability, in which only approximate linear equations for the disturbances are used. The stability analysis usually satisfies the assumption that any small disturbance of the laminar flow considered can be represented by a sum of normal modes that exponentially depend on time.

Instead of using the normal-mode method to deal with special "wave-like" infinitesimal disturbances, the Kelvin mode was used by Aristov and Gitman[18] to analyze the asymptotic behavior of periodical one-dimensional disturbance. When the disks move apart from each other, there is an instability that wave structures with different configurations are formed with the evolution of perturbation. In order to deal with the global stability of dynamic systems with slow time dependence or weakly non-parallel flows, i.e., steady or unsteady periodic flows, low-dimensional Garlerkin method (LDGM) is developed by Zhu *et al.*[19] to investigate the asymptotic behavior in a long period of time or the transient behavior in a short time interval. It has been found that wall boundaries have a stabilizing influence due to the inertial terms in the squeeze lubrication film. With the increase in the Reynolds number, the effect of the inertial term has to be considered.[20] However, the resulting viscous shear may tend to destabilize the flow because of its viscosity diffusion. In this case, similarity solutions have been developed to include both the viscous and inertial effects in the momentum equation. Meanwhile, approximation methods were developed using series solutions due to the non-linear squeeze characteristics. Engmann *et al.*[21] conducted a thorough review of the squeezing flow theory about the non-linear term in the momentum equation. Most studies established the validity limits of self-similarity solutions by comparing them with numerical results. However, this does not mean that all branches of the self-similar solutions can occur under all conditions. For example, if the Reynolds number is larger than 500 for accelerating flows, Espin and Papageorgiou[22] found it difficult to obtain the exact solution due to the dimensionality and nonlinear nature of the system. Another limitation is the approximate results for unsteady axisymmetric squeezing flow of non-Newtonian fluid in the presence of a magnetic field.[23] It can be seen that squeeze films appear not subjected to a comprehensive evaluation under extreme conditions.

Particularly, it is necessary to examine unsteady squeezing flow where the fluid inertia and the viscous effect are equally important.[24] In this case, the reduced quasi-steady linear (QSL) model provided excellent comparisons between the velocity measurements and computational fluid dynamics (CFD) analysis results. Velocity oscillation can be attributed to the interplay between temporal inertia, spatial inertia, and viscous effects.[25] Given that the application limits for the similarity method that the gap has to be the form $h = (At + B)^{1/2}$, where t represents the time, and A and B have to be the constant, the families of exact non-self-similar solutions of the axisymmetric Karman equations[26] and two-dimensional Hiemenz equations[27] were considered. Likewise, when the distance between plates changes over time according to a power-law $h \sim |t|^s$ or an arbitrary-power law, there exists a self-similar solution for $s = 1/2$, and the best approximations of the solutions are found by means of asymptotic series for $s = 1$, 2, or in the case of uniform motion and uniformly accelerated motion of the plates.[28–30] Then, the critical Reynolds number can be determined,

which corresponds to the development of counterflow near the boundary where the velocity is directly opposite to the average velocity.

There are inherent limitations about the perturbation methods assuming small parameters, in spite of their advantages in analytically solving nonlinear boundary value problems. Many constructive methods were put forward for more efficient solutions with various complicated boundary conditions. In 2008, the Optimal Homotopy Asymptotic Method (OHAM) was introduced to find approximate solution of nonlinear differential equations in thin film flow.[31] By comparison, it was found that OHAM is more appropriate for controlling the convergence to the exact solution.[32,33] Based on this method, Qayyum *et al.*[34] solved an unsteady squeezing fluid flow between two circular disks with slip and non-slip boundary conditions. They observed that the Reynolds number has opposite effects on the normal velocity and longitudinal velocity near the central axis of the gap. Hayat *et al.*[35] investigated the Cattaneo–Christov heat flux effect in the two-dimensional squeezing flow of second grade fluid between two parallel plates. The homotopy analysis method was employed for the development of convergent series solutions for velocity and temperature. It was observed that the velocity profile is enhanced by increasing the squeezing parameter. Similarly, analytical approaches such as the collocation method, the homotopy perturbation method, and the homotopy analysis method demonstrate highly accurate and rapid solutions for nonlinear differential equations, in comparison to the fourth-order Runge–Kutta method.[36,37]

More recently, in order to precisely capture the instantaneous fluid flow response inside a very thin gap during a sudden impact, analytical approaches including an exact solution, i.e., the Laplace transform method, and an approximate method, i.e., the boundary layer integral method, were proposed.[38] It was found that the time-dependent local acceleration of the fluid cannot be neglected since the magnitude of the viscous effect and the inertia effect are comparable. Later, Lang *et al.*[39] demonstrated that the pressure gradient in the radial direction is balanced by the local acceleration, the viscous force, and the porous resistance. As the squeezing depth increases, the oscillation of the velocity profile will be intensified due to the alternating dominance of the viscous and inertial effects.[40] They concluded that porous media significantly stabilize the fluid field and decrease the fluctuation in the velocity profiles. In addition, it should be noted that the flow detachment may be caused by the moving boundaries and the force wall motion induced by fluid dynamic forces, which results in oscillatory flows downstream of the moving wall. Because of the complex fluid–solid interaction mechanism, a simplified analytical model considering asymptotic solutions of the Navier–Stokes equations was developed with a perturbation technique.[41] Therein, it was found that the mean velocity in the channel with one wall periodically pulsating, is larger than that for the horizontal squeeze flow. Last but not least, electric/magnetic lubricants have been widely used as smart lubrication in modern tribological systems since they can be manipulated for regulating the load-carrying capacity of the lubricants through external electric/magnetic fields.[42] It was observed that the load-carrying capacity of squeeze film lubrication could be significantly increased by the applied magnetic field. The mean squeeze time is lengthened as compared to the corresponding non-magnetic case.[43,44] The electroviscous effect modifies the velocity profiles inside thin films to be much sharper, which reflects an interplay of electrostatic body force and the law of mass conservation.[45] Based on the spectral local linearization method (SLLM), increasing the film squeezing ratio is helpful in intensifying the velocity profiles, which also plays a significant role in controlling the friction factor of radiative squeezing flow.[46]

For quick reference, Table I summarizes representative instability analyses for plane squeeze flow.

B. Plane shear flow

For the shear flow of viscous incompressible fluids between two parallel plates, although the laminar-turbulent transition mechanism about PCF or PCPF has been investigated intensively, there is still a significant difference in the critical Reynolds number between experimental and theory results.[47–49] So far, the stability of plane shear flow has been insufficiently understood. The disturbance growth mechanism in plane shear flow has always been the object of a series of theoretical and experimental studies. In general, the main interest is to determine whether a laminar flow, which experiences a perturbation, is able to return its original stable state or evolves toward a new state, either steady or unsteady.[50,51] There exist extensive specific analytical and numerical solutions that have been devoted to this issue, so the following review is by no means exhaustive. Emphasis is placed on recent representative developments in the flow instability of plane shear flow.

There are two classical methods that yield rigorous stability results, i.e., the linearized stability analysis and the energy method. The former method deals with the evolution of infinitesimal disturbances satisfying the linearized Navier–Stokes equations. Whether the dynamic system is stable or not depends on the critical Reynolds number that is obtained from the O-S eigenvalues. The initial linear stability theory focused on PPF in which the stability problem can be reduced to a one-dimensional problem, an approach usually referred to as the local stability approach.[47] However, the transition to turbulence may occur at Reynolds numbers much lower than the critical value provided by linear stability theory.[52] This is due to the fact that the critical Reynolds number is found to increase monotonically with the decrease in the aspect ratio. The classical linear stability theory of plane shear flow is concerned with the development in space and time of infinitesimal perturbations around a given basic flow.[48] For wall-bounded shear flows, the mean-velocity profile is non-uniform in the streamwise direction. In order to characterize the impulse response of the baseflow when subjected to disturbances in different regions, the spatiotemporal evolution mechanism is analyzed to reflect the local and global instability properties, which indicates the instability of the local velocity profile and of the entire flow field, respectively.[53] The growth of localized disturbances spreading in both upstream and downstream directions will result in absolute instability. By contrast, locally convective instability occurs as the disturbances develop only in the downstream direction from the source.[54] Furthermore, Monkewitz *et al.*[55] assumed that the mean flow is weakly non-parallel or nearly plane-parallel, i.e., varies slowly in the streamwise direction. Then the complete solutions are obtained through the study of the temporal evolution of global modes. Specifically, the recent development of high-performance computers and computational methods offers an opportunity for extending the classical linear stability analysis into the global instability analysis. Instead of solving the ordinary-differential O-S and Squire equations, the system of partial differential equations is considered to analyze the global instability problem in a three-dimensional domain with two inhomogeneous and one homogeneous

TABLE I. Selected studies on the stability in plane squeeze flow.

References	Methods	Instability mechanism	Remark
Stuart *et al.*[16]	LSA/WKJB	*Re*	Damping rate of transition for the dilatation case is larger than that for the squeezing case.
Hamza[15]	LSA	Injection/suction	Velocity profiles are decreased or increased due to the effect of suction and injection.
Aristov and Gitman[18]	LSA/Kelvin mode	Dilatation/squeezing	Different types of stability depend on whether the disks move toward or away from each other.
Zhu *et al.*[19]	LSA/LDGM	Wall boundaries	Velocity shear is diffused by viscosity and tends to destabilize the flows.
Moss *et al.*[24]	XP/LSA	Visous/spatial/temporal inertia effects	A primary pressure spike is mainly caused by the temporal inertia effects.
Krassnokutski *et al.*[25]	XP/LSA	A constant energy impact	Small values of initial film thickness lead to the uncertainty of pressure spike between the initial and final stages.
Petrov and Kharlamova[29]	Asymptotic expansions	The distance between plates changes in time	The counterflow at plates moving apart occurs when the Reynolds number exceeds its critical value.
Qayyum *et al.*[34]	OHAM/RK4	Slip boundaries	Reynolds number has opposite effects on the normal velocity in case of slip and no-slip boundaries.
Lang *et al.*[38]	Boundary layer integral method/CFD	Viscous effects/local acceleration	The pressure drop in the radial direction is balanced by the viscous force and the local acceleration of the fluid.
Zhao *et al.*[45]	Lubrication approximation	Electroviscous effects	Electroviscous effects modifies the velocity profiles to be much sharper.
Prakash *et al.*[42]	Similarity transformations	Squeeze form/electroosmosis effects/zeta potential	Axial acceleration is affected by the squeeze form and also enhances with increasing electroosmosis parameter and zeta potential parameter.

directions (BiGlobal) or three inhomogeneous spatial directions (TriGlobal).[56–58]

Due to the strongly nonlinear characteristics, linear stability analysis does not predict the observed bifurcations in PCF or PCPF. The energy methods are based on a variational approach and yield global asymptotic stability for Reynolds numbers below some value at the order of 10^2.[59] According to Squire's transformation, an unstable 3D mode disturbance can be converted into a more unstable 2D mode disturbance at a lower Reynolds number. Then, the optimal perturbations using variational methods make construction of tight bounds on perturbation growth rate possible.[60] However, even though all eigenvalues may be stable, the non-normal O-S operator may cause the initial disturbances to grow at a greater rate than any single normal mode.[61] Based on energy methods, Hooper and Grimshaw[62] found the relationship between the maximum growth and the growth caused by the adjoint of the leading eigenmode for both PPF and PCF. It has been verified that the operators from the linear modal analysis in shear flows are exponentially far from normal, which indicates that the flow nonnormality increases with the shear rate. Consequently, the complex interplay between transient growth and nonlinear processes may result in the transition to turbulence.[63] In general, the linearized Navier–Stokes operators applied to most wall-bounded shear flows are non-normal, and the corresponding eigenmodes are non-orthogonal.[48] Nonmodal stability can be determined by analyzing the response of the linearized Navier–Stokes equations to general (deterministic or random) input variables, whether they be in the form of initial conditions, external disturbance environment, internal uncertainties, or geometric constraints.[64]

Until now, there are some discrepancies between the linear/nonlinear analysis and the experiments, i.e., the Couette–Sommerfeld paradox. For example, different from the Reynolds numbers between 300 and 450 of PCF obtained in the experiments, Kaiser *et al.*[65] found Reynolds numbers below $Re_\varepsilon = 44.3$ for PCF by presenting a generalized energy functional ε, which can be applied to a couple of hydrodynamic stability problems. Meanwhile, Kaiser and Mulone[66] proved conditional nonlinear stability for arbitrary plane-parallel shear flow in the case of $Re_\varepsilon > 44.3$. As a consequence, Re_ε turns out to be Re_E^x, which is the ordinary energy stability limit for perturbations that do not vary in the spanwise direction. Because of the complexity of the transition from laminar flows to instability, it is difficult to accurately obtain the solution to such a paradox. This is partly due to the fact that quasi-steady states in arbitrary small neighborhoods of the linear shear can be linearly unstable.[67,68] Small-amplitude and high spatial frequency sinusoidal perturbations may cause the shear flow to become more oscillatory. Then an attempt is made to find the initial conditions on the laminar-turbulent boundary closest to the laminar states, from which the route that leads directly to the statistically steady turbulent state can be optimized using non-equilibrium.[69] In order to determine the minimal seeds that triggers transition to turbulence in shear flows, Pringle *et al.*[70] constructed a variational problem that identifies turbulent velocity fields by taking significantly enhanced values compared to those for laminar fields. They utilized the ratio of the final to initial perturbation kinetic energies (energy growth) as the function, which proved that the converged optimal below the threshold smoothly converges to the minimal seed at the threshold. In the same year, Rabin *et al.*[71] found the critical energy for transition by using the energy gain at a fixed target time as the optimizing function, with the same associated minimal seed emerging. Interestingly, it has been verified that optimal disturbances obtained for large initial energies and target times induce bursting events, whereas for lower values of these parameters, the flow is directly attracted toward the turbulent state.[72] Furthermore, it was discovered that bursting events correspond to optimal energy flow structures embedded in the fully turbulent flow. Optimal structures inducing energy peaks at short times are initially composed of highly oscillating vortices and streaks near the wall.[73] From the framework of a finite-dimensional set of ordinary differential equations (ODEs) to a spatially extended system described by a set of partial differential equations (PDEs), Kerswell *et al.*[74] used a simple optimization technique for identifying the most efficient way to disturb the flow system, thereby bridging the gap between (linear) optimal perturbation theory and (nonlinear) dynamic system approach. This provides a useful tool for quantifying the nonlinear stability of a flow state, which opens up the possibility of subsequently manipulating or designing a better system.[75]

It is worth emphasizing that, the critical values obtained from linear instability are larger than those from nonlinear stability, and the critical values obtained through experiments are between these two. Falsaperla *et al.*[76] recently published their work on the energy-stability conditions under which PCF or PPF are stable against tilted perturbations. Based on the measured perturbation growth, the results showed that the critical Reynolds numbers are in good agreement both with the experiments of Prigent *et al.*[77] and the numerical simulation of Barkley *et al.*[78] For a fixed inclination angle and any wavelength, the Orr–Reynolds critical values $Re_{\text{orr}} = 44.3/\sin\theta$ for PCF, and $Re_{\text{orr}} = 87.6/\sin\theta$ for PPF (θ is the angle between the spanwise direction and the wavevector of the perturbations). Moreover, the nonlinear stability of plane Couette and Poiseuille flows was analyzed with the Lyapunov second method by using the classical L_2-energy.[79] It has been proven that the streamwise perturbations are L_2-energy stable for any Reynolds number, which is inconsistent with the results of Joseph *et al.*[80] who used the classic energy norm. In terms of a streamwise perturbation, it is probably due to the significant discrepancies between the growing effect of the classical energy method and the exponentially decaying effect of the classical L_2-energy method. However, it does not agree with the experimental results that most critical perturbations are neither spanwise nor streamwise. For example, the structure of the perturbation aligns with a certain angle to the streamwise direction experimentally.[77] In addition, localized nonlinear traveling wave solutions may emerge at $Re = 367$ with a tilt angle of 45°, which is lower than the non-localized solutions.[81]

Over the past several decades, many efforts have been devoted to reducing the gap between flow stability theory predictions and experimental data. To this end, the Lyapunov methods for improving the stability predictions have been widely used. For example, Goulart *et al.*[82] developed optimization methods based on sum-of-squares decomposition to construct a polynomial Lyapunov function. It can be seen that this function always shows better results than the classical energy methods in determining a lower-bound on the maximum Reynolds number at which a flow is globally stable. Moreover, much research results are heavily dependent on the monotonic decrease in perturbation energy, while the transient growth of energy is not fully considered. Fuentes *et al.*[83] proposed a general method for constructing polynomial Lyapunov functions to show global stability of fluid flows. Consequently, it effectively verified the stability of 2D PCF in a regime where energy grows transiently. In the same year, it is observed by Nagy *et al.*[84] that the predicted critical Reynolds number by using enstrophy as the norm of perturbations, is significantly smaller than that from the direct numerical simulations (DNS), as well as that with the energy method for tilted perturbations. However, the new critical value is much larger than that obtained from the classical theory or the results of Falsaperla *et al.*[79] In addition, the enstrophy change and the kinetic energy change are zero for the long-wave perturbations at the tilting angle 45°, which explains the reason why the tilted waves are critical values in the nonlinear stability analysis.[81]

More importantly, instead of the kinetic energy, the region of the wave-number-Reynolds-number map where the enstrophy of any initial disturbance cannot grow, can be found by using the vorticity norm. Then a critical Reynolds number for spanwise perturbations $Re_{\text{crit}} = 155$ was predicted by Fraternale *et al.*[85] Based on the viscous Arnolds's identity that are closely related to the perturbation's enstrophy identity, Lee *et al.*[86] established a novel weighted perturbation's enstrophy identity including general streamwise translation-invariant shear flows. This may be the reason why the stability of the disturbance can be determined. In fact, it reflects a subtle interaction between a critical layer and its adjacent boundary layer. Another important fact to mention is that the solution of the Navier–Stokes equation may be not regular in the presence of the wall-bounded conditions except when the compatibility condition is fulfilled. So, Nagy *et al.*[87] added the conditions to the original problem as non-linear constraints in the cases of PCF and PPF flow. As can be seen, adding the constraint significantly increases the critical Reynolds number in the case of a streamwise perturbation, but only slightly in the case of a spanwise

one. The application of physically reasonable constraints may reduce the gap between theory and experiments.

C. Rotating-disk flow

As introduced earlier, the open operating condition of HVD corresponds to the flow between a stationary and a rotating disk (rotor-stator configuration), while the soft-start and speed-regulating modes of HVD are associated with the flow between differentially rotating disks. Since the rotation of a flow system dramatically affects the stability characteristics of flows in many other practical situations, e.g., the cross-flow vortices that develop near the leading edge of a swept wing,[88] turbomachinery, rotating compressors, computer storage devices, and so on, a great number of theoretical and experimental research have dealt with the viscous flow that is confined between two rotating disks, or swirling flows, which has become a model for the study of instability and transition in three-dimensional flow.[89]

In the general context of rotating-disk flow, there are three different cases of stationary fluid above a rotating disk (von Kármán flow), rotating fluid above a stationary disk (Bödewadt flow) and both the disk and the fluid rotate at approximately equal rates (Ekman flow). These three scenarios are commonly referred to as the Bödewadt-Ekman-von Kármán family of flows.[90] Von Kármán was the first author to describe the flow and identify the boundary layer developing near a single rotating disk, whose thickness depends on the rotation velocity and the fluid kinematic viscosity.[91] As shown in Fig. 4, the fluid near the surface is pulled into azimuthal circulation by viscous stresses and, without a radial pressure gradient to balance the centrifugal forces, is thrown radially outward to be replaced by an axial downward flow; the radial velocity component exhibits a profile typical of wall jets being zero both on the wall and outside of the boundary layer and demonstrating a maximum (increasing with increasing radius r) in the vicinity of the wall. Thus, an inflection point in the radial flow component can be observed from the three-dimensional velocity distribution in the boundary layer, which represents the cross-flow component.[92]

1. Instability mechanisms

The flow between rotating disks can be represented by self-similar functions, which are exact solutions to the complete Navier–Stokes equations for steady laminar flow.[91] Both the shape of laminar velocity profiles and the boundary-layer thickness are independent of the radius. There is a wide variety of instability patterns resulting from these exact self-similar solutions about the flow, which have been found to be unstable with respect to infinitesimal unsteady disturbances.[93] In general, two types of local convective instabilities arise for different Rossby numbers, ranging from $Ro = -1$ (von Kármán flow[94]) $Ro = 0$ (Ekman flow), to $Ro = 1$ (Bödewadt flow).[89,95,96] The Type I instability, i.e., crossflow instability, is caused by the inflection point that appears in the radial mean velocity profile of the boundary layer, which is similar to the T-S instability of the flat-plate boundary layer.[97] This profile leads to a convectively unstable flow regime, which is shown in the form of co-rotating crossflow vortices. Based on the same crossflow instability, Type II instability is related to the combined effects of Coriolis and viscous forces, which occurs at a lower Reynolds number than Type I instability.[98,99] A sixth-order system of linear stability equations in which the effects of viscosity, Coriolis acceleration, and streamline curvature are included.[100] Both type I and II instabilities are unstable to stationary disturbances and also to disturbances traveling relative to the disk surface, but with different critical Reynolds numbers and over different parameter spaces.

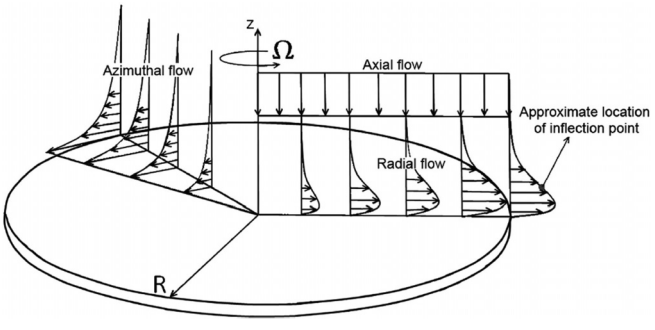

FIG. 4. The three velocity components of rotating-disk flow.

It should be mentioned that, both type I and II instabilities will appear as traveling vortices rolling up around a circular or spiral axis when there is vorticity in the disturbances.[101] In other words, the spatial structure consists of traveling vortices in the boundary layers that expand in rings or spirals along the azimuthal direction.[92] As the disturbances convect radially outward, the convectively unstable flow may become absolutely unstable at a critical radius, which causes the onset of transition to turbulent flow.[102] It is a very important theoretical study on absolute instability that comes neither from the Coriolis effects nor from streamline curvature effects. As the first example of a distinct instability characteristic, it provides a fixed Reynolds number that corresponds to the onset of nonlinearity and the subsequent transition process. Following this, the absolute instability above the critical Reynolds number was experimentally confirmed by introducing a traveling wavepacket into the boundary layer.[103] In this situation, the propagation velocity of the trailing edge decreases dramatically as the radius increases, until the wave packet reaches zero when the Reynolds number of 510 for the absolute instability is attained. It is important to emphasize that, absolute instability is a local concept in that it is theoretically defined by a stability analysis of the local velocity profiles. However, the instability analysis ignores the spatial development of the mean flow, which is equivalent to the parallel-flow approximation made for growing boundary layers, such as the Blasius boundary-layer flow.[104]

As the local Ro varies with the radius, the global stability properties of the boundary layers will be affected, which may reflect a certain amount of inconsistency between the non-parallel stabilizing effects and the destabilizing non-linear effects.[104,105] For a fixed rotation rate, the linear radial variation in Reynolds number leads to spatial inhomogeneity, which is often called the non-parallel effect, despite the similarity solution for the rotating-disk flow being physically parallel. The global response of locally absolutely unstable flow that is affected by the non-parallel effect, is investigated by Davies and Carpenter.[104] Based on DNS of the complete linearized Navier–Stokes equations, it is found that the rotating-disk boundary-layer flow is linearly globally stable. The conclusion is also confirmed by Davies *et al.*[106] because of the "detuning" effect arising from the radial variation of the temporal absolute frequency, i.e., a consequence of the non-parallel effects.

However, Healey[107] discovered that linear global instability can be induced by local absolute instability at the edge of the disk, provided the absolutely unstable region is sufficiently larger prior to the edge. As compared to the solutions of the Ginzburg–Landau equation, the experimental relationship between the onset of transition and the Reynolds number at the edge of the disk cannot be found by Imayama *et al.*[108] Following these contradictory results, Pier[109] found in his experiments that the flow over the edge of the disk acts as a strong source of fluctuations. The nonlinear results of Healey[107] and Imayama *et al.*[108] could align if the downstream boundary was modeled as a source of random noise rather than by a vanishing fluctuating amplitude.

In addition, the global self-sustained behavior of the rotating-disk flow can only be explained by resorting to the nonlinear framework.[104,109] In this situation, an absolutely unstable mode can easily lead to the occurrence of nonlinear global instability in connection to the nonlinear assumption that is made by Pier *et al.*,[111] Bassom *et al.*,[112] Pier and Huerre[113] and van Saarloos.[114] Pier[110] showed that the primary saturated waves initiated at the critical radius, are already absolutely unstable with respect to secondary perturbations. It revealed the secondary absolute instability properties of the naturally selected primary nonlinear crossflow vortices. Considering the primary absolute instability, Viaud *et al.*[115] performed a spectral DNS for the nonlinear stability properties of the rotating-disk flow. It was discovered that only large-amplitude initial perturbations will trigger the nonlinear global mode, which is made up of a front located at the upstream boundary of the absolutely unstable domain, followed by a saturated spiral mode, i.e., elephant mode. Furthermore, Viaud *et al.*[116] found a second front in the lee of the primary saturated waves, where small-scale instability develops by extending the flow both in the radial and azimuthal direction. Rapid turbulent breakdown at $Re = 565–590$ is correspond to the results from Imayama *et al.*,[117] who suggested that the nonlinear interaction of the traveling disturbances and the stationary vortices leads to a rapid transition to turbulence. On the other hand, previous studies have shown that the absolutely unstable mechanism was not sufficient to generate global instability.[104,118] To explain the transition process, Thomas and Davies[119] revealed that disturbances become globally linearly unstable for sufficiently large azimuthal mode numbers significantly greater than those associated with the onset of absolute instability. Subsequently, the regions of local-global linear stabilities in the (Re, n) space are described in Fig. 5, where Re is the Reynolds number, n is the azimuthal mode number, and n_a is the azimuthal mode number for the onset of absolute instability.[122]

More recently, Appelquist *et al.*[120] performed linear DNS of rotating-disk flow that is perturbed by an impulsive disturbance, which showed that there is a linear global instability, if the Reynolds number at the radial end is sufficiently larger than the critical Reynolds number for the onset of absolute instability. Based on the same growth of an impulsive disturbance, it was found that the critical Reynolds number for the nonlinear global instability is independent of the disk-edge configurations.[121] As having just been experimentally indicated by Imayama *et al.*,[108] the onset of nonlinearity is found to emerge at $Re = 510–520$. Both stationary disturbances and traveling disturbances in the transitional regime were identified by Imayama *et al.*[117] The former is excited by unavoidable surface roughness, which may modify the flow in such a way that transition occurs at a smaller radius.[121] Then the primary instability was found to be convectively unstable,

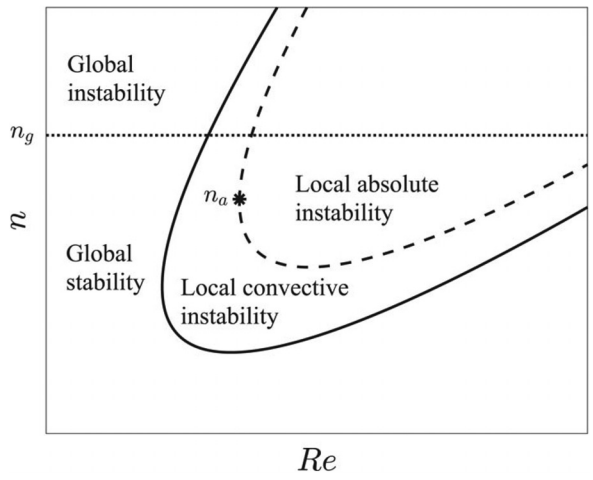

FIG. 5. Diagram illustrating the local and global linear stabilities of the rotating disk boundary layer. Reproduced from Thomas *et al.*, Phys. Fluids **32**, 074105 (2020) with the permission of AIP Publishing.[122]

and secondary instabilities were triggered spontaneously while the flow was developing. For sufficiently large azimuthal mode numbers, the transition to turbulence may be dominated by the huge spatial growth associated with local convective instabilities.[119] Similar behavior can also be found in the numerical results regarding the effects of small-scale surface roughness[122] and the receptivity characteristics relating closely to roughness distributions.[123]

For quick reference, Table II summarizes some representative instability analyses for the rotating-disk flow.

2. Open mode

When the flow is confined between a rotating (rotor) and a stationary disk (stator), i.e., the open mode, a system of ordinary differential equations is obtained from the reduction of the Navier–Stokes equations. As for the stability analysis of stationary and traveling disturbance waves, following the same instability mechanism as the Ekman layer,[95] there are two types of rotating-disk flow instability that is related to two separated layers: Ekman type on the rotating disk and Bödewadt type on the stationary disk.[124] In this situation, different instability patterns are controlled by two parameters: the Reynolds number Re_θ and the aspect ratio G, which are varied over large continuous range.[125] Thus, four flow regimes, including two separated boundary layers and two merged boundary layers, were first proposed by Daily and Nece[126] based on the combination of Re and G. For the merged boundary layers, it is closely related to a pure shear flow joined boundary layers, i.e., the torsional Couette flow, in which a quasi-linear profile of the azimuthal component of the flow velocity develops.[127] There are finite-size localized turbulent structures that characterize the subcritical transitions in the form of spots or solitary waves.[128] As shown in Fig. 6, the onset of transition is characterized by a regular pattern of spiral vortices, which can be observed when the rotating-disk velocity exceeds the critical value.[127] Both spiral waves and turbulent spirals can be sustained by wall compliance.[129]

In the case of separated boundary layers, the transition to turbulence is preceded by two types of waves: circular waves and spiral

TABLE II. Selected studies on the stability for the rotating-disk flow.

References	Methods	Instability mechanism	Remark
Lingwood[102]	LSA	Absolute instability	It is not caused by Coriolis effects nor by streamline curvature effects.
Lingwood[89]	LSA	Absolute instability	Absolute instability is caused by a pinch point between a spatially growing and a spatially damped branch of the dispersion relation.
Davies and Carpenter[104]	Linearized DNS	Convective behavior	Absolute instability may not give rise to the global instability mode.
Pier[110]	LSA	Secondary absolute instability	Primary absolute instability is essential for the transition location.
Viaud *et al.*[115]	DNS	Large-amplitude initial perturbations	Non-parallel effects counteract the absolute instability and restabilize the flow.
Healey[107]	Linearized complex Ginzburg–Landau equations with weakly spatially varying coefficients	Local absolute instability on a finite rotating disk	The Reynolds number at the edge of disk is the only global parameter.
Viaud *et al.*[116]	DNS	Large-amplitude impulsive perturbations	A second front appears in the lee of the primary bifurcation.
Pier[109]	XP	Locally absolute instability in the vicinity of the edge	The flow over the edge of the disk acts as a strong source of fluctuations.
Imayama *et al.*[108]	XP	Local absolute instability	The finite nature of the disk lead to linear global instability (supercritical) and then to a nonlinear steep-fronted global mode.
Imayama *et al.*[117]	XP	Traveling disturbances	A primary nonlinear steep-fronted global mode interacts with the stationary vortices, which leads to a secondary instability.
Appelquist *et al.*[118]	Linearized DNS	An impulsive disturbance within a linear global framework	Reynolds number at the radial end of the simulated linear region by linear global instability is sufficiently larger than the critical Reynolds number for the onset of absolute instability.
Appelquist *et al.*[120]	Nonlinear DNS	An impulsive disturbance	Nonlinear global instability depends on the outer turbulent region generating a linear inward-traveling mode.
Thomas and Davies[119]	Linearized complex Ginzburg–Landau equations and the radially homogeneous base flow	An impulsive disturbance for larger azimuthal mode numbers	Convective instability with large spatial growth may dominate the transition to turbulence.
Appelquist *et al.*[121]	Nonlinear DNS	Convective instability for primary modes/Global instability for secondary modes	High-amplitude roughness are more likely to give a turbulent flow as compared to low-amplitude roughness.
Thomas *et al.*[122]	LSA	Roughness patterns	Both concentric and radial roughness can be used for delaying the onset of local absolute instability.
Thomas and Davies[123]	Adjoint linearized NS equations/Monte-Carlo	Randomly generated surface roughness	Receptivity increases for roughness distributions near the conditions for neutral linear instability.

waves, due to the development of instabilities in the boundary layer of the stationary disk. The circular waves propagate in the flow direction, which can be recognized as a Type II instability.[130,131] It seems that the instability leading to circular rolls has the general properties of a shear instability in the radial velocity profile.[130] As the rotation rate increases, spiral waves develop at the periphery and co-exist with the previous circular waves.[125] As a type I instability, supercritical transition to turbulence occurs within the stationary disk boundary layer despite the confinement by viscous effects, which is caused by the mixing of spiral and circular rolls.[96] In addition, based on the peripheral

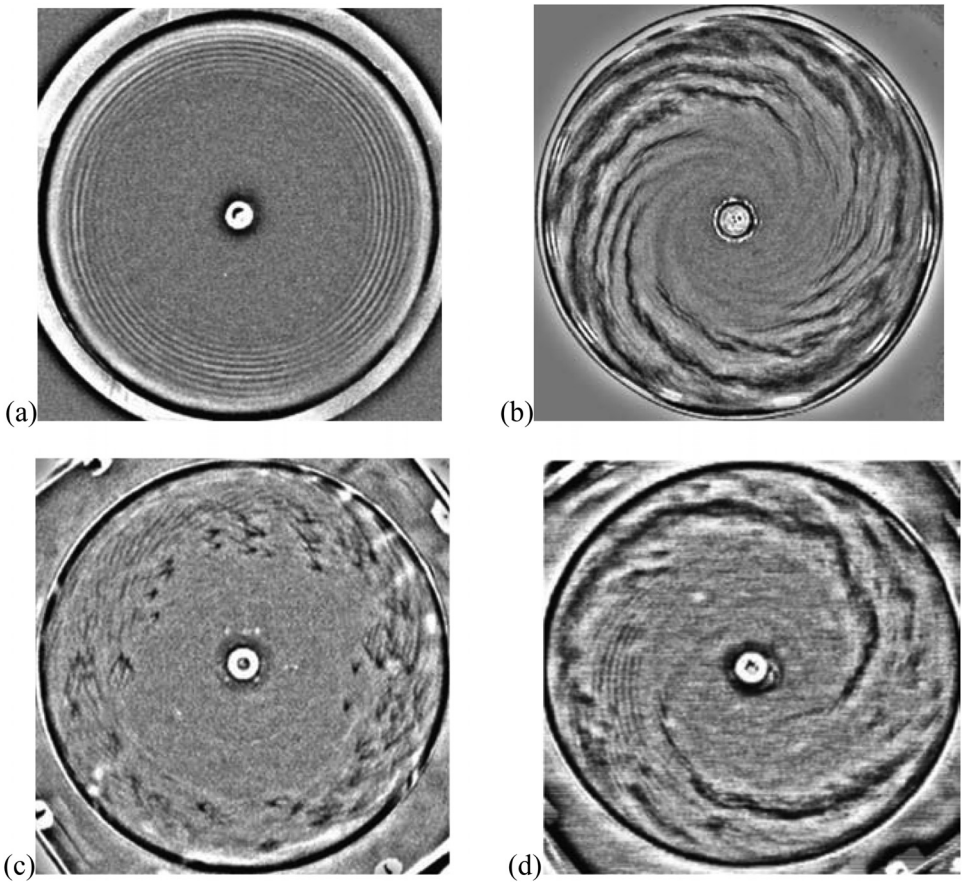

FIG. 6. Instability patterns observed in torsional Couette flows: (a) spiral waves SRIII; (b) turbulent spirals; (c) turbulent spots; and (d) mixed states. Reproduced with permission from Cros *et al.*, J. Fluid Mech. **481**, 177 (2003). Copyright 2003 Cambridge University Press.[129]

velocity of the rotating disk and the gap, the experimental study about two types of instability pattern via stereoscopic PIV (particle image velocity) highlight the existence of an absolute threshold for the Reynolds number.[132,133] It should be noted that the flow direction in these experiments (Fig. 7) is opposite to that of HVD, which may need further investigation.

In order to understand the nature of both circular and spiral rolls, Poncet *et al.*[134] particularly investigated the transition to turbulence in the flow of an annular rotor-stator cavity, as shown in Fig. 8. It is reported that the circular roll instability under permanent conditions can be sustained by noise, as indicated by a combined experimental and numerical study. A permanent perturbation induces the temporal coexistence of spiral and circular rolls, which appear through a supercritical Hopf bifurcation.[130] In other words, the transition to turbulence seems to be governed by the nonlinear interactions between the circular and spiral modes of the stationary disk flow.[101] Using visualization analysis and the Bi-Orthogonal Decomposition (BOD) technique, a torus doubling bifurcation is revealed before its complete destruction during the transition to weak turbulence.[135] With regard to the rotating boundary layer, the mean flow is qualitatively similar to the von Kármán self-similarity solution.[136] However, because of the shear and centrifugal effects, a locally unstable mean flow may act as a strong source of perturbations, which eventually leads to incipient turbulence. More specifically, the critical Reynolds number for the convective/absolute transition was found to be smaller than that for the equivalent von Kármán solution at the same Rossby number.[137] Due to the fluctuations in the form of a steep front followed by a saturated spiral wave, the superposition of various absolutely unstable modes with different azimuthal wavenumbers leads to convectively unstable rolls traveling outwards in the direction of the mean radial flow.[138] It can be seen that the characteristics of these flows are the coexistence of adjacent and coupled flow regions that are radially different in terms

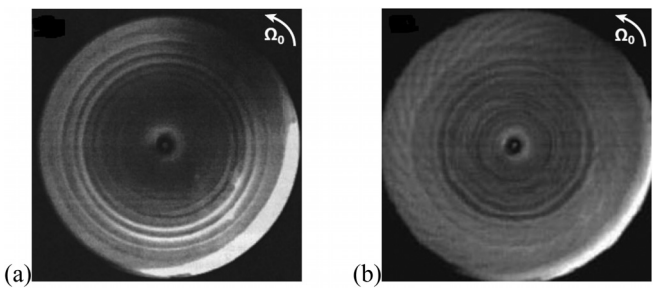

FIG. 7. Experimental visualizations of circular waves (a) alone, and circular waves and spiral arms (b) in the inward boundary layer close to the stationary disk. Reproduced with permission from Gauthier *et al.*, J. Fluid Mech. **386**, 105 (1999). Copyright 1999 Cambridge University Press.[130]

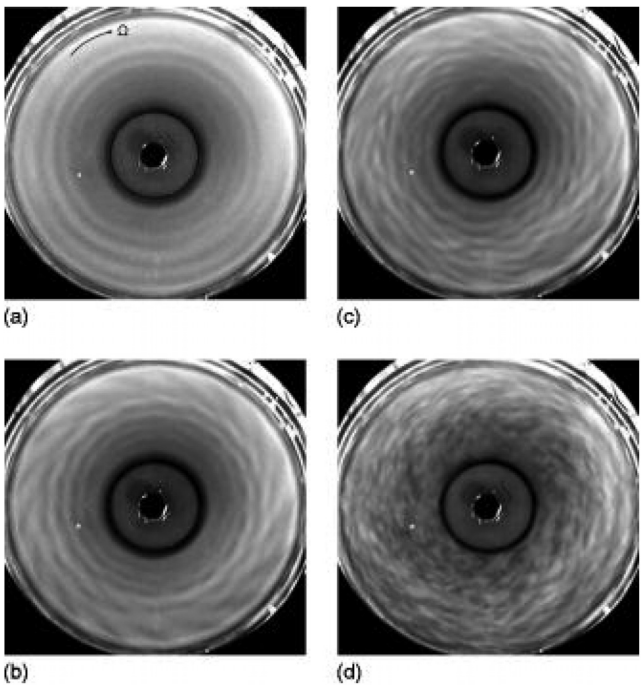

FIG. 8. Experimental flow visualizations for instability ($G = 0.114$). (a) Circular roll for $Re = 16\,400$. (b) Circular and spiral rolls for $Re = 26\,400$. (c) Circular and spiral rolls for $Re = 32\,500$. (d) Wave turbulence for $Re = 61\,600$. Reproduced from Poncet *et al.*, Phys. Fluids **21**, 064106 (2009) with the permission of AIP Publishing.[134]

of the flow properties and the thickness scales of the Ekman and Bödewadt boundary layers. According to the combination (G, Re), the flow structures mentioned above can be observed as mapped by Schouveiler *et al.*,[125] as shown in Fig. 9.

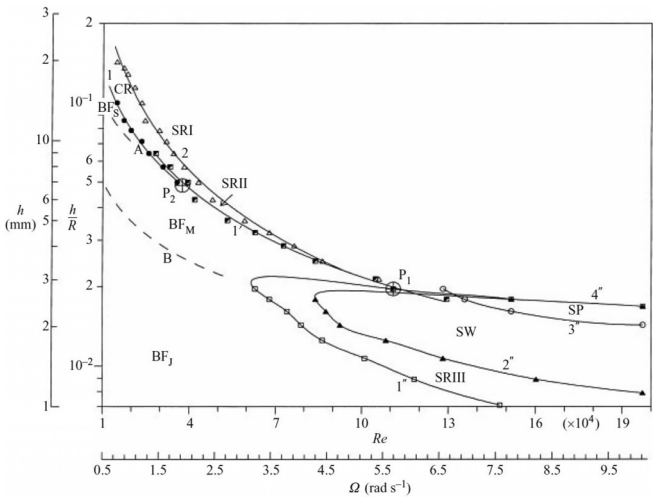

FIG. 9. Transition diagram. Reproduced with permission from Schouveiler *et al.*, J. Fluid Mech. **443**, 329 (2001). Copyright 2001 Cambridge University Press.[125]

3. Speed-regulating/soft-start/soft-brake mode

When two parallel disks are in relative motion, i.e., speed-regulating or soft-start mode, co-rotating and weak counter-rotating flows may affect the properties of boundary layer instabilities. Two Reynolds numbers based on the film thickness h: $Re_i = \Omega_i h^2/\upsilon(\Omega_i$ ($i = b, t$ for bottom and top disk) is the angular velocities), the rotation ratio $s = \Omega_b/\Omega_t$ ($|s| \leq 1$) and the aspect ratio G, are used for characterizing the flow. Then it is noted that $s > 0$ for the co-rotation case and $s < 0$ for the counter-rotation case, $s = 0$ corresponding to the rotor/stator case.[93] Two kinds of frequently encountered fluid flow with high rotation rate, Ekman-Poiseuille flow and Ekman-Couette flow, becomse first unstable to type II Ekman boundary layer instability, which is caused by the combined effects of Coriolis and viscous forces.[139] There is a continuum of codimension two points where both type I mode and type II mode become simultaneously unstable and where nonlinear interactions may occur. Also, the S-mode found by Hoffmann and Busse[139] correlates closely with the inflection point at the midplane corresponding to the extra mode of Hoffmann *et al.*[140]

In the case of co-rotating or weak counter-rotation flow, the basic flow is found to be of Batchelor type flow above a given radius[141] and of torsional Couette type flow below.[127] The flow is constituted by two boundary layers, but the core will be separated into two parts rotating in opposite directions, separated by a transition layer.[142] Two different kinds of instabilities lead to axisymmetric propagating vortices and positive spirals,[93] which have been investigated in the rotor-stator configuration by Schouveiler *et al.*[125] As shown in Fig. 10, different flow patterns, including propagating circular vortices, and the mixing of axisymmetric propagating vortices and positive spirals, appear successively on increasing Re_t, and then the flow becomes more and more disordered. It was found that positive spirals occur in the inward boundary layer of the bottom disk, while the boundary layer of the top disk, as well as the core, are found to remain stable. Furthermore, as the rotation ratio increases, the impact of additional global rotation on the instability threshold of the positive spirals is more pronounced when compared to that of the circles.[143]

On the other hand, when the disks rotate in opposite directions, there are both instabilities of boundary layer and free shear layer about counter-rotating flows, which is suitable for the soft-brake condition of HVD. As a consequence, the flow between counter-rotating disks appears to be much richer. Lopez *et al.*[144] observed rotating waves in the form of funnel-like vortices arising from a shear instability in the bulk of the flow. Based on the same free shear layer instability, a new instability pattern, i.e., negative spirals, rolls up from the periphery toward the center in the direction opposite to that of the faster disk.[93] As Re_t increases, the negative spirals, mixing of positive and negative spirals and positive spirals appear successively (Fig. 11). Increasing Re_t further, the structures become disorganized and the flow becomes turbulent. In other words, this instability leading to the propagating circles, can only take place in an axisymmetric region of the flow. The conclusions were experimentally confirmed by Moisy *et al.*[145] that vertical vortices are surrounded by these negative spirals. From the measurement results on the azimuthal wavenumber and phase velocity, it is found that the propagating negative spirals is controlled by the Reynolds number.[145] The internal shear layer that separates two regions of opposite azimuthal velocities is prone to azimuthal symmetry breaking, which can be described in terms of a classical Kelvin–Helmholtz instability. Such destabilization of the azimuthal shear layer

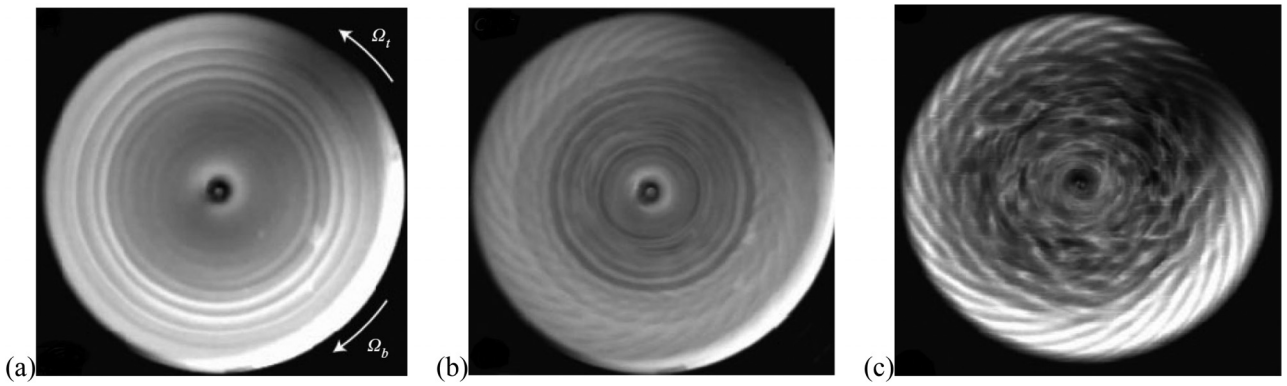

FIG. 10. Experimental flow visualizations for instability ($s \geq 0$): (a) propagating circular vortices. (b) Mixing of axisymmetric propagating vortices and positive spirals. (c) Disordered flow. Reproduced with permission from Gauthier *et al.*, J. Fluid Mech. **473**, 1–21 (2002). Copyright 2002 Cambridge University Press.[93]

always exhibits traveling waves, modulated traveling waves and chaos before the emergence of a turbulent spectrum.[146]

When the Reynolds number is increased, the axisymmetric region becomes unstable and gives rise to multiple complex dynamic behaviors: a single vortex associated with an azimuthal wavenumber of 1 instability; traveling waves; near-heteroclinic cycles; and a co-rotating vortex pair associated with an azimuthal wavenumber of 2 instability.[147–149] Furthermore, Nore *et al.*[150] found that the thresholds for axisymmetric instabilities are always higher than those of non-axisymmetric modes, thereby indicating the dominating role of the latter modes. Their findings also illuminate the feasibility of improving the stability of von Kármán swirling flow by actively controlling the height-to-radius aspect ratio.[151] More importantly, increasing the Reynolds number make the unstable flow to exhibit a two cat's eyes pattern. This is associated with vortices in 3D steady flows with characteristic azimuthal modes.[152] Another fact is that the time-dependent behavior at high Reynolds number is concerned with the pulsation of the two vortices found in the steady regime.[153]

In the presence of a stationary sidewall, it may substantially reduce the effectiveness of the counter-rotating endwalls in driving a torsional flow. For example, impellers are used for counteracting the sidewall effects in Giesecke *et al.*[154] Instead of having a stationary sidewall, Gutierrez-Castillo and Lopez[155,156] split the sidewall into two halves (top and bottom), with each half rotating with the corresponding end wall, as shown in Fig. 12. Obviously, the $O(2)$ symmetric basic state is dominated by the shear layer at the midplane separating the two counter-rotating bodies of fluid. Due to the mode competition between different non-axisymmetric steady states, primary circle-pitchfork bifurcations lead to different time-dependent state, including rotating waves, direction-reversing waves, and a variety of pulse waves dominating the unsteady flow regimes.[157] Particularly, for a codimension-2 point in the *Re-G* space, pulse waves occur because of the interaction between two steady states with the azimuthal wavenumbers $m = 1$ and $m = 2$.[158] Furthermore, the split at midheight provides a localized perturbation from the corners where the endwalls and the sidewall meet. The ensuing inertial wave beams produce intricate patterns that are very sensitive to the modulation frequency.[159,160]

III. INFLUENCE FACTORS FROM FLUID–SOLID INTERACTION SYSTEM

A. Wall conditions

1. Surface microstructure

Because of the requirements of load-bearing capacity and stabilization, thin films flow over micro-textured surfaces have drawn considerable attention over the years. Due to the small scale of these

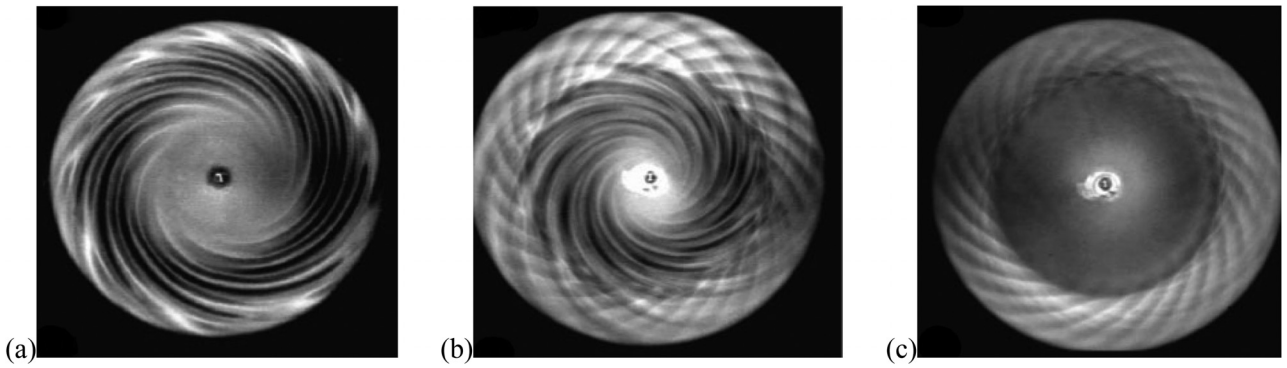

FIG. 11. Experimental flow visualizations for instability ($s < 0$): (a) negative spirals. (b) Mixing of positive and negative spirals. (c) Positive spirals. Reproduced with permission from Gauthier *et al.*, J. Fluid Mech. **473**, 1–21 (2002). Copyright 2002 Cambridge University Press.[93]

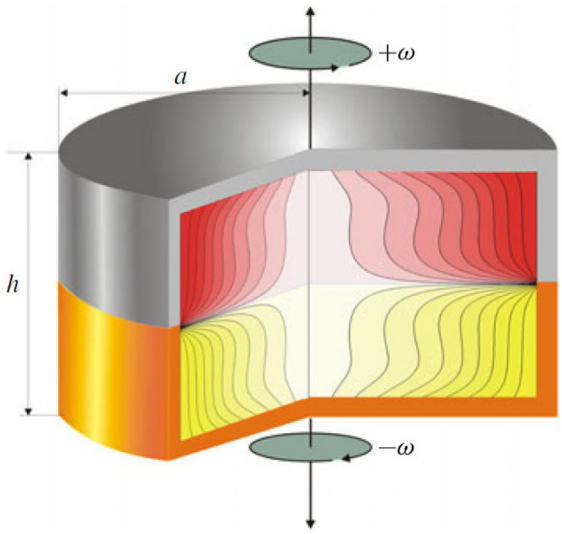

FIG. 12. Schematic of the counter-rotating split-cylinder flow system. Reproduced with permission from Gutierrez-Castillo and Lopez, J. Fluid Mech. **816**, 719 (2017). Copyright 2017 Cambridge University Press.[159]

well-designed features, surface microtextures are generally associated with the fluid dynamics of the oil film between sliding surfaces, which have an influence on the tribological performance of lubricated contacts. When the oil film surpasses the cavities of the substrates resulting in air encapsulation, it may significantly affect the vibration damping effect.[161,162] With the development of efficient algorithms and solution techniques combined with the increase in computational power, most of the research in the field of surface microtexturing has been based on theoretical modeling, which use different forms of Navier–Stokes equations with sophisticated models about viscosity, density and temperature. Examples of such models can be found in Papadopoulos *et al.*,[163] Gherca *et al.*,[164] Marian *et al.*[165] for thrust bearings, Etsion *et al.*,[166] Feldman *et al.*,[167] Brunetiere *et al.*,[168] Adjemout *et al.*[169] for mechanical seals, and Zhou *et al.*,[170] Usman *et al.*,[171] Pawlus *et al.*[172] for cylinder liners. On the other hand, relatively small number of publications are based on experimental setups including pin-on-disk/ball-on-disk tests and reciprocating sliding tests. Examples of such tests can be found in Etsion *et al.*,[173] Henry *et al.*,[174] Liu *et al.*[175] for thrust bearings, Yu *et al.*,[176] Qiu *et al.*,[177] Chen *et al.*[178] for mechanical seals, and Borghi *et al.*,[179] Wang *et al.*,[180] Ma *et al.*[181] for cylinder liners.

2. Topography substrate

For the capillary ridge effect of the non-flat surface, the substrates generally exhibit a topography that leads to the variation of the film thickness. Viscous flow over varying topography substrates is closely related to the delicate interplay between the substrate features, which create interfacial shapes that reflects the topography, and surface tension which tends to flatten the surface.[182] It is found that the dynamics of thin films in microchannels are governed by three pertinent parameters corresponding to the feature depth, feature width, and the capillary scale. In view of the parametric research conclusions, Kalliadasis and Homsy[183] considered the stability of thin-film flows with respect to small disturbances. The flow in the streamwise direction driven by a body force is the only term that represents energy production, which reflects the rearrangement of fluid in the flow direction. Based on the coupling mechanism of perturbation with the base flow, the topography-driven ridge is expected to be linearly stable to transverse perturbations for a wide range of parameters.[184] This can be confirmed by Davis *et al.*,[185] who performed a transient nonmodal analysis because of nonlinear perturbations effects. They found that unstable ridge on a smooth, flat and homogeneous surface is more prone to experience flow instability when compared to closed, recirculating streamlines beneath the capillary ridge.

It should be mentioned that, as an important derivation of thin-film equations, the lubrication-based models for these pronounced capillary ridge effects were used to investigate the flow conditions above, which were observed experimentally by Decré and Baret[186] and were captured by Mazouchi and Homsy.[187] The lubrication approximation is based on the asymptotic reduction of the governing equations and boundary conditions to a simplified system. It often consists of a single nonlinear partial differential equation formulated in terms of the local thickness of the film.[188] However, since the solution of the equations governing the flow must include the precise location of the interface, the presence of the deformable interface that bounds the film makes the direct modeling of interfacial flows more complicated. Moreover, one has to track the interfacial position while simultaneously solving an evolution governing equation coupled to temperature, electric, or other fields.[189] Considering the problem, by extending the boundary-integral calculation work of Mazouchi and Homsy,[187] Gaskell *et al.*[190] studied the thin film flow over two- and three-dimensional topographies by means of multigrid finite difference predictions within the framework of the lubrication approximation. It was concluded that an increase in the Reynolds number increases the amplitude of the free-surface disturbances and slightly reduces their wavelength.

Other alternative methods have devoted extensive efforts to solving the increasingly complex system and number of equations. In 2007, they reported a finding that adaptive local mesh refinement and multigriding offer increased flexibility together with a significant reduction in memory requirements. They also put forward an efficient and accurate automatic local grid refinement strategy that effectively restricted the use of fine grids to regions of rapid flow development, e.g., the upstream capillary ridge and the downstream surge region.[191] In order to make it comparable to the adaptive multigrid approach, the authors exploited the finite element method (FEM) to solve a weak form of the governing equations, which offered an attractive alternative to the non-specialist user. It is revealed that occlusions may lead to many of the features inherent in the flow of thin liquid films over fully submerged micro-scale topographic features; namely, the presence of capillary ridges linked to the "bow wave" plus "comet-tail" free-surface disturbances.[192] As has been demonstrated, the disturbances induced by small-scale topography can persist over length scales several orders of magnitude larger than the size of the topographical feature itself.[186] This can be explained by the numerical work of Veremieiev *et al.*[193] in which a depth-averaged form of the Navier–Stokes equations, akin to the integral boundary-layer approximation of Mazouchi and Homsy,[187] was used to model the problem. In their subsequent work, Veremieiev *et al.*[194,195] further enabled inertia effects and surface tension effects to be incorporated within the long-wave approximation. In

addition, they have examined a discrete analog of the full Navier–Stokes equations, including continuity and the boundary conditions for both two- and three-dimensional flows using a finite element formulation. As a result, they successfully predicted the internal flow structure and the corresponding free surface disturbance. Based on the above analysis, it can be observed that the modeling strategy suffers from a lack of accurately predicting the instability threshold correctly.

More recently, Veremieiev and Wacks[196] presented a stability analysis of free-surface gravity-driven liquid film over a periodic corrugated substrate. They successfully extended the standard first- and second-order weighted residual integral boundary-layer method (WIBL), proposed by D'Alessio *et al.*,[197] to include third- and fourth-order terms in the long-wavelength expansion. Due to the trade-off between the accuracy of a full Navier–Stokes computation and the efficiency of an integral method, the model facilitated a valuable insight toward the understanding of the stability mechanism of thin film flows over topography. In particular, it has been shown that the accuracy decreases as the Reynolds number and corrugation amplitude increase, but increases with the steepness parameter and the ratio of wavelength to capillary length. Furthermore, as the most important factor, microstructure's shape and dimension have a great influence on the stability of the overflowing liquid film. To this end, Bonart *et al.*[198] reported their work on the dynamical modeling of two-phase flow through the coupling of the Cahn–Hilliard and Navier–Stokes equations. In this model, the linearization and decoupling of the equations and preconditioned Krylov methods were used to enable efficient and accurate simulations. Results indicated that the stabilizing effect could be the dissipation of energy in the film while flowing over these sharp corners. Likewise, from the perspective of energy balance, the energy integral method (EIM) developed by Usha and Uma[199] for examining the stability and dynamics of a continuous thin film over topography accounts for depth averaged kinetic energy balance, and is based on velocity weighted averaging of the Navier–Stokes equations. Evidently, the merit of this method is that it captures the effects of large Reynolds numbers and moderate surface tension. This eliminates the explicit depth-coordinate dependence from the full Navier–Stokes system of equations. Therefore, a weighted-depth averaged model, based on EIM was established to predict accurately the instability threshold.[200] The analysis paves the way for similar investigations on three-dimensional flows related to film flow over a substrate featuring topographies.

More in-depth investigations about the stability analysis including thermocapillary effects and electric fields effects have been taken into consideration. Davies and Rideal[201] found that a temperature gradient at the free-surface will produce a surface tension gradient or Marangoni stress on account of varying degrees of surface tension with temperature in the gas–liquid interface. This partly explains the occurrence of film deformation and spontaneous rupture of thin films when considering the interfacial instabilities caused by thermocapillary flows in the case of such stresses. When the microstructured wall is heated, the films tend to accumulate at the deepest locations of the wall, which may trigger flow instability compared to films covering flat walls.[202] Furthermore, it was found that the special characteristic of flow over topography is that a high cumulative length of contact lines becomes unstable with respect to transverse perturbations.[203] In this case, different kinds of rivulet instabilities, including the long-wave falling film instability, the capillary instability, and the thermocapillary instability, may lead to the development of wavy flow patterns and to the rupture of the rivulet.[204] In order to prevent such instability, the study by Tiwari and Davis[205] considered the influence of topographical features on the linear stability of liquid films flowing over surfaces with localized heating was considered using a long-wave lubrication analysis. Simple step-down and mound features were found to effectively stabilize the film effectively, as the Marangoni number Mc at the instability threshold increases substantially with the appropriate topography. In this situation, the optimal topographical features that suppress all variations in the free surface were determined. Then it is recommended to use an energy analysis to provide insight into the mechanism. Based on the same energy calculation as Kalliadasis and Homsy,[183] it is observed that the streamwise gradient in the capillary pressure is destabilizing for flow over the locally heated topographical surfaces. In contrast, despite the destabilization of the free surface response to the wall deformations, the amplitude growth remains independent of the evolution of time-dependent perturbations imposed on the free surface, which can be stabilized by cooling from the wall.[206] Alternatively, spatial resonance is more effective than cooling to stabilize the free surface time-dependent perturbations. Different from the above gas–liquid interface stability analysis, Yoo *et al.*[207] systematically investigated the effects of system parameters, including substrate topography, on the temperature and flow fields of two-dimensional steady thermocapillary flows. Because of the temperature gradient along the gas–liquid interface, recirculating flows occur under low Marangoni number and low capillary number. Consequently, horizontal diffusion of heat weakens the overall flow and the convection of heat intensifies it.

The interaction of an externally applied electric field with a thin liquid film can give rise to interesting flow instabilities and pattern formation. This is due to the fact that the electric field affects the flow through an additional Maxwell stress term in the stress balance at the film surface. The general conclusion is that the effect of an electric field is destabilizing.[208] To be specific, an electric field can either reduce or promote irregularities on the film surface, depending on the local geometry. It is capable of eliminating the capillary ridge found at a downward step but leads to the creation of a free-surface ridge at an upward step.[209] Research such as this work focused primarily on the interplay between the Maxwell stress at the free surface and the capillary force present due to surface tension. Of particular interest has been to see how this balance of forces can be exploited to manipulate the film shape, to influence the progress of surface waves, or mitigate instability.[210,211] Furthermore, as trains of periodic waves or solitary waves are generated, the electric field can serve as a local modification to the ambient film pressure at each point on the free surface. Under this condition, the shape of the liquid layer's surface can be manipulated to become wave-free.[212] It can be inferred that the interface deformation depends on various problem parameters. In this sense, the interface deformation mimics the cavity shape in the case of small-amplitude sinusoidal cavities. For trapezoidal cavities and perfect dielectrics, the interface deforms near the cavity edges, rising toward the top electrode. This behavior can be enhanced by the leaky dielectrics due to charge accumulation.[213] Following this mechanism, the effects of imposed flow and electric fields on the nonlinear dynamics of undulating channel walls were investigated.[214] For sinusoidal lower channel walls, nonlinear time-periodic traveling waves are strongly influenced by on the wall amplitude, the flow rate, and the applied electric field measured by the lower wall potential. A type of "walking"

motion emerges that causes the lower fluid to wash through the troughs and create strong vortices over the peaks of the lower boundary. It should be mentioned that electric fields can also modify contact angles. Therefore, in view of the stability of dynamic contact lines, Conroy *et al.*[215] studied the linear stability of gravity-driven spreading of a thin liquid film in the presence of electric and temperature fields. It was found that electric fields in the capillary ridge destabilize the film front to transverse perturbations, which is also responsible for the enhancement of the perturbation growth.

3. Superhydrophobic surfaces

Thin films are related to the wettability and spreading of fluids over superhydrophobic (SHP) nature of surfaces fabricated using nano- or microtechnology.[216] In pressure-driven laminar flows, the use of superhydrophobic surfaces represents a promising technique for delaying the transition to turbulence. In general, liquid wetting on rough surfaces is commonly elucidated by two classical models: Wenzel model[217] and Cassie–Baxter model.[218] In general, these two models dramatically exhibit different slippage effect, from which the Cassie–Baxter state (or partially wetted state) can provide a significant slip effect due to the presence of the inner liquid–gas interface.[219–221] It has been acknowledged that, when a fluid does not completely wet an atomically smooth substrate, i.e., under superhydrophobic conditions, even a small amount of slip on the surfaces is expected to ease the fluid transport appreciably. In particular, the presence and effects of molecular slip can no longer be neglected since the Knudsen number increases beyond the continuum limit ($Kn > 10^{-2}$).[222,223] To quantify the amount of slip, as shown in Fig. 13, Navier's slip boundary condition in which the slip velocity u_0, is proportional to the shear rate experienced by the film at the wall can be defined as:[224]

$$u_0 = \lambda \left| \frac{\partial u}{\partial y} \right|, \tag{2}$$

where λ is the slip length that is proportional to Kn. $\lambda = 0$ corresponds to a no-slip condition, and $\lambda = \infty$ to a fully slipping surface. A number of theoretical, numerical, and experimental studies have shown that the slip length can be structurally determined by the SHP surface features, such as the pitch, solid fraction, and pattern type, and further affected by secondary factors, such as the state of the liquid–gas interface, for laminar flows[222,225–228] and turbulent flows.[229–234]

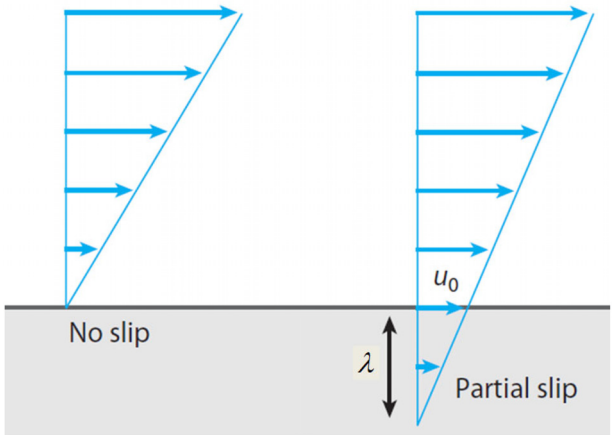

FIG. 13. Schematical diagram of slip at a fluid–solid interface.

The delay in transition, for example, can lead to a substantial reduction in the power required to move the fluid within the microchannel. Then based on the Navier–Stokes linear stability equations with slip boundary conditions, the influence of slip length on flow instability has been widely studied.[235–248] As the slip boundary condition on a smooth wall is a simplified treatment of complex superhydrophobic surfaces, most of the research above is applicable for the analysis of flow stability and the transition to turbulence associated with superhydrophobic surfaces. Min and Kim[249] performed a linear stability analysis with slip boundary conditions and a few direct numerical experiments of transition to turbulence initiated by two-dimensional Tollmien–Schlichting (TS) waves in different configurations. The results showed that velocity slip greatly suppresses linear instability and modestly affects the non-normality,[237] which agrees with that of Gersting,[250] Spille *et al.*,[251] Sahu *et al.*,[239] and Matthews and Hill.[252] In addition, as opposed to spanwise slip, streamwise slip increases the critical Reynolds number with the increase proportional to the slip length in wall-bounded shear flows. It can be inferred that streamwise (longitudinal) slip results in a decrease in frictional resistance, whereas spanwise (transverse) slip leads to an increase in overall frictional resistance. Following this study, Yu *et al.*[253] performed a modal analysis of pressure-driven flows through a channel patterned with superhydrophobic surfaces containing periodic grooves and ribs aligned longitudinally to the flow direction. By performing a BIGlobal linear stability analysis,[58] a stabilizing effect can be predicted for flows over longitudinal superhydrophobic grooves with small values of full-channel height, in agreement with the results obtained using local stability analysis that employs a homogeneous slip conditions along the walls, and also similar results have also been found accounting for anisotropic surfaces,[254,255] symmetric and asymmetric slip surfaces,[256] and spatially homogeneous slippery surfaces.[257,258]

However, the seemingly reasonable conclusion about the flow stability characteristics cannot always be achieved since most of the previous reports have been limited to the direct analysis of two-dimensional perturbations.[244] In fact, if a considerable amount of anisotropy in the slip length is considered within three-dimensional modes, both streamwise and spanwise slip will trigger different types of linear instability and different optimal nonmodal perturbations.[245,246,259] To be specific, the Navier slip boundary conditions at the channel wall for streamwise and spanwise velocities can be expressed as

$$\left(\lambda_{\{x,z\}} \frac{\partial u_{\{x,z\}}}{\partial m} + u_{\{x,z\}} \right) \Big|_{y=\pm 1} = 0, \tag{3}$$

where m is the outward wall-normal direction, and λ_x and λ_z are the streamwise and spanwise slip lengths, respectively. It was found that the critical Reynolds number first slightly decreases and then modestly increases as λ_x increases.[244] This is due to the fact that streamwise slip only enlarges the growth time window of 3D modes, which has no effects on the distribution of the maximal transient growth in the wave number plane. In the presence of equal slip length in the streamwise and spanwise directions, three-dimensional leading instabilities that would occur in pure streamwise with zero spanwise velocity. Furthermore, from the eigenvalue equations characterizing the least stable modes, Xiong and Tao[246] obtained the first-order

approximation $R^{E3D}_{l_x,l_z} \approx [1 + 2.41(l_x - l_z)]R^{E3D}_0$ of the critical Reynolds number for the nonlinear stability. Results showed that in the three-dimensional PPF with the anisotropic slip boundary condition, the critical Reynolds number increases with the increase in λ_x and with the decrease in λ_z. Regarding the case of the isotropic slip boundary condition, the critical Reynolds numbers are found to be $R^{E3D}_l \approx [1 + 8.37l^2]R^{E3D}_0$ for the 3D mode and $R^{E2D}_l \approx [1 + 14.95l^2]R^{E2D}_0$ for the 2D mode. From the results, it appears that developing a superhydrophobic surface with specified directional sensitivity is quite necessary and practical for delaying the early triggering of transition.

As shown in Fig. 14, in order to model more complex superhydrophobic surfaces, a slip tensorial Λ in the plane of the walls (x, z) is used for representing the anisotropic boundary condition,[225,226,254] as follows:

$$\begin{bmatrix} u \\ \omega \end{bmatrix} + \Lambda \frac{\partial}{\partial m} \begin{bmatrix} u \\ w \end{bmatrix} = 0, \tag{4}$$

$$\Lambda = Q \begin{bmatrix} \lambda^{\parallel} & 0 \\ 0 & \lambda^{\perp} \end{bmatrix} Q^T, \quad \text{with } Q = \begin{bmatrix} \cos\theta & -\sin\theta \\ \sin\theta & \cos\theta \end{bmatrix}, \tag{5}$$

where u and w denote the streamwise and spanwise velocity components, respectively. $\lambda^{\parallel}$ and $\lambda^{\perp}$ are the eigenvalues of the slip tensor Λ corresponding to the streamwise $(\theta = 0)$ and spanwise $(\theta = 90°)$ slip lengths, respectively, and θ represents a rotation of the tensor.

Such a tensorial slip boundary condition is then used for modeling the slip effect induced by microgroove-type superhydrophobic surfaces.[259] They showed that a proper tilt angle in the microgrooves along the streamwise direction can significantly reduce the critical Reynolds number for the onset of linear instability, which showed a good qualitative agreement with Pralits *et al.*[254] However, it is also worth noting that the lowest critical Reynolds number can be obtained with two superhydrophobic walls, which is significantly lower than those reported in Pralits *et al.*[254] Increasing the anisotropy in the slip length reduced the critical Reynolds number due to the decrease in the difference in tilt angles between the two walls. These results may be of interest for enhancing mixing or heat transfer in small flow systems where turbulence cannot be triggered.

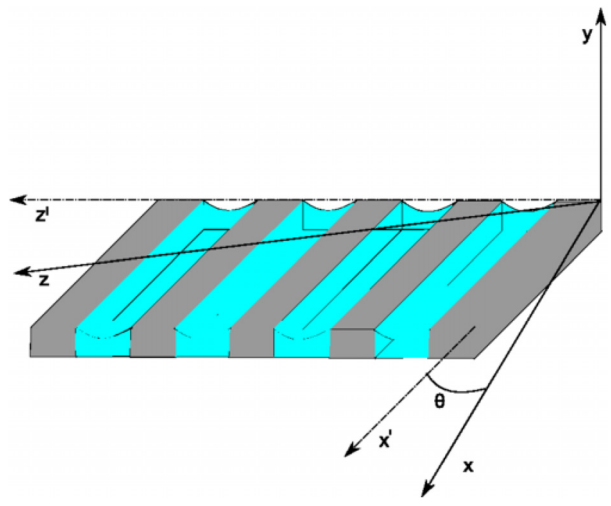

FIG. 14. Sketch of the wall pattern with definition of axes, angle θ, and ridges periodicity. Reproduced with permission from Pralits *et al.*, Phys. Rev. Fluids, **2**(1), 013901 (2017). Copyright 2017 American Physical Society.[254]

4. Porous media of the friction material

Since the grooved friction disk consists of a porous material, the permeability of the friction material may affect the squeeze velocity, which plays a major role in the torque profile. In general, increasing the permeability of a rotating porous disk effectively decreases the required time to arrive at a specific film thickness.[260] The maximum load capacity is sensitive to the anisotropic permeability of the friction material.[261] For such wall-bounded shear flows, the flexible dynamic model including porous walls plays a significant role in the prediction of the transition from laminar to turbulent flow. This is due to the fact that in the presence of porous boundaries, the turbulence can be attenuated and even inhibited by the effects of suction and blowing.[262] Hence, the instability analysis has been extensively used not only in the community of hydrodynamic flow control but also in reducing skin friction drag in wall-bounded shear flows.

When the viscous fluid flows past a porous surface, the effects of viscous shear appear to penetrate into the permeable material in a boundary layer region. For such fluid-porous system, most of the theoretical and numerical studies have been based on so-called the two-domain approach. The governing equations are prescribed on the fluid domain and the porous medium. The main aim is the derivation of appropriate boundary conditions rather than the solution of the transition layer at the fluid–porous interface, which is also quite challenging for unsteady flows.[263] When it comes to the two-domain approach, Beavers and Joseph proposed a velocity slip condition across the fluid–porous interface based on an experimental study of steady flow over a saturated porous medium,[264] which is theoretically justified by Saffman.[265] Subsequently, for the jump in tangential stress boundary conditions, Goyeau *et al.*,[263] Bars *et al.*,[266] and Valdéa-Parada *et al.*[267] deciphered the explicit expression of the jump coefficient that depends on the macroscopic variation of properties at the interface. Recently, using the homogenization approach, Lācis *et al.*[268] derived a tensorial generalized version of the empirical Beavers–Joseph interface condition. On the other hand, for the single-domain approach, a single set of governing equations that is simultaneously valid in both the fluid and porous domains can be derived via volume averaging.[266] Despite its suitability for numerical simulation of unsteady flows, such simulations are particularly scarce except some specific models, e.g., turbulent flow over a permeable wall.[269] Finally, comparisons between the two approaches for the fluid–porous system have been performed in the stability analysis by Hirata *et al.*[270] and Samanta *et al.*[271]

It is usually simply assumed to be governed by Darcy's law, which is the nature statistical result about the empirical equivalent of the Navier–Stokes equation. As far as we know, Chang *et al.*[272] first studied the linear instability of the PPF fluid overlying a porous medium by solving an eigenvalue problem for the O-S equation. The established model includes not only Darcy flow in the porous-layer but also the Beavers–Joseph interface condition,[264] i.e., the two-domain model. Three different modes of instability are found to be triggered by the shear stress of the Poiseuille flow in the fluid layer. Since the highly coupling effects about the viscous term in the Brinkman equation, it has been widely applied in the instability analysis.[241] Based on the

volume-averaging method, Bars *et al.*[266] employed the single-domain Darcy–Brinkman equation to eliminate the discontinuity in the velocity profile between the fluid and porous layers. They focused on studying the interaction between flow and solidification within the mushy layer during binary alloy solidification in a corner flow. There are difference velocity profiles only in the viscous transition zone based on the comparison with Beavers and Joseph.[264] By means of considering a three-layer configuration including a Brinkman porous transition layer, Hill and Straughan[273] found that the key parameters, which affect the bi-modal instability characteristics, are the depth ratio between the porous and fluid layers and the Brinkman transition layer depth. Only two instability modes of a fluid–porous system predicted by the Brinkman model, i.e., the porous mode and the even-fluid-layer mode, are found by Liu *et al.*[274] Wu *et al.*[275] investigated the instability of a coupled fluid–porous system, where the bottom plate was coated with various porous media. Depending on these parameters such as depth ratio, permeability and porosity of the porous medium, instability is dominated either by the fluid or by the porous region.

The effects of PCF on the instability of thermal convection in a fluid–porous system were investigated by Chang *et al.*[276] The neutral curves of both modes, including longitudinal and transverse rolls, may be bimodal which depends on the depth ratio. Furthermore, an increase in the depth ratio leads to a more unstable system, while the increases of Reynolds number and Prandtl number make the system more stable.[277] Based on a variation of the unsteady Darcy–Brinkman model, Antoniadis *et al.*[278] studied the stability of plane-parallel shear flows over a highly porous medium. It is shown that the shear flow is always unstable at all porosities and exhibits similar flow dynamics characteristics with different porous microstructure. As regards to the case of PCPF flow, Chang *et al.*[279] found that Couette flow may destabilize Poiseuille flow at a small depth ratio $\hat{d}$ and induces the tri-modal shape of the neutral curve. With an increase in $\hat{d}$ in the fluid–porous system, the Couette flow enhances flow stability as the magnitude of the moving boundary velocity increases, until eventually pure Couette flow becomes unconditional stable. Furthermore, in order to apprehend the momentum diffusion effect at the interface, the modal and non-modal stability analyses of three-dimensional PCPF flow in a porous medium was investigated by Samanta[280] using the Darcy–Brinkman equations. Consequently, when the Couette flow is considered, the fluid layer and the porous layer exhibit virtually opposite stability trends, respectively. Also, the non-modal stability analysis shows that short time energy growth exists in the parameter space and becomes significant. Following the method of the energy budget, Kirthy *et al.*[281] revealed that negative energy production is located near the plate that has a higher relative velocity in the direction of the bulk flow. There is an additional unstable mode manifested in the neutral curves as a bifurcation of the unstable region into primary and secondary regions. In addition, the energy production due to the Reynolds stress causes disturbances that trigger instability.[282]

In addition, Tilton and Cortelezzi[262] adopted the volume-averaged Navier–Stokes equations to characterize the flow in the porous regions. In the case of two porous walls with identical or differing permeability, it was shown that wall permeability plays a dominating role in determining the O-S spectrum and can dramatically decrease the stability of the channel flow. The same model was solved by Rosti *et al.*,[269] who carried out a number of direct numerical simulations to determine the response of turbulent channel flow to a permeable wall, which is experimentally verified by Suga *et al.*[283] For the stability problem of convection in a porous medium, Chen *et al.*[284] found that the onset of thermal convection may be bi-modal in which whether the instability is dominated by the fluid layer or the porous layer depends on the depth ratio.

5. Surface roughness

Surface roughness plays a substantial effect on the stability characteristics of HVD.[285] It is of considerable practical importance to predict the stability of macroscopic or microscopic flow system, especially when the film thickness is of the same order as the roughness or when the system is at high Reynolds numbers. For example, compared with the smooth surfaces, the minimum value of the skin-friction drag coefficient increases in the range of 5%–30% with increasing the roughness size in the study of Abdel-Rahman *et al.*[286] The flow characteristics around the airfoil is greatly influenced by different roughness patterns. Carefully designed surface roughness could be used to enhance or reduce the drag coefficient in any particular application.[287] In classical fluid dynamics, the research about laminar-turbulent transition and the structure of turbulent flows is closely related to the rough surface,[288,289] as shown in Fig. 15. Also, the inclusion of surface roughness in the flow stability has recently become more and more valuable due to the advancement of microflow technology.

Due to free-stream unsteadiness, small amplitude roughness over the appropriate range of surface locations may excite traveling wave instabilities, or act as a direct source of stationary crossflow instabilities. Moreover, roughness at intermediate heights may have a significant impact on the growth characteristics of the boundary layer perturbations by scattering the instability waves.[290] One of the most important factors that affects the fluid characteristics is the distribution, amplitude and geometry of roughness elements. Watanabe *et al.*[291] experimentally investigated the laminar-turbulent transition of the boundary layer over a rotating cone. General distributed roughness level was found to be effective in stabilizing the type I mode with a reduction in the number of vortices from 32 to 26. In order to simulate distributed surface roughness, wall suction was introduced by Floryan[292] to establish a linear stability model for three types of flow, i.e., PPF, PCF, and Blasius boundary layer. The model predicted the effects of suction amplitude on the critical Reynolds number and the appearance of streamwise vortices. The formation criterion of suction Reynolds number corresponds to transitional Reynolds numbers of rotating-disk flow, from which the threshold relative roughness can be obtained.[293] Since viscous stresses at the wall/flow interface may result in an increase in energy production, the effect of wall compliance on the viscous type II mode can be strongly destabilizing,[100] which has been experimentally verified by Colley *et al.*[294]

Transition induced by isolated roughness has been extensively studied.[295–297] In view of the transition over distributed surface roughness, it mainly focuses on the effects of roughness height, roughness spacing, section feature and the streamwise proximity of roughness elements. Corke *et al.*[298] suggested that transition is most likely to be triggered by the few highest peaks. For roughness with small amplitudes, transition is induced through a linear amplification of the exponentially growing disturbances. Large-amplitude roughness, by contrast, creates so-called "bypass" transition where local separations occur. It also means that the linear instability processes such as T-S waves are bypassed.[299] By examining the mean wall pressure, Muppidi

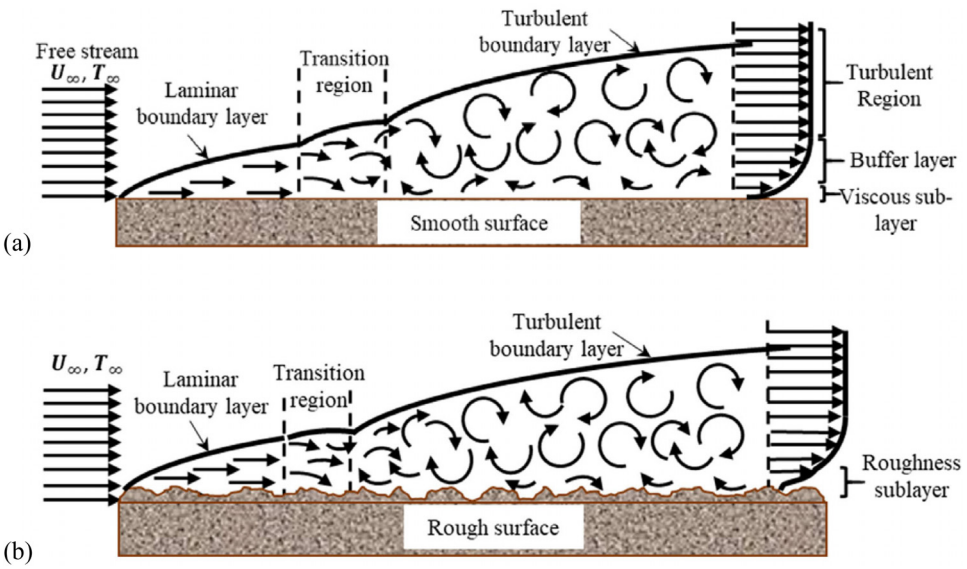

FIG. 15. A graphic illustrating boundary layer flows over two kinds of surfaces: (a) Smooth surfaces; (b) Rough surfaces. Reproduced with permission from Kadivar *et al.*, Int. J. Thermofluids **816**, 100077 (2021). Copyright 2021 Elsevier Ltd.[289]

and Mahesh[300] indicated that strong shear over the roughness surface generates counter-rotating pairs of streamwise vortices. The interaction of these vortices causes the shear layer to breakup and then are followed by a transition to turbulence. Particularly, with closely packed roughness elements, both upstream spacing and spanwise spacing are insufficient to induce transition. Loiseau *et al.*[301] showed that flow over a cylindrical roughness exhibits a sinuous global instability at low roughness aspect ratios and a varicose shape as the aspect ratio is increased, which is qualitatively similar to flow over the cuboid roughness element.[302] Also, a cylindrical roughness seems to delay the transition to turbulence, when compared to the cuboid roughness element. Vadlamani *et al.*[303] suggested that for roughness elements inside the boundary layer, secondary sinuous instabilities on the streaks promote transition to turbulence due to the occurrence of an elevated layer. In contrast, transition occurs due to the shedding from the roughness elements that are higher than the boundary layer. In the context of the instability wavelengths, they are governed by the roughness spacing between the roughness elements. von Deyn *et al.*[304] also found that the streak instability in the presence of roughness occurs within the boundary layer. Both the roughness height and density have an impact on the onset of transition.

There are two distinct theoretical models for the steady boundary-layer flow over rough surfaces. Miklavčič and Wang[305] proposed the MW model that is empirically modeled by converting the no-slip boundary conditions to partial-slip conditions at the disk surface. Two forms of anisotropic roughness (radial grooves and concentric grooves) and isotropic (general) roughness were used for the convective stability of the boundary-layer flow over a rotating disk.[306] Instead of independent modeling about the roughness level in both the radial and azimuthal directions of the MW model, Yoon *et al.*[307] imposed a particular mathematic form of surface distribution as a function of radial position only and a rotational symmetry, as presented by Garrett *et al.*,[308] i.e., the YHP model. Due to the limitations of the YHP model, the MW model is more suitable for modeling various forms of distributed roughness, including anisotropic and isotropic roughness.

Recently, based on the MW model, Alveroglu *et al.*[309] revealed that stabilization of the Type II mode in terms of radially anisotropic roughness is achieved for all boundary layers. Isotropic surface roughness can be used as a passive drag-reduction mechanism for a wide range of rotating boundary-layer flows.[308] Similarly, the linear instability of the non-Newtonian boundary-layer flow over rough rotating disks was investigated by Alqarni *et al.*[310] to account for the effects of isotropic and azimuthally anisotropic surface roughness on the behavior of the critical Reynolds number and growth rates of two modes of instability. With due consideration of the enforced axial flow, both radially anisotropic and isotropic surface roughness have a strong stabilizing effect on the boundary-layer flow for the type I mode. However, for the type II mode, both energy production and dissipation decrease for higher levels of radially anisotropic roughness, which showed a strong destabilizing effect.[311,312] This conclusion is not applicable for traveling modes studies of crossflow instability due to the increase in the frequency at which the most dangerous modes occur.[313] In addition, following the azimuthal velocity profile, it has been found that the resemblance between roughness-induced and confinement-induced effects[294] on the rotating-disk flow is remarkable. The effects induced by changes in the geometric boundary conditions is of the same nature and magnitude as the effects induced by roughness.[90]

B. Working media

1. Temperature-dependent viscosity

There has been a vast amount of research concerning the flow analysis of Newtonian fluid in HVD. Viscosity is one of the most considered factors that subjected to viscous dissipation. Under temperature–viscosity dependency, the fluid viscosity decreases with increase in temperature rise.[314] Viscous heating plays an important role in the fluid dynamics with temperature-dependent viscosity because of the coupling between the energy and momentum equations causing profound changes in the flow structure.[315,316]

In the case of flow with temperature-dependent viscosity, the velocity profile is affected by the viscosity dissipation heat, which induces unstable mode in the flow system.[317] From the existing literature, there are two types of temperature–viscosity relationship, namely Arrhenius-type and Nahme-type. Sukanek *et al.*[318] used the Nahme-type law to investigate the stability of PCF with viscous heating. Four different modes of instability are found: an inviscid mode, a viscous mode, a coupled mode, and a purely thermal mode. They indicated that the flow may become unstable for moderate Reynolds and Brinkman numbers. This finding is also verified by Yueh and Weng,[319] who indicated the difference between the two models mentioned above. They found that the fluids obeying the Arrhenius-type model are more stable than those of the Nahme-type model if both are based on the same temperature-sensitive viscosity. However, the second viscous mode for the instability is not observed by Eldabe *et al.*[320] who examine the effect of shear thinning and shear thickening on the pow-law fluid that obeys the Arrhenius-type model. Also, the Brinkman numbers for the instability of the shear thinning/thickening fluid occurs are different from the Newtian fluid. Based on the Nahme-type model, Sahu and Matar[316] showed that the critical Reynolds number decreases by one order of magnitude with increase in the Nahme number.

One of the well-known methods for delaying a transition to turbulence, for example, in boundary layers, has been to reduce the viscosity at the wall. Such a reduction could be brought about by heating the surface.[316] Wall and Wilson[321] included the effects of temperature-dependent viscosity and heating of the channel walls to analyze the linear stability of the viscous channel flow. A non-uniform increase in the viscosity will stabilize the flow whereas a non-uniform decrease in the viscosity may either destabilize or stabilize the flow.[322] In order to more fully understand the differences between different viscosity models, the nonlinear secondary flows that bifurcate from the basic flows were analyzed. It was found that the secondary flow is destabilized relative to the corresponding isothermal flow when the viscosity decreases with increasing temperature, and vice versa.[323] Govindarajan *et al.*[324] studied the effects of a weakly space-dependent viscosity on the stability of hydrodynamic flows. Due to reduced energy intake from the mean flow to the fluctuations, about 10% viscosity changes may lead to obvious increase in the threshold Reynolds numbers for instability. Jasmine *et al.*[325] investigated the linear absolute and convective instability of rotating disk flow by taking the fluid viscosity to be an inverse linear function of temperature. It is established that the flow stability is sensitive to changes in viscosity. More specifically, flows with temperature-dependent viscosity are found to be less stable than cases with temperature-independent viscosity.[326]

Furthermore, detailed mechanisms such as temperature-dependent viscosity, viscosity stratification and buoyancy were considered by Sameen *et al.*[327] They found that the temperature difference between the walls has a stabilizing effect whereas buoyancy, even at fairly low levels, gives rise to high levels of subcritical energy growth. As compared to the primary instability, wall heating has a converse effect on the secondary instabilities, destabilizing significantly when viscosity decreases toward the wall. Sahu and Matar[316] considered the linear stability of pressure-driven flow undergoing viscous heating through an asymmetrically heating channel. It was found that increasing the temperature difference between two walls can help to promote instability for viscous heating. However, since the temperature at the walls due to viscous heating is expected to increase continuously, such an assumption about the boundary condition at the walls is unphysical. In view of that, Srivastava *et al.*[328] investigated the non-isothermal flow behavior via direct numerical simulations and a temporal linear stability analysis. They found that increasing the Reynolds number or decreasing the Prandtl number enhances the instability behavior. In particular, the Grashof number does not change the stability characteristics qualitatively.

2. Non-Newtonian fluids

Many fluids are non-Newtonian, for which the slope of the shear stress vs shear rate curve is a function of the shear rate tensor. In general, non-Newtonian fluid exhibits certain distinct features, such as shear-rate dependency of viscosity (related to shear-shinning or shear-thickening aspects of the fluid), etc.[329] The constitutive equations of non-Newtonian fluids are usually too complex to solve because of high nonlinearity than Navier–Stokes equations. For power-law fluids, Andersson *et al.*[330] presented numerical solutions for the extremely non-linear ODEs arising in the presence of the shear-thinning and shear-thickening fluids, which may have a stabilizing effect on the flow. Based on two viscous models, Pinarbasi *et al.*[331] investigated the effect of temperature-dependent and shear-thinning viscosity on the stability of a channel flow, which showed different instable mode for the same temperature-sensitive viscosity. The decrease in the viscosity with temperature leads to flow instability.[332] For a PCF of a power-law fluid with viscous heating, it was observed that shear thinning has a destabilizing effect on the fluid flow, while shear-thickening has a stabilizing effect.[320] Following that, Nouar *et al.*[333] conducted a linear stability analysis on the effects of shear-thinning fluid on PPF, and they concluded that viscosity stratification delays the transition. As for PCF, since there is no viscosity stratification, the stress tensor is anisotropic aligned with the strain rate perturbation. Shear-thinning significantly increases the amplitude of the response to external excitations and initial conditions.[334] For the stability problem of PCPF, the influence of the velocity of the moving wall on the critical conditions is qualitatively similar to that for a Newtonian fluid.[335]

For the rotating-disk flows, Ming *et al.*[336] solved the non-linear ODEs over a rotating disk, assuming that the thermal conductivity follows the same function as the viscosity. It was indicated that the parameters of the power-law index and Prandtl number have significant effects on the velocity and temperature fields. The presence of non-Newtonian fluids causes the thickness of the boundary layer to decay with a power-law index. In addition, under the assumptions of a large Reynolds number and generalized Fourier heat conduction, it has been found that the relationship between the viscous coefficient and heat conductivity of fluids is nonlinear which depend strongly on the power-law index.[337] Griffiths *et al.*[338] considered a rigorous asymptotic stability analysis of the shear-thinning boundary-layer flow over a rotating disk. Predictions for the wavenumber and wave angle of the disturbances suggest that shear-thinning fluids may have a stabilizing effect on the flow, which is also applicable to the convective instability analysis of the BEK (Bödewart, Ekman, and von Kármán flows) family by Abdulameer *et al.*,[339] Using the Carreau model for a range of shear-thinning and shear-thickening fluids, local convective instability of the incompressible boundary layer flows over rough rotating disks is analyzed by Alqarni *et al.*[310] It was indicated that isotropic and azimuthally anisotropic surface roughness leads to the stabilization of both

shear-thinning and -thickening fluids. With the occurrence of non-uniform heat source/sink, the temperature decreases along with the similarity variable with the increasing Prandtl number but enhances with the enhancement in heat source/sink parameters.[340] Instead of the power law model that predicts both shear thinning/thickening impacts, the Ree–Eyring model from kinetic theory can be utilized for the study of flow behavior. With the assistance of the particle swarm optimization algorithm and artificial neural networks (ANN), substantial optimization has been achieved for the nonlinear mixed convective behavior of Ree–Eyring fluid between two rotating disks.[341] The results showed that enhancing the viscous effect of the Ree–Eyring fluid has a dramatic effect on flow instability.

In addition, the Bingham model is often used to describe the rheological behavior of a viscoplastic fluid. Peng *et al.*[342] and Landry *et al.*[343] found that the yield stress fluid flow is less stable than the corresponding Newtonian fluid flow, which is caused by an increase in the rate of strain of the basic flow. Nouar *et al.*[344] performed a linear stability analysis of plane Poiseuille flow of a Bingham fluid using modal and non-modal approaches. Within the range of parameters considered, plane Bingham–Poiseuille flow is found to be linearly stable. Ahmadpour *et al.*[345] derived numerical results for the swirling flow of Bingham fluids above a rotating disk. The effects of the Bingham number on the velocity profiles and wall shear stress distribution were presented. With the increase in the Bingham number, the heat penetration depth grows and the variation in solution profiles reduces in magnitude. Also, Bingham fluids have led to an increase in the rate of entropy generation within the boundary layer.[346]

The use of an magento-hydro dynamics (MHD) fluid as a lubricant in industrial applications is appealing because it prevents the anticipated variation of lubricant viscosity with temperature. There is a strong coupling between the unsteady equations of mass and momentum conservation and the variable magnetic field and energy equations. Alam *et al.*[347] and Jayavel *et al.*[348] considered the effects of a magnetic field on the squeezing flow between parallel plate. Based on the similarity transformations from nonlinear PDEs to nonlinear ODEs, they found that the thermo-fluid properties in the lubrication regime are strongly affected by the combination effects of the electromagnetic field and plate squeezing/separating.

3. Cavitation

As the relative angular velocity of the friction disk increases, or the film truly occupies the clearance space with increasing volume in the divergent region, air bubbles are formed, i.e., cavitation effect. This effect in the transmission oil needs to be considered in order to anticipate the accurate dynamic torque behavior.[8] There has been very little research on the stability analysis of HVD or wet clutch considering cavitation effects. It is observed that based on the same flow shear mechanism, the fluid film in the converging-diverging geometry of the hydrodynamic journal bearing will cavitate within the divergent region. Rao *et al.*[349] presented a two-dimensional linear stability analysis considering the fluid film in both the full film and cavitation regions. Based on the infinitesimal perturbation amplitude, the stability threshold increases with an increase in supply pressure in the case of a grooved journal bearing. Then, Rao *et al.*[350] developed a numerical procedure for stability analysis of a lubricated rough journal bearing using the same Elrod's cavitation model. They found that the threshold speed for instability increases significantly for the roughness patterns on the grooved bearing surface only at higher eccentricity ratios.

Despite the limitations of these studies investigating the dynamic characteristics, interfacial waves that exist on the interface of a gas–liquid two-phase flow have a significant effect on the heat and mass transfer characteristics of the system. In terms of two-phase flow in the microchannel, some of the frictional heat that is convectively transferred from the oil to the disks, will regenerate a relatively stable heat flux on the oil–disk interface.[351] As has been proved, some physical effects, such as capillary or shear, can cause large pressure drop excursions, and occasionally result in a negative drop with a corresponding flow reversal in the channel.[352] The resulting two-phase flow instabilities may take place which may induce some undesired effects, such as mechanical vibrations in the system or a decrease in hydrodynamic performances, etc. Therefore, it is necessary to perform an in-depth instability analysis about the gas–liquid two-phase flow instability.

As an important part of static instability, Ledinegg instability, which are relevant to pressure drop excursions, is a system-level instability that deals with internal and external pressure characteristics within a two-phase flow system. Stelling *et al.*[353] obtained the pressure drop in a heated tube under downflow conditions. The occurrence of Ledinegg instability depends on the L/D (L is the length of heated channel and D is the tube inner diameter) ratio of the channel, the inlet temperature, exit pressure, and surface heat flux, which may effectively predict the minimum point velocity, i.e., the onset of flow instability (OFI). Similarly, demand curves (pressure drop vs mass flow rate curves for fixed wall heat flux and channel exit pressure) were experimentally investigated, and thereby the onset of flow instability points can be specified.[354] In this case, it can be summarized as follows: For a nonzero heat flux, with the reduction of the flow velocity, pressure drop behavior begins to deviate from that for single-phase flow and then two-phase effects become more pronounced with OFI as demonstrated in Fig. 16. As mass velocity is reduced further, pressure drop

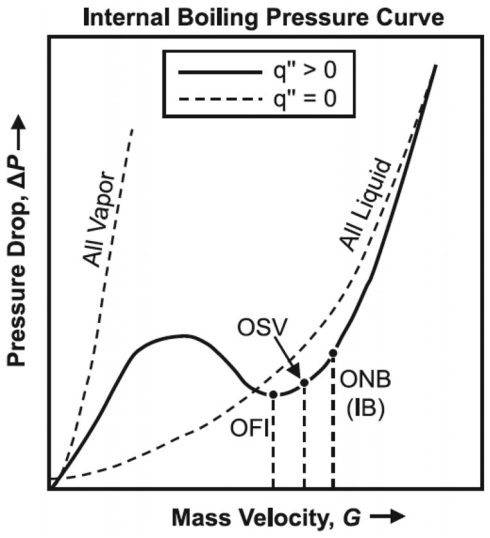

FIG. 16. Pressure vs mass velocity characteristics curves for flow boiling (internal characteristics, $q'' > 0$). Reproduced with permission from O'Neill and Mudawar, Int. J. Heat Mass Transfer **157**, 119738 (2020). Copyright 2020 Elsevier Ltd.[354]

begins to increase due to added body force and acceleration effects present in two-phase flows.[355] As observed in the experiments, the OFI always occurred when the bubbles at the channel exit began to coalesce, which corresponded to the beginning of the bubbly churn transition in flow pattern.[356] For more information, the identified minimum mass flux conditions imply that flow excursion points that were close to the onset of a significant void. This highlights the fact that the flow excursion is triggered by the coalescence of facing bubbles (for $Pe < 14\,000$) or wavy vapors (for $Pe > 14\,000$) on opposing heated surfaces.[357] Furthermore, in order to make it comparable with the concurrent thermal hydraulic behaviors, the ONB, OSV, and OFI under constant heat flux and constant mass flux conditions were sequentially investigated. Based on the two experimental methods, the OFI can be identified using pressure drop and inlet pressure fluctuations.[358] More recently, Lu *et al.*[359] defined OFI as the point at which significant flow oscillations were observed. On account of the significant channel restriction and surface tension, the flow patterns rapidly evolved to the annular flow for OFI, while the flow state simultaneously transferring from a stable state to an unstable state.

For high heat fluxes in micro-channels, the phase change will cause the bubble to expand toward the channel exit as well as the inlet. Then, an increase in the pressure drop will lead to a delayed response in the mass flow rate, i.e., density wave oscillations (DWOs). More specifically, local instabilities are caused by the rapid expansion of confined bubbles. Under specific conditions, there are inlet pressure signals that exhibit fluctuations with high amplitudes, which showed how confined growth could lead to a rapid transition from bubbly flow to annular flow,[360] as shown in Fig. 5. When using a compliant buffer tank, unsteady flows are observed with a different intensity and across a different range of operating conditions. A critical Reynolds number to delimit steady and unsteady states behaviors was determined.[361] Wang *et al.*[362] found that in the stable regime, isolated bubbles were generated and then squeezed out of the microchannel. Two unstable regimes showed the effects of heat fluxes and mass fluxes on flow instability, including the expansion of vapor bubbles and the transition of flow pattern. Later, due to the difficulties in local accurate measurements of wall temperatures, platinum microheaters were fabricated on a Pyrex glass wall in the single microchannel. Pressure drop oscillations (PDOs) with superimposed DWOs may lead to reverse flow.[363] Similar to measuring local temperature, local heat transfer coefficients were measured in conjunction with visualizing local flow.[364] It was found that vapor recoil instabilities are responsible for triggering flow reversal and high fluctuations in both temperature and pressure. This also greatly implies the fact that reverse flow in the upstream direction does not absolutely correspond to back and forth oscillations with flow instabilities.[365] In order to damp out or even eliminate DWOs, Fan and Hassan[366] investigated the effects of an orifice on flow oscillation, pressure drop, and heat flux at the onset of flow stability under uniform heating conditions. This method provides a way to avoid the adverse impact of DWOs. It was reported that the heat flux at the onset of flow instability for the microtubes with orifices of 50% and 35% area ratios was much larger than that of the microtube without an orifice, which effectively shows the potential to stabilize the flow without active control. More importantly, given that bubble dynamic processes are usually related to quantitative instability criteria, He *et al.*[367] presented an analytical model to predict pressure fluctuation through the analysis of bubble growth. The relationship between bubble reversal flow and pressure fluctuation is determined by solving the conservation equations for the momentum of the liquid column, coupled with the equations of the force balance at the bubble interface. Furthermore, based on a similar model, Li and Hrnjak[368] made a comparison between the simulation and available experimental measurements. It is shown that the model is capable of capturing the transient flow regime and quantitatively demonstrates the mechanism of flow reversal.

The rapid growth of the bubble toward the inlet leads to DWOs, while the interaction of the bubbles with the upstream compressible volume triggers PDOs. As discussed for Ledinegg instability, pressure drop instability is also a system-level instability. This instability occurs when the system is operating on the negative-slope portion of the internal pressure curve and there is a compressible volume within the system.[369] According to Maulbetsch and Griffith,[370] in high power density systems, the amount of compressible volume needed to sustain the oscillation is very low. The frequency of the oscillations is partly controlled by the compressible volume dynamics in which PDOs mode were experimentally investigated. More experimental studies about PDOs can be found in Yuncu,[371] Qu and Mudawar,[372] Huh *et al.*,[373] Zhang *et al.*,[374] Kuang *et al.*,[375] etc. It can be found that PDOs with high amplitude and low frequency are usually characterized by the transition of flow pattern (a bubbly/slug flow and elongated slug/semi-annular flow), which can be used as an index for the appearance of reversed flow.[376] Due to the changes in flow patterns, heat transfer is enhanced both in the downstream region and in the upstream region. The effect of instabilities on heat transfer is amplified in micro-channels.[377] Based on the amplitude-frequency characteristics, five different flow pattern evolution modes are caused by the coupling effects of inertial force, evaporation momentum, heating wall, etc.[378] Some influencing parameters leading to the onset of PDOs are concentrated in inlet mass flow rate, inlet subcooling degree, mass and heat flux, compressible volume, etc.[379] On the other hand, most of the theoretical studies concerning two-phase flow commonly use correlations synthesized from experimental data. A lumped model for pressure-drop type instabilities in an upflow boiling system is developed for predicting the oscillation amplitude and period.[380] The upstream compressibility and the associated oscillatory transients can be quantified using the lumped model.[374] Also, the effects of upstream compressible volume, heat flux, mass flow rate, and inlet sub-cooling degree on the pressure drop instability were comprehensively investigated.[375] Then the flow oscillation amplitude can be regulated based on a family of state and dynamic output-feedback active flow controllers. The controllable parameters of the system, including the valve setting, can be chosen to avoid pressure drop oscillation.[381] Moreover, the model revealed that a fully confined bubble may result in bubble reversal flow and pressure fluctuations.[367] The local pressure peak caused by the build-up of downstream flow resistance can cause negative pressure gradient, which induces flow reversal.[368] It has been demonstrated that the model can guide the selection of system inputs for efficient operation and support the development of effective control strategies to suppress PDOs.[382]

Moreover, Qu and Mudawar[372] found that large-amplitude flow oscillations are the result of the interaction between vapor generation in channels and the compressible volume in the upstream flow loop. As pressure drop oscillation becomes severe, pre-mature critical heat flux (CHF) can be eliminated simply by throttling the flow upstream. Particularly, in the case of higher pressures, the rapid growth instability of bubbles can be inhibited by the low superheat temperature and then

boiling instability was significantly delayed.[383] Based on the results regarding the onset of flow oscillation and CHF, it was observed that system pressure has a significant impact on flow instabilities.

IV. CONCLUDING REMARKS AND PERSPECTIVES

A. Conclusions

Microscale flow stability of the incompressible viscous fluid in HVD plays a significant role, offering a maximum of versatility as power transmission elements, such as large-scale equipment with high-power and large reduction ratio. Although the nonlinear development of the tribodynamic behavior is complicated, the flow configurations leading to final flexible outcomes can be probably categorized as three simple idealized plane-parallel flow: plane squeeze flow, plane shear flow and rotating-disk flow. As a typical fluid–solid coupling system, it is no doubt that flow instability will be greatly affected by the physical characteristics of the coupling interface, from which the combined interaction may show a dramatic evolution trend according to the extreme working conditions. In addition, the presence of frictional heat, due to the tribodynamic behavior, also has a major influence on the boundary conditions, the oil viscosity, as well as the multi-physical coupling mechanisms of the friction pair system. These flow configurations, along with the wall conditions and the working media, provide analytical characterizations of key mechanisms and physical phenomena about flow instability. In this review, detailed elucidation of the laminar-to-turbulent transition in such a wall-bounded flow have been carried out, which may open new routes to prevention and control of system instability of HVD. Main highlights are as follows:

(1) Squeeze-film flow stability depends on whether the disks move toward or away from each other. The case of squeezing may help enhance the stability caused by the suppressive effects of wall boundaries. However, the resulting viscous shear may tend to destabilize the flow due to viscosity diffusion. Since, for the rotating-disk boundary layer, suction has a greater stabilizing effect on the absolute instability than the destabilizing effect of injections, it can be inferred that the rotating-disk flow has a comparative significance over the squeeze-film flow during the flexible drive process of HVD.
(2) Since there are discrepancies between the linear/nonlinear analysis and the experiments, it is necessary to first revisit the shear flow instability from the prospective of (linear) nonmodal stability analysis. This analysis should comprehensively incorporate time-dependent characteristics, spatially varying configurations, stochastic influences, and complex microstructures of the wall boundary. For the transition to turbulence in wall-bounded flows, nonlinear nonmodal analysis can be coupled with a search over disturbance amplitude to identify the critical disturbance, i.e., the minimal seed for transition, that first breaches the basin boundary of the reference state.
(3) As the local *Ro* varies with the radius, the affected global stability properties of the rotating-disk boundary-layer flow reflect the inconsistency between the non-parallel stabilizing effects and the destabilizing non-linear effects. Linear global instability can be created by local absolute instability at the edge of the disk. Moreover, for sufficiently large azimuthal mode numbers that are greater than those associated with the onset of absolute instability, disturbances become globally linearly unstable. The transition to turbulence may be dominated by the significant spatial growth associated with local convective instabilities.
(4) Whether for the merged boundary layers or the separated boundary layers, the transition to turbulence appears to be governed by the nonlinear interactions between the circular and spiral modes of the stationary disk flow. In the case of co-rotating or weak counter-rotation flow, various flow patterns including the propagating circular vortices, mixing of axisymmetric propagating vortices, and positive spirals appear successively on increasing Re_t. Subsequently, the flow transitions into a more disordered state. When the disks rotate in opposite directions, negative spirals, mixing of positive and negative spirals, and positive spirals appear successively as Re_t increases.
(5) Developing a superhydrophobic surface with specified directional sensitivity is useful for delaying the early onset of transition. Increasing the anisotropy in the slip length may reduce the critical Reynolds number due to the decrease in the difference in the tilt angles at the two walls. These results may be of interest for enhancing mixing or heat transfer in microchannel flow systems, such as HVD, where turbulence cannot be triggered.
(6) Depending on parameters such as depth ratio, permeability, and porosity of the porous medium, the stability over porous surfaces is influenced by the velocity slip at the liquid–porous interface. From the perspective of energy analysis, flow instability seems to be triggered by an increase in energy transfer from the base flow to disturbances. As regards PCPF, the presence of the Couette flow component intensifies the most unstable fluid layer mode while it attenuates the most unstable porous layer mode. It effectively highlights once again the dominating role of shear flow stability as a sufficient condition for flexible controllability in HVD.
(7) Surface roughness typically results in statistically inhomogeneous flow fields in the roughness sublayer on the length-scale of the roughness. This leads to an early transition from laminar to turbulence through bypass transition. As an effective passive flow-control method, understanding the flow stability mechanism of the boundary layer is crucial. The diverse variety of roughness, the chaotic and random nature of turbulent flows, and the lack of systematic studies on the structure of turbulent flows are possible reasons for considerable discrepancies.
(8) The critical Reynolds number decreases as the viscous heating increases. It may be caused by the coupling effects between velocity perturbations and the base temperature gradient, which ultimately reduce the dissipation energy of the disturbances. Increasing the temperature difference between two walls can help promote instability due to viscous heating. The instability behavior can be enhanced by increasing the Reynolds number or decreasing the Prandtl number. In terms of HVD, as there is obvious difference in thermal conductivity between the disks, the conclusions mentioned above are of great reference value for improving the flow stability.
(9) In light of the amplitude of response to external excitations and initial conditions, as well as the phase exchange of energy caused by viscosity stratification, the stability of PCPF of a power-law fluid may be influenced by the balance between PCF and PPF. With the increase in the power-law index of

shear-thinning fluids, a universal stabilizing effect on the entire BEK family of flows can be predicted, which can be utilized to delay laminar-turbulent transition in HVD under high rotational speeds.

(10) DWOs and PDOs are caused by the rapid growth of bubbles and the interaction of the bubbles with upstream compressible volume, respectively. Both types of instability are closely related to pressure fluctuations. For the two-phase flow of HVD, due to its high sensitivity to disturbances, the trigger mechanism of instability should be further studied by combining experiments with numerical simulation methods, especially focusing on the crucial factors such as squeeze-film flow and the physical properties of the working medium.

B. Perspectives

Although numerous valuable works on flow instability of basic flow patterns have been carried out in the past decades, and lots of progresses have been achieved with respect to the effects of key influence factors from the fluid–solid interaction system, there are still some aspects that should be further investigated.

(1) Regardless of whether the working mode is speed-regulating or soft-start or soft-brake, the tribodynamic behavior depends on the simultaneous motion of squeeze-film and shear-film. In particular, the shear flow is affected by both the centrifugal forces and the Coriolis forces, which are of great importance in rotating machinery. Such superimposed instabilities in wall-bounded microscale flows are of an entirely different character compared to the three aforementioned flow patterns. Therefore, understanding the complicated flow characteristics and establishing an appropriate analytical model or a specific numerical model, or both, including the most recent nonlinear developments, is an important further work.

(2) In a sliding system involving frictional heat, a disturbance might change the nominally uniform pressure distribution and hence the friction heat generation. The associated non-uniform thermoelastic distortion will eventually evolve into frictionally excited thermoelastic instability or TEI if the sliding speed is in excess of a certain threshold value. For the frictional system with lubrication, there is no doubt that flow instability can be influenced by TEI, in which the constantly evolving non-uniform distribution of frictional heat will transform the various physical characteristics of the oil film in turn. In order to further investigate the unsteady flow and heat transfer in HVD, there is an urgent need for analyzing the coupling mechanism between flow instability and TEI.

(3) Current studies mainly focus on the negative effects of flow instability. However, the positive effect of flow instability can be exploited to enhance the heat and mass transfer efficiency of the oil film, or to reduce the fluid transportation energy consumption, on condition that flow instability should be kept within a limited level. This, to some extent, depends on the implementation of flow control, which attempts to introduce perturbations into the flow field to alter the original flow development path toward an ideal state. Thus, the effects of different flow control methods need to be researched and assessed in terms of the operating range and performance of HVD.

ACKNOWLEDGMENTS

This work was sponsored by the National Natural Science Foundation of China (No. 51805464), China Postdoctoral Science Foundation (No. 2018M632199), Qinglan Project of Jiangsu Province of China, and also Jiangsu Overseas Visiting Scholar Program for University Prominent Young & Middle-aged Teachers and Presidents.

AUTHOR DECLARATIONS

Conflict of Interest

The authors have no conflicts to disclose.

Author Contributions

Jianzhong Cui: Data curation (equal); Formal analysis (equal); Investigation (equal); Methodology (equal); Resources (equal); Writing – original draft (equal). **Hui Tang:** Conceptualization (equal); Writing – review & editing (equal).

DATA AVAILABILITY

Data sharing is not applicable to this article as no new data were created or analyzed in this study.

NOMENCLATURE

a, b	inner, outer radius of disk, respectively
G	aspect ratio of the gap separating the two parallel disks
h_t	average gap height
Kn	Knudsen number
m	outward wall-normal direction
Mc	Marangoni number
n	azimuthal mode number
n_a	azimuthal mode number for the onset of absolute instability
Re_θ	tangential Reynolds number
Ro	Rossby number
u_0	slip velocity
εE	generalized energy functional
Λ	slip tensorial
λ_x, λ_z	streamwise and spanwise slip lengths, respectively
v_r, v_θ	radial and tangential velocity component
ρ	density of lubricating oil
υ	kinematic viscosity of the oil film
ω_1/Ω_t, ω_2/Ω_b, ω	angular velocity of separator/top and friction/bottom plate, and relative angular velocity, respectively

Abbreviations

ANN	Artificial neural networks
BEK	Bödewart, Ekman and von Kármán flows
BOD	Bi-orthogonal decomposition
CFD	Computational fluid dynamics
CFD	Computational fluid dynamics
CHF	Critical heat flux

CST	Controlled start transmission
DNS	Direct numerical simulations
DWOs	Density wave oscillations
EIM	Energy integral method
FEM	Finite element method
HVD	Hydroviscous drive
LDGM	Low-dimensional Garlerkin method
LSA	Linear stability analysis
MEMS	Microelectromechanical system
MHD	Magento-hydro dynamics
ODEs	Ordinary differential equations
OFI	Onset of flow instability
OHAM	Optimal homotopy asymptotic method
O-S	Orr–Sommerfeld
PCF	Plane Couette flow
PCPF	Plane Couette–Poiseuille flow
PDEs	Partial differential equations
PDOs	Pressure drop oscillations
PIV	Particle image velocity
PPF	Plane Poiseuille flow
QSL	Quasi-steady linear
RPCF	Rotating plane Couette flow
SHP	Superhydrophobic
SLLM	Spectral local linearization method
TBM	Tunnel boring machine
TCF	Taylor–Couette flow
TEI	Thermoelastic instability
T-S	Tollmien–Schlichting
WIBL	Weighted residual integral boundary-layer

REFERENCES

[1]J. Z. Cui, P. L. Hou, B. G. Zhang, and X. Y. Zhao, "Investigation of flow between deformed disks in hydro-viscous drive," Tribol. Int. **121**, 287–301 (2018).

[2]J. Y. Jang and M. M. Khonsari, "Thermal characteristics of a wet clutch," ASME J. Tribol. **121**, 610–617 (1999).

[3]J. Z. Cui, F. W. Xie, C. T. Wang, X. J. Zhang, and R. Xuan, "Dynamic transmission characteristics during soft-start of hydro-viscous drive considering fluid-inertia item," Tribol. Online **10**(1), 35–47 (2015).

[4]C. R. Aphale, J. Cho, and W. W. Schultz, "Modeling and parametric study of torque in open clutch plates," ASME J. Tribol. **128**, 422–430 (2006).

[5]H. B. Xie, H. S. Gong, L. Hu, and H. Y. Yang, "Coriolis effects on torque transmission of hydro-viscous film in parallel disks with imposed throughflow," Tribol. Int. **115**, 100–107 (2017).

[6]J. H. Huang, J. H. Wei, and M. X. Qiu, "Laminar flow in the gap between two rotating parallel frictional plates in hydro-viscous drive," Chin. J. Mech. Eng. **25**(1), 144–152 (2012).

[7]J. Z. Cui, H. Li, D. Zhang, Y. W. Xu, and F. W. Xie, "Multi-objective optimization of hydro-viscous flexible drive for dynamic characteristics using genetic algorithm," Ind. Lubr. Tribol. **73**(7), 1003–1010 (2021).

[8]Y. Yuan, P. Attibele, and Y. Dong, "CFD simulation of the flows within disengaged wet clutches of an automatic transmission," SAE Technical Paper No. 2003-01-0320, 2003.

[9]J. Z. Cui, F. W. Xie, H. Li, and X. Y. Zhao, "Influences of deformed film gaps on dynamic torque behavior of hydroviscous drive," Tribol. Trans. **64**(3), 477–500 (2021).

[10]J. Z. Cui, D. Zhang, Y. W. Xu, S. X. Ma, and G. T. Chen, "A coupling model for tribodynamic behavior of the hydroviscous flexible drive with consideration of saucer-warping deformation," Tribol. Trans. **66**(1), 73–91 (2023).

[11]X. X. Yin, Y. G. Lin, W. Li, and H. G. Gu, "Hydro-viscous transmission based maximum power extraction control for continuously variable speed wind turbine with enhanced efficiency," Renewable Energy **87**, 646–655 (2016).

[12]Q. R. Meng and Y. F. Hou, "Effect of oil film squeezing on hydro-viscous drive speed regulating start," Tribol. Int. **43**, 2134–2138 (2010).

[13]S. Ishizawa, "The unsteady laminar flow between two parallel discs with arbitrarily varying gap width," Bull. JSME **9**(35), 533–550 (1966).

[14]C. J. Lawrence, Y. Kuang, and S. Weinbaum, "The inertia draining of a thin fluid layer between parallel plates with a constant normal force. Part 2. Boundary layer and exact numerical solutions," J. Fluid Mech. **156**, 479–494 (1985).

[15]E. A. Hamza, "Impulsive squeezing with suction and injection," ASME J. Appl. Mech. **66**, 945–951 (1999).

[16]J. T. Stuart, R. DiPrima, P. Eagles, and A. Davey, "On the instability of the flow in a squeeze lubrication film," Proc. R. Soc. A **430**, 347–375 (1990).

[17]P. Hall and D. T. Papageorgiou, "The onset of chaos in a class of Navier-Stokes solutions," J. Fluid Mech. **393**, 59–87 (1999).

[18]S. N. Aristov and I. M. Gitman, "Viscous flow between two moving parallel disks: Exact solutions and stability analysis," J. Fluid Mech. **464**, 209–215 (2002).

[19]K. Q. Zhu, L. Ren, and Y. Liu, "Linear stability of flows in a squeeze film," Chin. Phys. Lett. **22**(6), 1460–1463 (2005).

[20]J. D. Jackson, "A study of squeezing flow," Appl. Sci. Res., Sect. A **11**(1), 148–152 (1963).

[21]J. Engmann, C. Servais, and A. S. Burbidge, "Squeeze flow theory and applications to rheometry: A review," J. Non-Newtonian Fluid Mech. **132**, 1–27 (2005).

[22]L. Espin and D. T. Papageorgiou, "Flow in a channel with accelerating or decelerating wall velocity: A comparison between self-similar solutions and Navier-Stokes computations in finite domains," Phys. Fluids **21**, 113601 (2009).

[23]T. Hayat, A. Qayyum, and A. Alsaedi, "MHD unsteady squeezing flow over a porous stretching plate," Eur. Phys. J. Plus **128**(12), 157 (2013).

[24]E. A. Moss, A. Krassnokutski, B. W. Skews, and R. T. Paton, "Highly transient squeeze-film flows," J. Fluid Mech. **671**, 384–398 (2011).

[25]A. Krassnokutski, E. A. Moss, and B. W. Skews, "An experimental study of highly transient squeeze-film flows," Phys. Fluids **25**, 063102 (2013).

[26]D. V. Knyazev, "Axisymmetric flows of an incompressible fluid between movable rotating disks," Fluid Dyn. **46**(4), 558–564 (2011).

[27]S. N. Aristov and D. V. Knyazev, "Viscous fluid flow between moving parallel plates," Fluid Dyn. **47**(4), 476–482 (2012).

[28]A. G. Petrov, "Exact solution of the Navier-Stokes equations in a fluid layer between the moving parallel layer," J. Appl. Mech. Tech. Phys. **53**, 642–646 (2012).

[29]A. G. Petrov and I. S. Kharlamova, "The solutions of Navier-Stokes equations in squeezing flow between parallel plates," Eur. J. Mech. B **48**, 40–48 (2014).

[30]A. G. Petrov, "Exact solution of the equations of axisymmetric viscous fluid between parallel plates approaching and moving apart from one another," Fluid Dyn. **54**, 56–66 (2019).

[31]V. Marinca, N. Herisanu, and I. Nemes, "Optimal homotopy asymptotic method with application to thin film flow," Cent. Eur. J. Phys. **6**(3), 648–653 (2008).

[32]V. Marinca, N. Herisanu, C. Bota, and B. Marinca, "An optimal homotopy asymptotic method applied to the steady flow of a fourth-grade fluid past a porous plate," Appl. Math. Lett. **22**(2), 245–251 (2009).

[33]M. Idrees, S. Islam, S. Haq, and S. Islam, "Application of the optimal homotopy asymptotic method to squeezing flow," Comput. Math. Appl. **59**(12), 3858–3866 (2010).

[34]M. Qayyum, H. Khan, M. T. Rahim, and I. Ullah, "Analysis of unsteady axisymmetric squeezing fluid flow with slip and non-slip boundaries using OHAM," Math. Problems Eng. **2015**, 1–11.

[35]T. Hayat, M. W. A. Khan, A. Alsaedi, and M. I. Khan, "Squeezing flow of second grade liquid subject to non-Fourier heat flux and heat generation/absorption," Colloid Polym. Sci. **295**, 967–975 (2017).

[36]M. R. Shirkhani, H. A. Hoshyar, I. Rahimipetroudi, H. Akhavan, and D. D. Ganji, "Unsteady time-dependent incompressible Newtonian fluid flow between two parallel plates by homotopy analysis method (HAM), homotopy

perturbation method (HPM) and collocation method (CM)," Propul. Power Res. **7**(3), 247–256 (2018).
[37]O. A. Ilhan, "Approximation solution of the squeezing flow by the modification of optimal homotopy asymptotic method," Eur.opean Phys. J. Plus **135**(9), 745 (2020).
[38]J. Lang, S. Santhanam, and Q. H. Wu, "Exact and approximate solutions for transient squeezing flow," Phys. Fluids **29**, 103606 (2017).
[39]J. Lang, R. Nathan, and Q. H. Wu, "Theoretical and experimental study of transient squeezing flow in a highly porous film," Tribol. Int. **135**, 259–268 (2019).
[40]J. Lang, L. Y. Wang, and Q. H. Wu, "Theoretical study of oscillating squeezing flow through a porous medium," Tribol. Int. **162**, 107110 (2021).
[41]D. Alviso, D. Sciamarella, A. Gronskis, and G. Artana, "Flow-induced self-sustained oscillations in a straight channel with rigid walls and elastic supports," Bioinspiration Biomimetics **17**(6), 065005 (2022).
[42]J. Prakash, D. Tripathi, O. A. Beg, and R. K. Sharma, "Electroosmotic modulated unsteady squeezing flow with temperature-dependent thermal conductivity, electric and magnetic fields effects," J. Phys. Condens. Matter **34**, 175701 (2022).
[43]N. B. Naduvinamani, B. N. Hanumagowda, and S. T. Fathima, "Combined effects of MHD and surface roughness on couple-stress squeeze film lubrication between porous circular stepped plates," Tribol. Int. **56**, 19–29 (2012).
[44]X. H. Su and Y. X. Yin, "Effects of an inclined magnetic field on the unsteady squeezing flow between parallel plates with suction/injection," J. Magn. Magn. Mater. **484**, 266–271 (2019).
[45]C. L. Zhao, W. Y. Zhang, D. V. D. Ende, and F. Mugele, "Electroviscous effects on the squeezing flow of thin electrolyte solution films," J. Fluid Mech. **888**, A29 (2020).
[46]T. Thumma and V. M. Magagula, "Transient electromagnetohydrodynamic radiative squeezing flow between two parallel Riga plates using a spectral local linearization approach," Heat Transfer-Asian Res. **49**(1), 67–85 (2020).
[47]P. Drazin and W. Reid, *Hydrodynamic Stability* (Cambridge University Press, Cambridge, UK, 2004).
[48]P. J. Schmid and D. S. Henningson, *Stability and Transition in Shear Flows* (Springer, New York, 2001).
[49]X. S. Wu, "Nonlinear theories for shear flow instabilities: Physical insights and practical implications," Annu. Rev. Fluid Mech. **51**, 451–485 (2019).
[50]B. J. Bayly and S. A. Orgzag, "Instability mechanism shear-flow transition," Ann. Rev. Fluid Mech. **20**, 359–391 (1988).
[51]P. G. Baines and H. Mitsudera, "On the mechanism of shear flow instabilities," J. Fluid Mech. **276**, 327–342 (1994).
[52]T. Tatsumi and T. Yoshimura, "Stability of the laminar flow in a rectangular duct," J. Fluid Mech. **212**, 437–449 (1990).
[53]L. Kleiser and T. A. Zang, "Numerical simulation of transition in wall-bounded shear flows," Annu. Rev. Fluid Mech. **23**, 495–537 (1991).
[54]P. Huerre and P. A. Monkewitz, "Local and global instabilities in spatially developing flows," Annu. Rev. Fluid Mech. **22**, 473–537 (1990).
[55]P. A. Monkewitz, P. Huerre, and J. Chomaz, "Global linear stability analysis of weakly non-parallel shear flows," J. Fluid Mech. **251**, 1–20 (1993).
[56]V. Theofilis, "Advances in global linear instability analysis of nonparallel and three-dimensional flows," Prog. Aerosp. Sci. **39**, 249–315 (2003).
[57]V. Theofilis, P. W. Duck, and J. Owen, "Viscous linear stability analysis of rectangular duct and cavity flows," J. Fluid Mech. **505**, 249–286 (2004).
[58]V. Theofilis, "Global linear instability," Annu. Rev. Fluid Mech. **43**(1), 319–352 (2011).
[59]L. N. Trefethen, A. E. Trefethen, S. C. Reddy, and T. A. Driscoll, "Hydrodynamic stability without eigenvalues," Science **261**(5121), 578–584 (1993).
[60]K. M. Butler and B. F. Farrell, "Three-dimensional optimal perturbations in viscous shear flow," Phys. Fluids A **4**(8), 1637–1650 (1992).
[61]S. C. Reddy and D. S. Henningson, "Energy growth in viscous channel flow," J. Fluid Mech. **252**, 209–238 (1993).
[62]A. P. Hooper and R. Grimshaw, "Two-dimensional disturbance growth of linearly stable viscous shear flows," Phys. Fluids **8**(6), 1424–1432 (1996).
[63]A. P. Hooper and R. Grimshaw, "Transient linear growth and nonlinear effects," Stud. Appl. Math. **106**(1), 47–68 (2001).
[64]P. J. Schmid, "Nonmodal stability theory," Annu. Rev. Fluid Mech. **39**(1), 129–162 (2007).
[65]R. Kaiser, A. Tilgner, and W. von Wahl, "A generalized energy functional for plane Couette flow," SIAM J. Math. Anal. **37**, 438–454 (2005).
[66]R. Kaiser and G. Mulone, "A note on nonlinear stability of plane parallel shear flows," J. Math. Anal. Appl. **302**, 543–556 (2005).
[67]Y. Li and Z. Lin, "A resolution of the Sommerfeld paradox," SIAM J. Math. Anal. **43**, 1923–1932 (2011).
[68]Y. Lan and Y. C. Li, "A resolution of the turbulent paradox: Numerical implementation," Int. J. Non-Linear Mech. **51**, 1–9 (2013).
[69]A. Monokrousos, A. Bottaro, L. Brandt, A. D. Vita, and D. S. Henningson, "Nonequilibrium thermodynamics and the optimal path to turbulence in shear flows," Phys. Rev. Lett. **106**, 134502 (2011).
[70]C. C. T. Pringle, A. P. Willis, and R. R. Kerswell, "Minimal seeds for shear flow turbulence: Using nonlinear transient growth to touch the edge of chaos," J. Fluid Mech. **702**, 415–443 (2012).
[71]S. M. E. Rabin, C. P. Caulfield, and R. R. Kerswell, "Triggering turbulence efficiently in plane Couette flow," J. Fluid Mech. **712**, 244–272 (2012).
[72]S. Cherubini and P. De Palma, "Nonlinear optimal perturbations in a Couette flow: Bursting and transition," J. Fluid Mech. **716**, 251–279 (2013).
[73]M. Farano, S. Cherubini, J. C. Robinet, and P. De Palma, "Optimal bursts in turbulent channel flow," J. Fluid Mech. **817**, 35–60 (2017).
[74]R. R. Kerswell, C. C. T. Pringle, and A. P. Willis, "An optimization approach for analysing nonlinear stability with transition to turbulence in fluids as an exemplar," Rep. Prog. Phys. **77**(8), 085901 (2014).
[75]R. R. Kerswell, "Nonlinear nonmodal stability theory," Annu. Rev. Fluid Mech. **50**, 319–345 (2018).
[76]P. Falsaperla, A. Giacobbe, and G. Mulone, "Nonlinear stability results for plane Couette and Poiseuille flows," Phys. Rev. E **100**, 013113 (2019).
[77]A. Prigent, G. Gregoire, H. Chate, and O. Dauchot, "Long-wavelength modulation of turbulent shear flows," Physica D **174**(1–4), 100–113 (2003).
[78]D. Barkey and L. S. Tuckerman, "Mean flow of turbulent-laminar patterns in plane Couette flow," J. Fluid Mech. **576**, 109–137 (2007).
[79]P. Falsaperla, G. Mulone, and C. Perrone, "Energy stability of plane Couette and Poiseuille flows: A conjecture," Eur. J. Mech. B **93**, 93–100 (2022).
[80]D. D. Joseph and S. Carmi, "Stability of Poiseuille flow in pipes, annuli, and channels," Q. Appl. Math. **26**, 575–599 (1969).
[81]C. S. Paranjape, Y. Duguet, and B. Hof, "Oblique stripe solutions of channel flow," J. Fluid Mech. **897**, A7 (2020).
[82]P. J. Goulart and S. Chernyshenko, "Global stability analysis of fluid flows using sum-of-squares," Physica D **241**(6), 692–704 (2012).
[83]F. Fuentes, D. Goluskin, and S. Chernyshenko, "Global stability of fluid flows despite transient growth energy," Phys. Rev. Lett. **128**(20), 204502 (2022).
[84]P. T. Nagy, M. Kiss, and G. Paal, "Analytic investigation of the compatibility condition and the initial evolution of a smooth velocity field for the Navier–Stokes equation in a channel configuration," Fluid Dyn. Res. **54**, 055502 (2022).
[85]F. Fraternale, L. Domenicale, G. Staffilani, and D. Tordella, "Internal waves in sheared flows: Lower bound of the vorticity growth and propagation discontinuities in the parameter space," Phys. Rev. E **97**, 063102 (2018).
[86]H. Lee and S. X. Wang, "Extension of classical stability theory to viscous planar wall-bounded shear flows," J. Fluid Mech. **877**, 1134–1162 (2019).
[87]P. T. Nagy, G. Paal, and M. Kiss, "Imposing a constraint on the discrete Reynolds-Orr equation demonstrated in shear flows," Phys. Fluids **35**, 034115 (2023).
[88]W. S. Saric, H. L. Reed, and E. B. White, "Stability and transition of three-dimensional boundary layers," Annu. Rev. Fluid Mech. **35**, 413–440 (2003).
[89]R. J. Lingwood, "Absolute instability of the Ekman layer and related rotating flows," J. Fluid Mech. **331**, 405–428 (1997).
[90]M. Özkan, P. J. Thomas, A. J. Cooper, and S. J. Garrette, "Comparison of the effects of surface roughness and confinement on rotor-stator cavity flow," Eng. Appl. Comput. Fluid Dyn. **11**(1), 142–158 (2017).
[91]T. von Kármán, "Über laminare and turbulente reibung," Z. Angew. Math. Mech. **1**, 233–251 (1921).
[92]R. J. Lingwood and P. H. Alfredsson, "Instabilities of the von Kármán boundary layer," ASME Appl. Mech. Rev. **67**, 030803 (2015).

[93]G. Gauthier, P. Gondret, F. Moisy, and M. Rabaud, "Instabilities in the flow between co- and counter-rotating disks," J. Fluid Mech. **473**, 1–21 (2002).
[94]R. J. Lingwood and S. J. Garrett, "The effects of surface mass flux on the instability of the BEK system of rotating boundary-layer flows," Eur. J. Mech. B **30**, 299–310 (2011).
[95]A. J. Faller, "Instability and transition of the disturbed flow over a rotating disk," J. Fluid Mech. **230**, 245–269 (1991).
[96]E. Serre, E. Tuliszka-Sznitko, and P. Bontoux, "Coupled numerical and theoretical study of the flow transition between a rotating and a stationary disk," Phys. Fluids **16**(3), 688–706 (2004).
[97]H. L. Reed and W. S. Saric, "Stability of three-dimensional boundary layers," Annu. Rev. Fluid. Mech. **21**, 235–284 (1989).
[98]P. Hall, "An asymptotic investigation of the stationary modes of instability of the boundary layer on a rotating disc," Proc. R. Soc. London A **406**, 93–106 (1986).
[99]Y. Y. Lee, Y. K. Hwang, and K. W. Lee, "The flow instability over the infinite rotating disk," KSME Int. J. **17**, 1388–1395 (2003).
[100]A. J. Cooper and P. W. Carpenter, "The stability of rotating-disc boundary layer flow over a compliant wall. Part 1. Type I and Π instabilities," J. Fluid Mech. **350**, 231–259 (1997).
[101]B. Launder, S. Poncet, and E. Serre, "Laminar, transitional, and turbulent flows in rotor-stator cavities," Annu. Rev. Fluid Mech. **42**, 229–248 (2010).
[102]R. J. Lingwood, "Absolute instability of the boundary layer on a rotating disk," J. Fluid Mech. **299**, 17–33 (1995).
[103]R. J. Lingwood, "An experimental study of absolute instability of the rotating-disk boundary layer," J. Fluid Mech. **314**, 373–405 (1996).
[104]C. Davies and P. W. Carpenter, "Global behavior corresponding to the absolute instability of the rotating-disc boundary layer," J. Fluid Mech. **486**, 287–329 (2003).
[105]H. Othman and T. Corke, "Experimental investigation of absolute instability of a rotating-disk boundary layer," J. Fluid Mech. **565**, 63–94 (2006).
[106]C. Davies, C. Thomas, and P. W. Carpenter, "Global instability of the rotating-disk boundary layer," J. Eng. Math. **57**(3), 219–236 (2007).
[107]J. J. Healey, "Model for unstable global modes in the rotating-disk boundary layer," J. Fluid Mech. **663**, 148–159 (2010).
[108]S. Imayama, P. H. Alfredsson, and R. J. Lingwood, "An experimental study of edge effects on rotating-disk transition," J. Fluid Mech. **716**, 638–657 (2013).
[109]B. Pier, "Transition near the edge of a rotating disk," J. Fluid Mech. **737**, R1 (2013).
[110]B. Pier, "Finite-amplitude crossflow vortices, secondary instability and transition in the rotating-disk boundary layer," J. Fluid Mech. **487**, 315–343 (2003).
[111]B. Pier, P. Huerre, J. M. Chomaz, and A. Couairon, "Steep nonlinear global modes in spatially developing media," Phys. Fluids **10**(10), 2433–2435 (1998).
[112]A. P. Bassom, K. M. Kuzanyan, and A. M. Soward, "A nonlinear dynamo wave riding on a spatially varying background," Proc. R. Soc. London A **455**, 1443–1481 (1999).
[113]B. Pier and P. Huerre, "Nonlinear self-sustained structures and fronts in spatially developing wake flows," J. Fluid Mech. **435**, 145–174 (2001).
[114]W. Van Saarloos, "Front propagation into unstable states," Phys. Rep. **386**(2–6), 29–222 (2003).
[115]B. Viaud, E. Serre, and J. M. Chomaz, "The elephant mode between two rotating disks," J. Fluid Mech. **598**, 451–464 (2008).
[116]B. Viaud, E. Serre, and J. M. Chomaz, "Transition to turbulence through steep global-modes cascade in an open rotating cavity," J. Fluid Mech. **688**, 493–506 (2011).
[117]S. Imayama, P. H. Alfredsson, and R. J. Lingwood, "On the laminar-turbulent transition of the rotating-disk flow: The role of absolute instability," J. Fluid Mech. **745**, 132–163 (2014).
[118]E. Appelquist, P. Schlatter, P. H. Alfredsson, and R. J. Lingwood, "Global linear instability of the rotating-disk flow investigated through simulations," J. Fluid Mech. **765**, 612–631 (2015).
[119]C. Thomas and C. Davies, "On the impulse response and global instability development of the infinite rotating-disc boundary layer," J. Fluid Mech. **857**, 239–269 (2018).
[120]E. Appelquist, P. Schlatter, P. H. Alfredsson, and R. J. Lingwood, "On the global nonlinear instability of the rotating-disk flow over a finite domain," J. Fluid Mech. **803**, 332–355 (2016).
[121]E. Appelquist, P. Schlatter, P. H. Alfredsson, and R. J. Lingwood, "Transition to turbulence in the rotating-disk boundary-layer flow with stationary vortices," J. Fluid Mech. **836**, 43–71 (2018).
[122]C. Thomas, S. O. Stephen, and C. Davies, "Effects of partial-slip on the local-global linear stability of the infinite rotating disk boundary layer," Phys. Fluids **32**, 074105 (2020).
[123]C. Thomas and C. Davies, "An adjoint approach for computing the receptivity of the rotating disc boundary layer to surface roughness," J. Fluid Mech. **926**, A16 (2021).
[124]L. Schouveiler, P. Le Gai, and M. P. Chauve, "Stability of a travelling roll system in a rotating disk flow," Phys. Fluids **10**(11), 2695–2697 (1998).
[125]L. Schouveiler, P. Le Gai, and M. P. Chauve, "Instabilities of the flow between a rotating and a stationary disk," J. Fluid Mech. **443**, 329–350 (2001).
[126]J. W. Daily and R. E. Nece, "Chamber dimension effects on induced flow and frictional resistance of enclosed rotating disks," ASME J. Basic Eng. **82**, 217–232 (1960).
[127]A. Cros and P. Le Gai, "Spatiotemporal intermittency in the torsional Couette flow between a rotating and a stationary disk," Phys. Fluids **14**(11), 3755–3765 (2002).
[128]P. I. San'kov and E. M. Smirnov, "Bifurcation and transition to turbulence in the gap between rotating and stationary parallel disks," Fluid. Dyn. **19**, 695–702 (1985).
[129]A. Cros, R. Ali, P. Legal, P. J. Thomas, L. Schouveiler, P. W. Carpenter, and M. P. Chauve, "Effects of wall compliance on the laminar-turbulent transition of torsional Couette flow," J. Fluid Mech. **481**, 177–186 (2003).
[130]G. Gauthier, P. Gondret, and M. Rabaud, "Axisymmetric propagating vortices in the flow between a stationary and a rotating disk enclosed by a cylinder," J. Fluid Mech. **386**, 105–126 (1999).
[131]L. Schouveiler, M. P. Chauve, P. Le Gai, and Y. Takeda, "Spiral and circular waves in the flow between a rotating and a stationary disk," Exp. Fluids **26**, 179–187 (1999).
[132]D. Remy, G. Gauthier, and D. Buisine, "Instabilities between rotating and stationary parallel disks with suction," Phys. Fluids **17**, 018102 (2005).
[133]S. Poncet and M. P. Chauve, "Crossflow instability in rotor-stator flows with axial inward throughflow," J. Fluid Mech. **545**, 281–289 (2005).
[134]S. Poncet, E. Serre, and P. Le Gal, "Revisiting the two first instabilities of the flow in an annular rotor-stator cavity," Phys. Fluids **21**, 064106 (2009).
[135]A. Cros, E. Floriani, P. Le Gal, and R. Lima, "Transition to turbulence of the Batchelor flow in a rotor/stator device," Eur. J. Mech. B **24**, 409–424 (2005).
[136]E. Yim, J. –M. Chomaz, D. Martinand, and E. Serre, "Transition to turbulence in the rotating disk boundary layer of a rotor-stator cavity," J. Fluid Mech. **848**, 631–647 (2018).
[137]D. Martinand, E. Serre, and B. Viaud, "Instabilities and routes to turbulence in rotating disc boundary layers and cavities," Proc. R. Soc. London A **381**(2243), 20220135 (2023).
[138]E. Serre, S. Hugues, E. Crespo del Arco, A. Randriamampianina, and P. Bontoux, "Axisymmetric and three-dimensional instabilities in an Ekman boundary-layer flow," Int. J. Heat Fluid Flow **22**, 82–93 (2001).
[139]N. P. Hoffmann and F. H. Busse, "Linear instability of Poiseuille-Couette-Ekman flows: Local results for flows between differentially rotating disks with throughflow," Phys. Fluids **13**(9), 2735–2738 (2001).
[140]N. P. Hoffmann, F. H. Busse, and W. L. Chen, "Transition to complex flows in the Ekman-Couette layer," J. Fluid Mech. **366**, 311–331 (1998).
[141]G. K. Batchelor, "Note on a class of solutions of the Navier-Stokes equations representing steady rotationally-symmetric flow," Q. J. Mech. Appl. Math. **4**, 29–41 (1951).
[142]S. Poncet, M. P. Chauve, and P. Legal, "Turbulent rotating disk flow with inward throughflow," J. Fluid Mech. **522**, 253–262 (2005).
[143]A. Singh, "Inward flow between stationary and rotating disks," ASME J. Fluids Eng. **136**, 101205 (2014).
[144]J. M. Lopez, J. E. Hart, F. Marques, S. Kittelman, and J. Shen, "Instability and mode interactions in a differentially-driven rotating cylinder," J. Fluid Mech. **462**, 383–409 (2002).
[145]F. Moisy, O. Doare, T. Pasutto, O. Dause, and M. Rabaud, "Experimental and numerical study of the shear layer instability between two counter-rotating disks," J. Fluid Mech. **507**, 175–202 (2004).

[146]F. Ravelet, A. Chiffaudel, and F. Daviaud, "Supercritical transition to turbulence in an inertially driven von Kármán closed flow," J. Fluid Mech. **601**, 339–364 (2008).
[147]C. Nore, L. S. Tuckerman, O. Daube, and S. Xin, "The 1:2 mode interaction in exactly counter-rotating von Kármán swirling flow," J. Fluid Mech. **477**, 51–88 (2003).
[148]C. Nore, F. Moisy, and L. Quartier, "Experimental observation of near-heteroclinic cycles in the von Kármán swirling flow," Phys. Fluids **17**, 064103 (2005).
[149]M. C. Navarro, L. Martin Witkowski, L. S. Tuckerman, and P. Le Quere, "Building a reduced model for nonlinear dynamics in Rayleigh-Bénard convection with counter-rotating disks," Phys. Rev. E **81**, 036323 (2010).
[150]C. Nore, M. Tartar, O. Daube, and L. S. Tuckerman, "Survey of instability thresholds of flow between exactly counter-rotating disks," J. Fluid Mech. **511**, 45–65 (2004).
[151]C. Nore, L. Martin Witkowski, E. Foucault, J. Pecheux, O. Daube, and P. Le Quere, "Competition between axisymmetric and three-dimensional patterns between exactly counter-rotating disks," Phys. Fluids **18**, 054102 (2006).
[152]T. C. Lackey and F. Sotiropoulos, "Relationship between stirring rate and Reynolds number in the chaotically advected steady flow in a container with exactly counter-rotating lids," Phys. Fluids **18**, 053601 (2006).
[153]E. C. Del Arco, J. J. Sanchez-Alvarez, E. Serre, A. De La Torre, and J. Burguete, "Numerical and experimental study of the time-dependent states and the slow dynamics in a von Kármán swirling flow," Geophys. Astrophys. Fluid Dyn. **103**(2–3), 163–177 (2009).
[154]A. Giesecke, F. Stefani, and J. Burguete, "Impact of time-dependent nonaxisymmetric velocity perturbations on dynamo action of von Kármán-like flows," Phys. Rev. E **86**, 066303 (2012).
[155]P. Gutierrez-Castillo and J. M. Lopez, "Instabilities of the sidewall boundary layer in a rapidly rotating split cylinder," Eur. J. Mech. B **52**, 76–84 (2015).
[156]P. Gutierrez-Castillo and J. M. Lopez, "Nonlinear mode interactions in a counter-rotating split-cylinder flow," J. Fluid Mech. **816**, 719–745 (2017).
[157]J. Pecheux and E. Foucault, "Axisymmetric instabilities between coaxial rotating disks," J. Fluid Mech. **563**, 293–318 (2006).
[158]P. Gutierrez-Castillo and J. M. Lopez, "Imperfect O(2) symmetry in counter-rotating split-cylinder flow," Phys. Fluids **34**, 014105 (2022).
[159]P. Gutierrez-Castillo and J. M. Lopez, "Differentially rotating split-cylinder flow: Responses to weak harmonic forcing in the rapid rotation regime," Phys. Rev. E **2**(8), 084802 (2017).
[160]Y. Burnishev and V. Steinberg, "Torque and pressure fluctuations in turbulent von Karman swirling flow between two counter-rotating disks," Phys. Fluids **26**(5), 055102 (2014).
[161]L. Y. Chen, R. T. Li, F. W. Xie, and Y. Wang, "Load-bearing capacity research in wet clutches with surface texture," Measurement **142**, 96–104 (2019).
[162]H. W. Cui, Y. Y. Jiang, and Q. L. Wang, "Load-bearing capacity investigation of friction pairs in hydro-viscous drive based on fractal contact theory," ASME J. Tribol. **143**(12), 121801 (2021).
[163]C. I. Papadopoulos, L. Kaiktsis, and M. Fillon, "Computational fluid dynamics thermohydrodynamic analysis of three-dimensional sector-pad thrust bearings with rectangular dimples," ASME J. Tribol. **136**, 011702 (2014).
[164]A. Gherca, A. Fatu, M. Hajjam, and P. Maspeyrot, "Influence of surface texturing on the hydrodynamic performance of a thrust bearing operating in steady-state and transient lubrication regime," Tribol. Int. **102**, 305–318 (2016).
[165]M. Marian, A. Almqvist, A. Rosenkranz, and M. Fillon, "Numerical micro-texture optimization for lubricated contacts-A critical discussion," Friction **10**(11), 1772–1809 (2022).
[166]I. Etsion, Y. Kligerman, and G. Halperin, "Analytical and experimental investigation of laser-textured mechanical seal faces," Tribol. Trans **42**, 511–516 (1999).
[167]Y. Feldman, Y. Kligerman, and I. Etsion, "A hydrostatic laser surface textured gas seal," Tribol. Lett. **22**(1), 21–28 (2006).
[168]N. Brunetiere and B. Tournerie, "Numerical analysis of s surface-textured mechanical seal operating in mixed lubrication regime," Tribol. Int. **49**, 80–89 (2012).
[169]M. Adjemout, A. Andrieux, J. Bouyer, N. Brunetiere, G. Marcos, and T. Czerwiec, "Influence of the real dimple shape on the performance of a textured mechanical seal," Tribol. Int. **115**, 409–416 (2017).
[170]Y. K. Zhou, H. Zhu, W. Tang, C. B. Ma, and W. Q. Zhang, "Development of the theoretical model for the optimal design of surface texturing on cylinder liner," Tribol. Int. **52**, 1–6 (2012).
[171]A. Usman and C. W. Park, "Optimizing the tribological performance of textured piston ring-liner contact for reduced frictional losses in SI engine: Warm operating conditions," Tribol. Int. **99**, 224–236 (2016).
[172]P. Pawlus, W. Koszela, and R. Reizer, "Surface texturing of cylinder liners: A review," Materials **15**(23), 8629 (2022).
[173]I. Etsion, G. Halperin, V. Brizmer, and Y. Kligerman, "Experimental investigation of laser surface textured parallel thrust bearing," Tribol. Lett. **17**, 295–300 (2004).
[174]Y. Henry, J. Bouyer, and M. Fillon, "An experimental analysis of the hydrodynamic contribution of textured thrust bearing during steady-state operation: A comparison with the untextured parallel surface configuration," Proc. Inst. Mech. Eng. Part J **229**, 362–375 (2014).
[175]W. L. Liu, H. J. Ni, P. Wang, and H. L. Chen, "Investigation on the tribological performance of micro-dimples textured surface combined with longitudinal or transverse vibration under hydrodynamic lubrication," Int. J. Mech. Sci. **174**, 105474 (2020).
[176]X. Q. Yu, S. He, and R. L. Cai, "Frictional characteristics of mechanical seals with a laser-textured seal face," J. Mater. Process Technol. **129**, 463–466 (2002).
[177]Y. Qiu and M. M. Khonsari, "Experimental investigation of tribological performance of laser textured stainless steel rings," Tribol. Int. **44**, 635–644 (2011).
[178]T. Y. Chen, J. H. Ji, Y. H. Fu, X. P. Yang, H. Fu, and L. N. Fang, "Tribological performance of UV picosecond laser multi-scale composite textures for C/SiC mechanical seals: Theoretical analysis and experimental verification," Ceram. Int. **47**(16), 23162–23180 (2021).
[179]A. Borghi, E. Gualtieri, D. Marchetto, L. Moretti, and S. Valeri, "Tribological effects of surface texturing on nitriding steel for high-performance engine applications," Wear **265**(7–8), 1046–1051 (2008).
[180]H. T. Wang, H. Zhu, Y. K. Zhou, and H. F. Yang, "Experimental study on the friction characteristics of textured steel surface with ring-shaped pits under lubricated sliding conditions," Tribol. Trans. **58**(4), 712–717 (2015).
[181]K. Ma, Z. W. Guo, and C. Q. Yuan, "Insight into friction and lubrication performances of surface-textured cylinder liners and piston rings," Int. J. Engine Res. **24**(2), 408–419 (2021).
[182]S. Kalliadasis, C. Bielarz, and G. M. Homsy, "Steady free-surface thin film flows over topography," Phys. Fluids **12**, 1889–1898 (2000).
[183]S. Kalliadasis and G. M. Homsy, "Stability of free-surface thin-film flows over topography," J. Fluid Mech. **448**, 387–410 (2001).
[184]C. Bielarz and S. Kalliadasis, "Time-dependent free-surface thin film flows over topography," Phys. Fluids **15**, 2512–2524 (2003).
[185]J. M. Davis and S. M. Troian, "Generalized linear stability of nonlinear coating flows over topographical features," Phys. Fluids **17**, 072103 (2005).
[186]M. M. J. Decré and J. C. Baret, "Gravity-driven flows of low viscosity liquids over two-dimensional topographies," J. Fluid Mech. **487**, 147–166 (2003).
[187]A. Mazouchi and G. M. Homsy, "Free surface Stokes flow over topography," Phys. Fluids **13**(10), 2751–2761 (2001).
[188]A. Oron, S. H. Davis, and S. G. Bankoff, "Long-scale evolution of thin liquid films," Rev. Mod. Phys. **69**, 931–980 (1997).
[189]R. V. Craster and O. K. Matar, "Dynamics and stability of thin liquid films," Rev. Mod. Phys. **81**(3), 1131–1198 (2009).
[190]P. H. Gaskell, P. K. Jimack, M. Sellier, H. M. Thompson, and M. C. T. Wilson, "Gravity-driven flow of continuous thin liquid flows on non-porous substrates with topography," J. Fluid Mech. **509**, 253–280 (2004).
[191]Y. C. Lee, H. M. Thompson, and P. H. Gaskell, "An efficient adaptive multigrid algorithm for predicting thin film flow on surfaces containing localised topographical features," Comput. Fluids **36**, 838–855 (2007).
[192]M. Sellier, Y. C. Lee, H. M. Thompson, and P. H. Gaskell, "Thin film flow on surfaces containing arbitrary occlusions," Comput. Fluids **38**, 171–182 (2009).
[193]S. Veremieiev, H. M. Thompson, and P. H. Gaskell, "Inertial thin film flow on planar surfaces featuring topography," Comput. Fluids **39**, 431–450 (2010).
[194]S. Veremieiev, H. M. Thompson, Y. C. Lee, and P. H. Gaskell, "Inertial two- and three-dimensional thin film flow over topography," Chem. Eng. Process. **50**(5–6), 537–542 (2011).

[195]S. Veremieiev, H. M. Thompson, and P. H. Gaskell, "Free-surface film flow over topography: Full three-dimensional finite element solutions," Comput. Fluids **122**, 66–82 (2015).
[196]S. Veremieiev and D. H. Wacks, "Modelling gravity-driven film flow on inclined corrugated substrate using a high fidelity weighted residual integral boundary-layer method," Phys. Fluids **31**(2), 022101 (2019).
[197]S. J. D. D'Alessio, J. P. Pascal, and H. A. Jasmine, "Instability in gravity-driven flow over uneven surfaces," Phys. Fluids **21**(6), 062105 (2009).
[198]H. Bonart, J. Jung, and J. U. Repke, "On the stability of gravity-driven liquid films overflowing microstructures with sharp corners," Phys. Rev. Fluids **5**(9), 094001 (2020).
[199]R. Usha and B. Uma, "Modeling of stationary waves on a thin viscous film down an inclined plane at high Reynolds numbers and moderate Weber numbers using energy integral method," Phys. Fluids **16**(7), 2679–2696 (2004).
[200]S. K. Pal, Y. V. S. S. Sanyasiraju, and R. Usha, "A consistent energy integral model for a film over a substrate featuring topographies," Int. J. Numer. Methods Fluids **93**, 3424–3446 (2021).
[201]J. Davies and E. Rideal, *Interfacial Phenomena* (Academic Press, 1963).
[202]Y. O. Kabova, A. Alexeev, T. Gambaryan-Roisman, and P. Stephan, "Marangoni-induced deformation and rupture of a liquid film on a heated microstructured wall," Phys. Fluids **18**, 012104 (2006).
[203]J. A. Diez and L. Kondic, "Contact line instabilities of thin liquid films," Phys. Rev. Lett. **86**(4), 632–635 (2001).
[204]T. Gambaryan-Roisman and P. Stephan, "Flow and stability of rivulets on heated surfaces with topography," ASME J. Heat Mass Transfer **131**(3), 033101 (2009).
[205]N. Tiwari and J. M. Davis, "Stabilization of thin liquid films flowing over locally heated surfaces via substrate topography," Phys. Fluids **22**(4), 042106 (2010).
[206]L. A. Davalos-Orozco, "Non-linear instability of a thin film flowing down a cooled wavy thick wall of finite thermal conductivity," Phys. Lett. A **379**(12–13), 962–967 (2015).
[207]J. Yoo, J. Nam, and K. H. Ahn, "Thermocapillary flows on heated substrates with sinusoidal topography," J. Fluid Mech. **859**, 992–1021 (2019).
[208]D. Tseluiko and D. T. Papageorgiou, "Wave evolution on electrified falling films," J. Fluid Mech. **556**, 361–386 (2006).
[209]D. Tseluiko, M. G. Blyth, D. T. Papageorgiou, and J. M. Vanden-Broeck, "Electrified viscous thin film flow over topography," J. Fluid Mech. **597**, 449–475 (2008).
[210]D. Tseluiko, M. G. Blyth, D. T. Papageorgiou, and J. M. Vanden-Broeck, "Viscous electrified film flow over step topography," SIAM J. Appl. Math. **70**, 845–865 (2009).
[211]D. Tseluiko, M. G. Blyth, D. T. Papageorgiou, and J. M. Vanden-Broeck, "Electrified film flow over step topography at zero Reynolds number: An analytical and computational study," J. Eng. Math. **69**, 169–183 (2011).
[212]B. J. Binder and M. G. Blyth, "Electrified free-surface flow of an inviscid liquid past topography," Phys. Fluids **24**(10), 102112 (2012).
[213]A. Ramkrishnan and S. Kumar, "Electrohydrodynamic deformation of thin liquid films near surfaces with topography," Phys. Fluids **26**, 122110 (2014).
[214]E. Dubrovina, R. V. Craster, and D. T. Papageorgiou, "Two-layer electrified pressure-driven flow in topographically structured channels," J. Fluid Mech. **814**, 222–248 (2017).
[215]D. T. Conroy, L. Espin, O. K. Matar, and S. Kumar, "Thermocapillary and electrohydrodynamic effects on the stability of dynamic contact lines," Phys. Rev. Fluids **4**(3), 034001 (2019).
[216]T. Min and J. Kim, "Effects of hydrophobic surface on skin-friction drag," Phys. Fluids **16**, L55–L58 (2004).
[217]R. Z. Wenzel, "Resistance of solid surfaces to wetting by water," Ind. Eng. Chem. **28**, 988–994 (1936).
[218]A. B. D. Cassie and S. Baxter, "Wettability of porous surfaces," Trans. Faraday Soc. **40**, 546–551 (1944).
[219]J. P. Rothstein, "Slip on superhydrophobic surfaces," Annu. Rev. Fluid Mech. **42**, 89–109 (2010).
[220]D. Gropper, L. Wang, and T. J. Harvey, "Hydrodynamic lubrication of textured surfaces: A review of modeling techniques and key findings," Tribol. Int. **94**, 509–529 (2016).
[221]H. Li, Z. Li, X. Tan, X. Wang, S. Huang, Y. Xiang, P. Lv, and H. Duan, "Three-dimensional backflow at liquid-gas interface induced by surfactant," J. Fluid Mech. **899**, A8 (2020).
[222]E. Lauga and H. A. Stone, "Effective slip in pressure-driven Stokes flow," J. Fluid Mech. **489**, 55–77 (2003).
[223]E. Lauga, M. P. Brenner, and H. A. Stone, "Microfluidics: The no-slip boundary condition," in *Handbook of Experimental Fluid Mechanics* (Springer Press, 2007).
[224]C. L. M. H. Navier, "Memoire sur les lois du mouvement des fluides," Mem. Acad. R. Sci. Inst. **6**, 389–440 (1823).
[225]A. V. Belyaev and O. I. Vinogradova, "Effective slip in pressure-driven flow past super-hydrophobic stripes," J. Fluid Mech. **652**, 489–499 (2010).
[226]E. S. Asmolov and O. I. Vinogradova, "Effective slip boundary condition for arbitrary one-dimensional surfaces," J. Fluid Mech. **706**, 108–117 (2012).
[227]C. Ybert, C. Barentin, C. Cottin-Bizonne, P. Joseph, and L. Bocquet, "Achieving large slip with superhydrophobic surface: Scaling laws for generic geometries," Phys. Fluids **19**, 123601 (2007).
[228]A. M. J. Davis and E. Lauga, "Hydrodynamic friction of fakir-like superhydrophobic surfaces," J. Fluid Mech. **661**, 402–411 (2010).
[229]M. B. Martell, J. B. Perot, and J. P. Rothstein, "Direct numerical simulations of turbulent flows over superhydrophobic surfaces," J. Fluid Mech. **620**, 31–41 (2009).
[230]M. B. Martell, J. P. Rothstein, and J. B. Perot, "An analysis of superhydrophobic turbulent drag reduction mechanisms using direct numerical simulation," Phys. Fluids **22**, 065102 (2010).
[231]H. Park, H. Park, and J. Kim, "A numerical study of the effects of superhydrophobic surface on skin-friction drag in turbulent channel flow," Phys. Fluids **25**, 110815 (2013).
[232]H. Park, G. Y. Sun, and C. J. Kim, "Superhydrophobic turbulent drag reduction as a function of surface grating parameters," J. Fluid Mech. **747**, 722–734 (2014).
[233]R. J. Daniello, N. E. Waterhouse, and J. P. Rothstein, "Drag reduction in turbulent flows over superhydrophobic surfaces," Phys. Fluids **21**, 085103 (2009).
[234]E. Aljallis, M. A. Sarshar, R. Dala, V. Sikka, A. Jones, and C. H. Choi, "Experimental study of skin friction drag reduction on superhydrophobic flat plates in high Reynolds number boundary layer flow," Phys. Fluids **25**, 025103 (2013).
[235]A. K. H. Chu, "Stability of slip flows in a peristaltic transport," Europhys. Lett. **64**, 435–440 (2003).
[236]A. K. H. Chu, "Instability of Navier slip flow of liquids," C. R. Mec. **332**, 895–900 (2004).
[237]E. Lauga and C. Cossu, "A note on the stability of slip channel flows," Phys. Fluids **17**, 088106 (2005).
[238]C. J. Gan and Z. N. Wu, "Short-wave instability due to wall slip and numerical observation of wall-slip instability for microchannel flows," J. Fluid Mech. **550**, 289–306 (2006).
[239]K. C. Sahu, A. Sameen, and R. Govindarajan, "The relative role of divergence and velocity slip in the stability of plane channel flow," Eur. Phys. J. Appl. Phys. **44**(1), 101–107 (2008).
[240]Q. L. He and X. P. Wang, "The effect of the boundary slip on the stability of shear flow," Z. Angew. Math. Mech. **88**(9), 729–734 (2008).
[241]B. Straughan and A. J. Harfash, "Instability in Poiseuille flow in a porous medium with slip boundary conditions," Microfluid. Nanofluid. **15**(1), 109–115 (2013).
[242]S. Ghosh, R. Usha, and K. C. Sahu, "Linear stability analysis of miscible two-fluid flow in a channel with velocity slip at the walls," Phys. Fluids **26**(1), 014107 (2014).
[243]S. Ghosh, R. Usha, and K. C. Sahu, "Absolute and convective instabilities in double-diffusive two-fluid flow in a slippery channel," Chem. Eng. Sci. **134**, 1–11 (2015).
[244]C. S. Chai and B. F. Song, "Stability of slip channel flow revisited," Phys. Fluids **31**, 084105 (2019).
[245]K. W. Chen and B. F. Song, "Linear stability of slip pipe flow," J. Fluid Mech. **910**, A35 (2021).
[246]X. M. Xiong and J. J. Tao, "Linear stability and energy stability of plane Poiseuille flow with isotropic and anisotropic slip boundary conditions," Phys. Fluids **32**(9), 094104 (2020).

[247]Y. Xiao, L. S. Zhang, and J. J. Tao, "Slip boundary effect on the critical Reynolds number of subcritical transition in channel flow," Theor. Appl. Mech. Lett. **13**(2), 100431 (2023).
[248]S. Zou, B. Lin, C. W. Zhong, X. X. Yuan, and Z. G. Tang, "A novel linear stability analysis method for plane Couette flow considering rarefaction effects," J. Fluid Mech. **963**, A33 (2023).
[249]T. Min and J. Kim, "Effects of hydrophobic surface on stability and transition," Phys. Fluids **17**, 108106 (2005).
[250]J. M. Gersting, "Hydrodynamic stability of plane porous slip flow," Phys. Fluids **17**, 2126–2127 (1974).
[251]A. Spille, A. Rauh, and H. Bühring, "Critical curves of plane Poiseuille flow with slip boundary conditions," Nonlinear Phenom. Complex Syst. **3**, 171–173 (2000).
[252]M. T. Matthews and J. M. Hill, "Effect of slip on the linear stability of flow through a tube," Z. Angew. Math. Phys. **59**, 360–379 (2008).
[253]K. H. Yu, C. J. Teo, and B. C. Khoo, "Linear stability of pressure-driven flow over longitudinal superhydrophobic grooves," Phys. Fluids **28**, 022001 (2016).
[254]J. O. Pralits, E. Alinovi, and A. Bottaro, "Stability of the flow in a plane microchannel with one or two superhydrophobic walls," Phys. Rev. Fluids **2**(1), 013901 (2017).
[255]E. Alinovi, "Modelling the flow over superhydrophobic and liquid-impregnated surfaces," Ph.D. dissertation (DICCA, University of Genova, 2018).
[256]S. Ceccacci, S. A. W. Calabretto, C. Thomas, and J. P. Denier, "The linear stability of slip channel flows," Phys. Fluids **34**, 074103 (2022).
[257]F. Picella, J. C. Robinet, and S. Cherubini, "Laminar-turbulent transition in channel flow with superhydrophobic surfaces modelled as a partial slip wall," J. Fluid Mech. **881**, 462–497 (2019b).
[258]F. Picella, J. C. Robinet, and S. Cherubini, "On the influence of the modelling of superhydrophobic surfaces on laminar-turbulent transition," J. Fluid Mech. **901**, A15 (2020).
[259]X. Y. Zhai, K. W. Chen, and B. F. Song, "Linear instability of channel flow with microgroove-type anisotropic superhydrophobic walls," Phys. Rev. Fluids **8**, 023901 (2023).
[260]D. T. Gethin, M. M. H. M. Ahmad, T. C. Claypole, and B. J. Roylance, "Numerical and experimental investigation into porous squeeze films," Tribol. Int. **31**, 189–199 (1998).
[261]N. M. Bujurke and N. B. Naduvinamani, "A note on squeeze film between rough anisotropic porous rectangular plates," Wear **217**, 225–230 (1998).
[262]N. Tilton and L. Cortelezzi, "Linear stability analysis of pressure-driven flows in channels with porous walls," J. Fluid Mech. **604**, 411–445 (2008).
[263]B. Goyeau, D. Lhuillier, D. Gobin, and M. G. Velarde, "Momentum transport at a fluid-porous interface," Int. J. Heat Mass Transfer **46**(21), 4071–4081 (2003).
[264]G. S. Beavers and D. D. Joseph, "Boundary conditions at a naturally permeable wall," J. Fluid Mech. **30**(1), 197–207 (1967).
[265]P. Saffman, "On the boundary condition at the surface of a porous medium," Stud. Appl. Math. **50**, 93–101 (1971).
[266]M. L. Bars and M. G. Worster, "Interfacial conditions between a pure fluid and a porous medium: Implications for binary alloy solidification," J. Fluid Mech. **550**, 149–173 (2006).
[267]F. Valdéa-Parada, B. Goyeau, and J. Ochoa-Tapia, "Jump momentum boundary condition at a fluid-porous dividing surface: Derivation of the closure problem," Chem. Eng. Sci. **62**, 4025–4039 (2007).
[268]U. Lācis and S. Bagheri, "A framework for computing effective boundary conditions at the interface between free fluid and a porous medium," J. Fluid Mech. **812**, 866–889 (2017).
[269]M. E. Rosti, L. Cortelezzi, and M. Quadrio, "Direct numerical simulation of turbulent channel flow over porous walls," J. Fluid Mech. **784**, 396–442 (2015).
[270]S. C. Hirata, B. Goyeau, D. Gobin, M. Carr, and R. M. Cotta, "Linear stability of natural convection in superposed fluid and porous layers: Influence of the interfacial modelling," Int. J. Heat Mass Transfer **50**(7–8), 1356–1367 (2007).
[271]A. Samanta, "Nonmodal and modal analyses of a flow through inhomogeneous and anisotropic porous channel," Int. J. Multiphase Flow **157**, 104230 (2022).
[272]M.-H. Chang, F. Chen, and B. Straughan, "Instability of Poiseuille flow in a fluid overlying a porous layer," J. Fluid Mech. **564**, 287–303 (2006).
[273]A. A. Hill and B. Straughan, "Poiseuille flow in a fluid overlying a porous medium," J. Fluid Mech. **603**, 137–149 (2008).
[274]R. Liu, Q. S. Liu, and S. C. Zhao, "Instability of plane Poiseuille flow in a fluid-porous system," Phys. Fluids **20**, 104105 (2008).
[275]Z. Wu and P. Mirbod, "Instability analysis of the flow between two parallel plates where the bottom one coated with porous media," Adv. Water Resour. **130**, 221–228 (2019).
[276]M. H. Chang, "Thermal convection in superposed fluid and porous layers subjected to a horizontal plane Couette flow," Phys. Fluids **17**, 064106 (2005).
[277]C. Yin, J. Niu, C. J. Fu, and W. C. Tan, "Thermal convection of a viscoelastic fluid in a fluid-porous system subjected to a horizontal plane Couette flow," Int. J. Heat Fluid Flow **44**, 711–718 (2013).
[278]P. D. Antoniadis and M. V. Papalexandris, "Dynamics of shear layers at the interface of a highly porous medium and a pure fluid," Phys. Fluids **27**, 014104 (2015).
[279]T.-Y. Chang, F. Chen, and M.-H. Chang, "Stability of plane Poiseuille-Couette flow in a fluid layer overlying a porous layer," J. Fluid Mech. **826**, 376–395 (2017).
[280]A. Samanta, "Linear stability of a plane Couette-Poiseuille flow overlying a porous layer," Int. J. Multiphase Flow **123**, 103160 (2020).
[281]K. S. Kirthy and S. S. Diwan, "Energy budget analysis and neutral curve characteristics for the linear instability of Couette-Poiseuille flow," Phys. Fluids **33**, 034102 (2021).
[282]S. Hooshyar, H. N. Yoshikawa, and P. Mirbod, "The impact of imposed Couette flow on the stability of pressure-driven flows over porous surfaces," J. Eng. Math. **132**(1), 15 (2022).
[283]K. Suga, Y. Nakagawa, and M. Kaneda, "Spanwise turbulence structure over permeable walls," J. Fluid Mech. **822**, 186–201 (2017).
[284]F. Chen and C. F. Chen, "Onset of finger convection in a horizontal porous layer underlying a fluid layer," ASME J. Heat Mass Transfer **110**, 403–409 (1988).
[285]F. W. Xie, J. Zhu, J. Z. Cui, X. D. Zheng, X. J. Guo, Y. Wang, and R. K. Agarwal, "Dynamic transmission of oil film in soft-start process of HVD considering surface roughness," Ind. Lubr. Tribol. **70**(3), 463–473 (2018).
[286]A. A. Abdel-Rahman and W. M. Chakroun, "Surface roughness effects on flow aerofoils," Wind Eng. **21**(3), 125–137 (1997).
[287]P. Carpenter, "The right sort of roughness," Nature **388**(6644), 713–714 (1997).
[288]D. Fernando, S. Gao, and S. J. Garrett, "The effect of surface roughness on rotor-stator cavity flows," Phys. Fluids **30**, 064103 (2018).
[289]M. Kadivar, D. Tormey, and G. McGranaghan, "A review on turbulent flow over rough surfaces: Fundamentals and theories," Int. J. Thermofluids **10**, 100077 (2021).
[290]E. Reshotko and A. Tumin, "Role of transient growth in roughness-induced transition," AIAA J. **42**(4), 766–770 (2004).
[291]T. Watanabe, H. M. Warui, and N. Fujisawa, "Effect of distributed roughness on laminar-turbulent transition in the boundary layer over a rotating cone," Exp. Fluids **14**, 390–392 (1993).
[292]J. M. Floryan, "Stability of wall-bounded shear layers in the presence of simulated distributed surface roughness," J. Fluid Mech. **335**, 29–55 (1997).
[293]F. Zoueshtiagh, R. Ali, A. J. Colley, P. J. Thomas, and P. W. Carpenter, "Laminar-turbulent boundary-layer transition over a rough rotating disk," Phys. Fluids **15**(8), 2441–2444 (2003).
[294]A. J. Colley, P. Carpenter, P. J. Thomas, R. Ali, and F. Zoueshtiagh, "Experimental verification of the type Π eigenmode destabilization in the boundary layer over a compliant rotating disk," Phys. Fluids **18**, 054107 (2006).
[295]M. Bernardini, S. Pirozzoli, and P. Orlandi, "Compressibility effects on roughness-induced boundary layer transition," Int. J. Heat Fluid Flow **35**, 45–51 (2012).
[296]Y. Shin, U. Rist, and E. Krämer, "Stability of the laminar boundary-layer flow behind a roughness element," Exp. Fluids **56**(1), 1–18 (2015).
[297]D. K. Puckert and U. Rist, "Experiments on critical Reynolds number and global instability in roughness-induced laminar-turbulent transition," J. Fluid Mech. **844**, 878–903 (2018).

[298]T. C. Corke, A. Bar-Sever, and M. V. Morkovin, "Experiments on transition enhancement by distributed roughness," Phys. Fluids **29**(10), 3199–3213 (1986).
[299]E. Reshotko, "Transient growth: A factor in bypass transition," Phys. Fluids **13**(5), 1067–1075 (2001).
[300]S. Muppidi and K. Mahesh, "Direct numerical simulations of roughness-induced transition in supersonic boundary layers," J. Fluid Mech. **693**, 28–56 (2012).
[301]J. C. Loiseau, J. C. Robinet, S. Cherubini, and E. Leriche, "Investigation of the roughness-induced transition: Global stability analyses and direct numerical simulations," J. Fluid Mech. **760**, 175–211 (2014).
[302]R. Ma and K. Mahesh, "Global stability analysis and direct numerical simulation of boundary layers with isolated roughness element," J. Fluid Mech. **949**, A12 (2022).
[303]N. R. Vadlamani, P. G. Tucker, and P. Durbin, "Distributed roughness effects on transitional and turbulent boundary layers," Flow Turbul. Combust. **100**(3), 627–649 (2018).
[304]L. H. von Deyn, P. Forooghi, B. Frohnapfel, P. Schlatter, A. Hanifi, and D. S. Henningson, "Direct numerical simulations of bypass transition over distributed roughness," AIAA J. **58**(2), 702–711 (2020).
[305]M. Miklavčič and C. Wang, "The flow due to a rough rotating disk," Z. Angew. Math. Phys. **55**, 235–246 (2004).
[306]A. J. Cooper, J. H. Harris, S. J. Garrett, M. Özkan, and P. J. Thomas, "The effect of anisotropic and isotropic roughness on the convective stability of the rotating disk boundary layer," Phys. Fluids **27**, 014107 (2015).
[307]M. S. Yoon, J. M. Hyun, and J. S. Park, "Flow and heat transfer over a rotating disk with surface roughness," Int. J. Heat Fluid Flow **28**(2), 262–267 (2007).
[308]S. J. Garrette, A. J. Cooper, J. H. Harris, M. Özkan, A. Segalini, and P. J. Thomas, "On the stability of von Kármán rotating-disk boundary layers with radial anisotropic surface roughness," Phys. Fluids **28**(1), 014104 (2016).
[309]B. Alveroglu, A. Segalini, and S. J. Garrette, "The effect of surface roughness on the convective instability of the BEK family of boundary-layer flows," Eur. J. Mech. B **56**, 178–187 (2016).
[310]A. A. Alqarni, B. Alveroglu, P. T. Griffiths, and S. J. Garrett, "The instability of non-Newtonian boundary-layer flows over rough rotating disks," J. Non-Newtonian Fluid Mech. **273**, 104174 (2019).
[311]B. Alveroglu, A. Segalini, and S. J. Garrette, "An energy analysis of convective instabilities of the Bödewadt and Ekman boundary layers over rough surfaces," Eur. J. Mech. B **61**, 310–315 (2017).
[312]M. A. S. Al-Malki, S. J. Garrett, S. Camarri, and Z. Hussain, "The effects of roughnesss levels on the instability of the boundary-layer flow over a rotating disk with an enforced axial flow," Phys. Fluids **33**(10), 104109 (2021).
[313]M. A. S. Al-Malki, M. Fildes, and Z. Hussain, "Competing roughness effects on the non-stationary crossflow instability of the boundary-layer over a rotating broad cone," Phys. Fluids **34**(10), 104103 (2022).
[314]H. S. Gong, H. B. Xie, L. Hu, and H. Y. Yang, "Combined effects of Coriolis force and temperature-viscosity dependency on hydro-viscous transmission of rotating parallel disks," Tribol. Int. **117**, 168–173 (2018).
[315]A. Costa and G. Macedonio, "Viscous heating effects in fluids with temperature-dependent viscosity: Triggering of secondary flows," J. Fluid Mech. **540**, 21–38 (2005).
[316]K. C. Sahu and O. K. Matar, "Stability of plane channel flow with viscous heating," ASME J. Fluids Eng. **132**(1), 011202 (2010).
[317]D. D. Joseph, "Variable viscosity effects on the flow and stability of flow in channel and pipes," Phys. Fluids **7**, 1761–1771 (1964).
[318]P. C. Sukanek, R. L. Goldstein, and R. L. Laurence, "The stability of plane Couette flow with viscous heating," J. Fluid Mech. **57**, 651–670 (1973).
[319]C. S. Yueh and C. I. Weng, "Linear stability analysis of plane Couette flow with viscous heating," Phys. Fluids **8**(7), 1802–1813 (1996).
[320]N. T. M. Eldabe, M. F. El-Sabbagh, and M. A. S. El-Sayed, "The stability of plane Couette flow of a power-law fluid with viscous heating," Phys. Fluids **19**, 094107 (2007).
[321]D. P. Wall and S. K. Wilson, "The linear stability of channel flow of fluid with temperature-dependent viscosity," J. Fluid Mech. **323**, 107–132 (1996).
[322]D. P. Wall and S. K. Wilson, "The linear stability of flat-plate boundary-layer flow of fluid with temperature-dependent viscosity," Phys. Fluids **9**(10), 2885–2898 (1997).
[323]D. P. Wall and M. Nagata, "Nonlinear equilibrium solutions for channel flow of fluid with temperature-dependent viscosity," J. Fluid Mech. **406**, 1–26 (2000).
[324]R. Govindarajan, V. S. L'vov, I. Procaccia, and A. Sameen, "Stabilization of hydrodynamic flows by small viscosity variations," Phys. Rev. E **67**, 026310 (2003).
[325]H. A. Jasmine and J. S. B. Gajjar, "Absolute and convective instabilities in the incompressible boundary layer on a rotating disk with temperature-dependent viscosity," Int. J. Heat Mass Transfer **48**, 1022–1037 (2005).
[326]R. Miller, P. T. Griffiths, Z. Hussain, and S. J. Garrett, "On the stability of a heated rotating-disk boundary layer in a temperature-dependent viscosity fluid," Phys. Fluids **32**, 024105 (2020).
[327]A. Sameen and R. Govindarajan, "The effect of wall heating on instability of channel flow," J. Fluid Mech. **577**, 417–442 (2007).
[328]H. Srivastava, A. Dalal, K. C. Sahu, and G. Biswas, "Temporal linear stability analysis of an entry flow in a channel with viscous heating," Int. J. Heat Mass Transfer **109**, 922–929 (2017).
[329]W. T. Wu and M. Massoudi, "Recent advances in mechanics of non-Newtonian fluids," Fluids **5**(1), 10 (2020).
[330]H. I. Andersson, E. De Korte, and R. Meland, "Flow of a power-law fluid over a rotating disk revisited," Fluid Dyn. Res. **28**(2), 75–88 (2001).
[331]A. Pinarbasi and C. Ozalp, "Effect of viscous models on the stability of a Non-Newtonian fluid in a channel with heat transfer," Int. Commun. Heat Mass Transfer **28**(3), 369–378 (2001).
[332]A. Pinarbasi and M. Imal, "Viscous heating effects on the linear stability of Poiseuille flow of an inelastic fluid," J. Non-Newtonian Fluid Mech. **127**, 67–71 (2005).
[333]C. Nouar and I. Frigaard, "Delaying transition to turbulence in channel flow: Revisiting the stability of shear-thinning fluids," J. Fluid Mech. **592**, 177–194 (2007).
[334]R. Liu and Q. S. Liu, "Non-modal instability in plane Couette flow of a power-law fluid," J. Fluid Mech. **676**, 145–171 (2011).
[335]C. Nouar and I. Frigaard, "Stability of plane Couette-Poiseuille flow of shear-thinning fluid," Phys. Fluids **21**, 064104 (2009).
[336]C. Y. Ming, L. C. Zheng, and X. X. Zhang, "Steady flow and heat transfer of the power-law fluid over a rotating disk," Int. Commun. Heat Mass Transfer **38**(3), 280–284 (2011).
[337]C. Y. Ming, L. C. Zheng, X. X. Zhang, F. W. Liu, and V. Anh, "Flow and heat transfer of power-law fluid over a rotating disk with generalized diffusion," Int. Commun. Heat Mass Transfer **79**, 81–88 (2016).
[338]P. T. Griffiths, S. O. Stephen, A. P. Bassom, and S. J. Garrett, "Stability of the boundary layer on a rotating disk for pow law fluids," J. Non-Newtonian Fluid Mech. **207**, 1–6 (2014).
[339]M. A. Abdulameer, P. T. Griffiths, B. Alveroglu, and S. J. Garrett, "On the stability of the BEK family of rotating boundary-layer flows for power-law fluids," J. Non-Newtonian Fluid Mech. **236**, 63–72 (2016).
[340]Usman, P. Lin, and A. Ghaffari, "Steady flow and heat transfer of the power-law fluid between two stretchable rotating disks with non-uniform heat source/sink," J. Therm. Anal. Calorim. **146**(4), 1735–1749 (2021).
[341]T. H. Zhao, M. I. Khan, and Y. M. Chu, "Artificial neural networking (ANN) analysis for heat and entropy generation in flow of non-Newtonian fluid between two rotating disks," Math. Methods Appl. Sci. **46**(3), 3012–3030 (2021).
[342]J. Peng and K. Q. Zhu, "Linear stability of Bingham fluids in spiral Couette flow," J. Fluid Mech. **512**, 21–45 (2004).
[343]M. P. Landry, I. A. Frigaard, and D. M. Martinez, "Stability and instability of Taylor-Couette flows of a Bingham fluid," J. Fluid Mech. **560**, 321–353 (2006).
[344]C. Nouar, N. Kabouya, J. Dusek, and M. Mamou, "Modal and non-modal linear stability of the plane Bingham-Poiseuille flow," J. Fluid Mech. **577**, 211–239 (2007).
[345]A. Ahmadpour and K. Sadeghy, "Swirling flow of Bingham fluids above a rotating disk: An exact solution," J. Non-Newtonian Fluid Mech. **197**, 41–47 (2013).
[346]M. Mustafa, M. Tabassum, and M. Rahi, "Second law analysis of heat transfer in swirling flow of Bingham fluid by a rotating disk subjected to suction effect," Therm. Sci. **25**(1), 13–24 (2021).
[347]M. K. Alam, K. Bibi, A. Khan, and S. Noeiaghdam, "Dufour and Soret effect on viscous fluid flow between squeezing plates under the influence of variable magnetic field," Mathematics **9**(19), 2404 (2021).

[348]P. Jayavel, R. Katta, and R. K. Lodhi, "Numerical analysis of electromagnetic squeezing flow through a parallel porous medium plate with impact of suction/injection," Waves Random Complex Media **2022**, 1–24.
[349]T. V. V. L. N. Rao and J. T. Sawicki, "Linear stability analysis for a hydrodynamic journal bearing considering cavitation effects," Tribol. Trans. **45**(4), 450–456 (2002).
[350]T. V. V. L. N. Rao and J. T. Sawicki, "Stability analysis for a rough journal bearing considering cavitation effects," ASME J. Tribol. **127**(1), 112–119 (2005).
[351]J. Z. Cui, F. W. Xie, and C. T. Wang, "Numerical investigation on thermal deformation behavior of friction pair in hydro-viscous drive," Appl. Therm. Eng. **90**, 460–470 (2015).
[352]M. Ledinegg, "Instability of flow during natural and forced circulation," Die Wärme **61**(8), 891–898 (1938).
[353]R. Stelling, E. V. McAssey, T. Dougherty, and B. W. Yang, "The onset of flow instability for downward flow in vertical channels," ASME J. Heat Transfer **118**(3), 709–714 (1996).
[354]L. E. O'Neill and I. Mudawar, "Review of two-phase flow instabilities in macro- and micro-channel systems," Int. J. Heat Mass Transfer **157**, 119738 (2020).
[355]G. H. Yeoh, J. Y. Tu, and Y. Li, "On void fraction distribution during two-phase boiling flow instability," Int. J. Heat Mass Transfer **47**(2), 413–417 (2004).
[356]J. F. Wang, Y. P. Huang, and Y. L. Wang, "Visualized study on specific points on demand curves and flow patterns in a single-side heated narrow rectangular channel," Int. J. Heat Fluid Flow **32**(5), 982–992 (2011).
[357]J. Lee, H. Chae, and S. H. Chang, "Flow instability during subcooled boiling for a downward flow at low pressure in a vertical narrow rectangular channel," Int. J. Heat Mass Transfer **67**, 1170–1180 (2013).
[358]O. S. Al-Yahia and D. Jo, "ONB, OSV, and OFI for subcooled flow boiling through a narrow rectangular channel heated on one-side," Int. J. Heat Mass Transfer **116**, 136–151 (2018).
[359]Q. Lu, Y. Zhang, Y. Liu, L. L. Zhou, C. F. Shen, and D. Q. Chen, "An experimental investigation on the characteristics of flow instability with the evolution of two-phase interface morphology," Int. J. Heat Mass Transfer **138**, 468–482 (2019).
[360]D. Brutin, F. Topin, and L. Tadrist, "Experimental study of unsteady convective boiling in heated minichannels," Int. J. Heat Mass Transfer **46**, 2957–2965 (2003).
[361]D. Brutin and L. Tadrist, "Pressure drop and heat transfer analysis of flow boiling in a minichannel: Influence of the inlet condition on two-phase flow stability," Int. J. Heat Mass Transfer **47**, 2365–2377 (2004).
[362]G. Wang, P. Cheng, and H. Wu, "Unstable and stable flow boiling in parallel microchannels and in a single microchannel," Int. J. Heat Mass Transfer **50**, 4297–4310 (2007).
[363]G. Wang and P. Cheng, "An experimental study of flow boiling instability in a single microchannel," Int. Commun. Heat Mass Transfer **35**, 1229–1234 (2008).
[364]J. Barber, K. Sefiane, D. Brutin, and L. Tadrist, "Hydrodynamics and heat transfer during flow boiling instabilities in a single microchannel," Appl. Therm. Eng. **29**(7), 1299–1308 (2009).
[365]G. P. Celata, S. K. Saha, G. Zummo, and D. Dossevi, "Heat transfer characteristics of flow boiling in a single horizontal microchannel," Int. J. Therm. Sci. **49**, 1086–1094 (2010).
[366]Y. F. Fan and I. Hassan, "Experimental investigation of flow boiling instability in a single horizontal microtube with and without inlet restriction," ASME J. Heat Mass Transfer **134**(8), 081501 (2012).
[367]H. He, P. F. Li, R. G. Yan, and L. M. Pan, "Modeling of reversal flow and pressure fluctuation in rectangular microchannel," Int. J. Heat Mass Transfer **102**, 1024–1033 (2016).
[368]H. Z. Li and P. Hrnjak, "Modeling of bubble dynamics in single diabatic microchannel," Int. J. Heat Mass Transfer **107**, 96–104 (2017).
[369]L. C. Ruspini, C. P. Marcel, and A. Clausse, "Two-phase flow instabilities: A review," Int. J. Heat Mass Transfer **71**, 521–548 (2014).
[370]J. Maulbetsch and P. Griffith, "System induced instabilities in forced-convection flows with subcooled boiling," Int. Heat Transfer Conf. **3**(7–12), 247–257 (1966).
[371]H. Yuncu, "An experimental and theoretical study of density wave and pressure drop oscillations," Heat Transfer Eng. **11**(3), 45–56 (1990).
[372]W. L. Qu and I. Mudawar, "Measurement and prediction of pressure drop in two-phase micro-channel heat sinks," Int. J. Heat Mass Transfer **46**(15), 2737–2753 (2003).
[373]C. Huh, J. Kim, and M. H. Kim, "Flow pattern transition instability during flow boiling in a single microchannel," Int. J. Heat Mass Transfer **50**(5–6), 1049–1060 (2007).
[374]T. J. Zhang, Y. Peles, J. T. Wen, T. Tong, J. Y. Chang, R. Prasher, and M. K. Jensen, "Analysis and active control of pressure-drop flow instabilities in boiling microchannel systems," Int. J. Heat Mass Transfer **53**(11–12), 2347–2360 (2010).
[375]Y. Kuang, W. Wang, J. Miao, X. Yu, and R. Zhuan, "Theoretical analysis and modeling of flow instability in a mini-channel evaporator," Int. J. Heat Mass Transfer **104**, 149–162 (2017).
[376]K. H. Chang and C. Pan, "Two-phase flow instability for boiling in a microchannel heat sink," Int. J. Heat Mass Transfer **50**(11–12), 2078–2088 (2007).
[377]T. L. Chen and S. V. Garimella, "Local heat transfer distribution and effect of instabilities during flow boiling in a silicon microchannel heat sink," Int. J. Heat Mass Transfer **54**(15–16), 3179–3190 (2011).
[378]Z. R. Jiang, Z. Y. Ma, R. G. Yan, L. T. Zhang, W. Sun, S. S. Bu, and L. M. Pan, "Experimental study on the flow boiling oscillation characteristics in a rectangular multiple micro-channel," Exp. Therm. Fluid Sci. **109**, 109902 (2019).
[379]B. Wang, Y. W. Hu, Y. R. He, N. Rodionov, and J. Q. Zhu, "Dynamic instabilities of flow boiling in micro-channels: A review," Appl. Therm. Eng. **214**, 118773 (2022).
[380]L. Cao, S. Kakac, H. Liu, and P. Sarma, "Theoretical analysis of pressure-drop type instabilities in an upflow boiling system with an exit restriction," Heat Mass Transfer **37**, 475–483 (2001).
[381]Q. Jin, J. T. Wen, and S. Narayanan, "Characteristics of pressure drop oscillation in a microchannel cooling system," Appl. Therm. Eng. **160**, 113849 (2019).
[382]Q. Jin, J. T. Wen, and S. Narayanan, "The analysis and prediction of pressure drop oscillation in phase-change cooling systems," Int. J. Heat Mass Transfer **165**, 120621 (2021).
[383]C. J. Kuo and Y. Peles, "Pressure effects on flow boiling instabilities in parallel microchannels," Int. J. Heat Mass Transfer **52**, 271–280 (2009).